Universitetet i Stavanger

FACULTY OF SCIENCE AND TECHNOLOGY

MASTER'S THESIS

Study programme/specialisation: Master of Science in Petroleum Engineering, Drilling and Well Technology	Spring semester, 2017 Open
Author: Andreas Holsen	…… (signature of author)
Programme coordinator: Supervisor(s): Helge Hodne, University of Stavanger Vegar Haraldsen, Oilfield Innovations	
Title of master's thesis: **Evaluation of Downhole Tubing Disposal for Permanent Plug and Abandonment**	
Credits: 30	
Keywords: Plug and abandonment New technology Tubing compaction Rigless P&A	Number of pages: 133 + supplemental material/other: 11 Stavanger, 15/06/2017. date/year

Abstract

A new method called Downhole Tubing Disposal developed by Oilfield Innovations for performing rigless permanent plug and abandonment is presented. Instead of pulling the production tubing, the tubing is weakened with longitudinal cuts which enables crushing of the tubing into the available liquid space of the constraining casing, effectively providing an unobstructed casing length where cement plugs can be set. By eliminating the requirement for a drilling rig, significant cost savings can be achieved. Evaluation of a full-scale experiment with a 2 3/8" tubing is given, and the plans for conducting a full-scale experiment with 4 ½" tubing is presented and discussed. Furthermore, a small-scale experiment was performed with the main objective being investigation of the influence of cutting pattern and radial clearance between compaction tube and constraint. The discussions from the three experiments are combined and further developed in terms of a real case of Downhole Tubing Disposal.

No studies on chaotic crushing of constrained tubes have been found in the literature except for an experiment conducted by the inventors of Downhole Tubing Disposal. The data on the matter were therefore limited, which motivated the small-scale experiment. This experiment clearly shows that weakening a tube with longitudinal cuts reduces its axial compressive strength, and an increasing number of cuts further reduces this strength. Moreover, the compaction ratio increased significantly at moderate loads when more than two cuts were used. Calculations revealed that while a smaller constraining tube gave a reduced compaction ratio, the occupied cross-sectional area of the constraining tube increased at high loads. At moderate loads, the occupied cross-sectional area was identical for the different constraining tubes.

Acknowledgements

This thesis is submitted as part of my Master of Science degree in Petroleum Technology at the University of Stavanger. It would not have been possible without the help of several individuals, and I would therefore like to use this opportunity to express my gratitude towards them.

First and foremost, I would like to thank my faculty supervisor, Helge Hodne, who has given me valuable guidance and structural feedback during the writing of this thesis. He has continuously guided me along the right path and helped shape the thesis into what it is today.

My sincere appreciation goes to Oilfield Innovations for the opportunity they gave me to work on this thesis. The exciting field of new technology within plug and abandonment has made this an interesting journey from the beginning to the end. I would also like to thank Vegar Haraldsen, who has been my external supervisor at Oilfield Innovations. He has introduced me to various parts of the industry and provided me with the necessary information to make this thesis possible.

I would also like to express my gratitude to Mesfin Agonafir Belayneh, who have given me motivation and insights throughout the work of this thesis. Although not being my supervisor, he has stayed close and followed my work from the beginning. His wealth of knowledge has been of great importance for my work.

I am thankful to everyone at the university who have helped me with my inquiries, especially Bernt Sigve Aadnøy, Jan Aage Aasen, Jan Magne Nygård, and Samdar Kakay.

Finally, I want to thank my partner Ida Karoline Baustad for always supporting me, and my son for bringing me joy and laughter every day.

Table of Contents

List of Figures

List of Tables

Abbreviations

API	American Petroleum Institute
ASV	Annular Safety Valve
DTD	Downhole Tubing Disposal
ERD	Extended Reach Drilling
ID	Inner Diameter
LOT	Leak Off Test
NCS	Norwegian Continental Shelf
OD	Outer Diameter
P&A	Plug and Abandonment
PBR	Polished Bore Receptacle
PP&A	Permanent Plug and Abandonment
PPF	Pounds Per Foot
RLWI	Riserless Light Well Intervention
WBE	Well Barrier Element
XMT	Christmas Tree

Chapter 1

Introduction

1.1. Background

Production wells that are either no longer economically viable or require closure due to wellbore issues need to be plugged to prevent future leaks after the well is abandoned. On the Norwegian continental shelf (NCS) alone there were 4,535 active and inactive development wells in May 2017 (NPD n.d.). Almost half of these wells have been permanently plugged and abandoned, as seen in Fig. 1. As all wells need to be abandoned at some point, the industry has an enormous job ahead. The oil industry is looking for ways to cut costs, and many people have lost their jobs due to the currently low oil price. Reducing the expenses related to permanent plug and abandonment (PP&A) can save millions of dollars in the future. For most offshore wells, rig related costs are usually the major contributor to the total cost of PP&A. The aim should therefore be to use smaller and cheaper vessels where applicable, or perform necessary operations from fixed installations using wireline and coiled tubing.

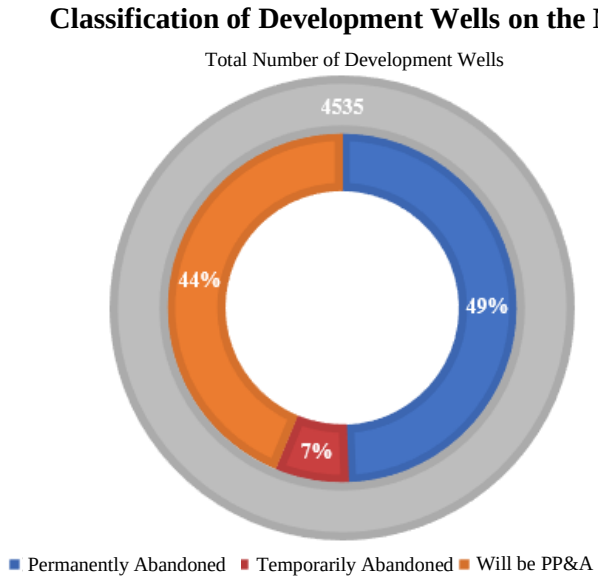

Fig. 1. Classification of development wells on the Norwegian Continental Shelf (NPD n.d.).

One of the main problems with performing rigless PP&A is the lifting capacity of the equipment. Many wells require the tubing to be removed in order to place a cement plug to seal the wellbore. As

of 2017, no riserless light well intervention (RLWI) vessel have retrieved tubing to surface. Therefore, the industry has been looking for ways to remove the tubing without lifting it out of the hole. The Norwegian company Interwell have developed a method where thermite is used to melt the tubing, casing and even the rock. The melted mass is meant to form an impermeable plug once it has cooled down (Interwell 2016).

Another way to avoid lifting the tubing out of the hole is to compact it further down. Buckling theory describes the effect of axial force on a constrained cylinder. Sufficient axial load will transform the initially straight tubing into a helical shape. Further increase in axial load will direct the force to the casing wall and the tubing will experience lock-up, inhibiting any further transfer of axial load to the bottom of the tubing. The total displacement of a 100 m long tubing can be calculated to be under 4 m, which makes this method very impractical[1]. To solve this problem, Oilfield Innovations have patented the process of weakening the tubing before compacting it, currently called Downhole Tubing Disposal (DTD). By splitting the tubing longitudinally, the strength of the cylinder is considerably reduced. Rather than just buckle, it will bend and fold as axial force is applied, and be effectively crushed inside the casing (Oilfield Innovations 2013).

1.2. Purpose and Scope

The aim of this thesis is to give an evaluation of DTD as a method for creating sufficient space to place a cement plug during PP&A, where the focus area will be the compaction process. DTD can save the petroleum industry millions, if not even billions, of dollars if the method is verified and becomes the main abandonment strategy for offshore wells. The thesis was initially meant to be built upon a full-scale experiment of the patented method performed in Norway, but the test has not been conducted as of the filing of this thesis. Instead, the planned test is reviewed and a theoretical evaluation of the different parameters that may influence the compaction process is given. A small-scale experiment was also conducted to investigate the effect of different cutting patterns and constraints on a compaction tube. A brief description of the chapters found in this thesis is as follows:

- Chapter 2 provides the necessary theory to understand the different concepts of the thesis, which includes friction, effective forces, buckling, and deformation.

- Chapter 3 presents guidelines used for P&A, both on the Norwegian and English sector. A general PP&A procedure is also given.

- Chapter 4 introduces the method of DTD.

- Chapter 5 considers the first full-scale test of DTD which was performed in the US in 2013. The results are discussed and the limitations of the experiment are highlighted.

- Chapter 6 covers the planned full-scale experiment in Norway, including the setup, procedure, and discussion of important compaction parameters.

[1] Calculated with Eq. 6, 10, and 11 assuming lock-up when initiating helical buckling, using 4 ½” 12.6 ppf tubing within 9 5/8” 47 ppf casing.

- Chapter 7 presents a small-scale compaction experiment conducted at the University of Stavanger.

- Chapter 8 discusses the method of DTD with respect to a real case scenario, which is an extension of the discussion of the experiments in Chapter 5, 6, and 7.

- Chapter 9 concludes with a summary of the most important learnings and conclusions from the thesis. Recommendations for future work are also given.

Chapter 2

Theory

This chapter contains theory required to recognize the different concepts found in this thesis. To understand the method of DTD, and to justify the weakening of the tubing before compaction, one should be aware of constrained tubular mechanics. First, a short overview of the theory behind friction will be presented, followed by the concept of effective forces. This serves as an introduction to constrained buckling theory and subsequently elasticity and plastic behavior of steel. An introduction to absorber deformation is given at the end of this chapter.

Different conventions are used when defining the sign of compression and tension within the petroleum industry. In rock mechanics, compression is usually defined positive, while in mechanical engineering, the practice has been to define compression as negative. In this thesis, compression is defined as positive.

2.1. Friction

Friction is defined as the force that resists motion between two bodies in contact and moving relative to each other (Oxford University Press n.d.). It is not a fundamental force in itself, but comprises a combined effect of other forces. Some parameters that influence friction are inter-surface adhesion, electromagnetic attraction, surface roughness, and deformation. Analyzing friction with respect to all parameters of importance is often very complex, which lead scientists to a simpler expression that is based on experiments. The force of friction can be expressed as:

$$F_f = \mu N \tag{1}$$

where F_f is the friction force, μ is the coefficient of friction between two surfaces, and N is the normal force between the surfaces. The coefficient of friction may either be the kinetic coefficient μ_k, or the static coefficient μ_s, depending on whether the objects are moving relative to each other or not. This parameter is an empirical factor and can only be found through experiments. The kinetic coefficient is usually lower than the static, which means that it is easier for a body to maintain motion rather than to initiate motion. It is important to note that frictional force is not dependent on contact area between surfaces. An increased contact area also increases the distribution of the normal force, and these two effects cancel each other out (Persson 2000).

2.1.1. Dry Friction

No object is completely smooth, especially not on an atomic scale. During sliding of clean and dry metal surfaces, the asperities, as illustrated in Fig. 2, weld together and break apart, and this process produces wear debris of metallic particles. This is believed to be the main source of dry friction between clean metal surfaces (Persson 2000).

Fig. 2. Asperities before and after an axial load is applied.

2.1.2. Lubricated Friction

A lubricant can be used to lower the coefficient of friction and reduce wear, and is usually a liquid placed between solid parts that move relative to one another. A high viscosity fluid will usually lead to a lower sliding friction compared to a lower viscosity fluid, because the viscous fluid will not have sufficient time to be squeezed out between the contact areas. However, if the relative motion between the sliding objects is low enough, the fluid may have time to be squeezed out, and this will result in direct contact between the surfaces. As dry friction is usually greater than lubricated friction, the friction force will then increase (Persson 2000).

2.2. Effective Forces

Archimedes found that a body submerged in a fluid experiences an upward force equal to the weight of the fluid displaced by the body (Aasen 2007). This force is called buoyancy. The buoyant force can be described using a buoyancy factor (BF), and this factor can be multiplied by a force to account for buoyancy. Lubinski (1962) came up with the concept of effective weight, which was used to incorporate the buoyant force into the buckling equations. Effective forces differ from "real" forces by including the influence of buoyancy. The effective weight per foot (w_e) of a steel pipe can be described as (Aasen 2007):

$$w_e = w_s BF \tag{2}$$

where w_s is the weight per foot of the steel pipe in air. The buoyancy factor of an object can generally be described as (Aasen 2007):

$$BF = \frac{\rho_s - \left(\rho_o \frac{A_o}{A_s} - \rho_i \frac{A_i}{A_s}\right)}{\rho_s} \tag{3}$$

where ρ_s is the density of steel, ρ_o and ρ_i are the densities of the fluids outside and inside the pipe, respectively, A_s is the cross-sectional area of the steel pipe, and A_o and A_i are the cross-sectional areas created by the outside and inside diameters, respectively. Given a pipe with the same fluid density (ρ_f) inside and outside, the above equation simplifies to:

$$BF = \frac{\rho_s - \rho_f}{\rho_s} \tag{4}$$

2.3. Constrained Buckling

Buckling of cylindrically constrained tubulars is of great importance to the petroleum industry. A cylinder is said to buckle when introduced to a sufficiently large compressive force (R. F. Mitchell, Tubing Buckling - The State of the Art 2006). In a vertical well, buckling is only resisted by the stiffness of the pipe. In a deviated or horizontal well, buckling is also resisted by the increase in potential energy required to lift the pipe up along the curvature of the constraining cylinder (R. F. Mitchell, Tubing Buckling - The State of the Art 2006). Lubinski (1950) was the first to model the behavior for vertical wells, and the concept was later described in deviated and horizontal wells. Effective weights and forces should be used in calculations regarding buckling (Lubinksi, Althouse and Logan 1962).

It is assumed that primarily two types of buckling occur in an oil well; lateral (sinusoidal) and helical buckling, as seen in Fig. 3 (R. F. Mitchell, Tubing Buckling - The State of the Art 2006). When the axial load on a tubular passes some critical value, the tubular will no longer remain straight. This critical value is called the lateral buckling limit (LBL), and loading beyond this point makes the tubular develop a snake-like shape (Wicks, Wardle and Pafitis 2007). At the helical buckling limit (HBL), the shape of the tubular transforms further into a helix (Wicks, Wardle and Pafitis 2007). The well geometry influences the buckling loads, and different models have been developed to predict the buckling behavior for vertical, horizontal, and deviated well bores. It should be noted that none of the buckling equations in this chapter are dependent on the length of the tubular.

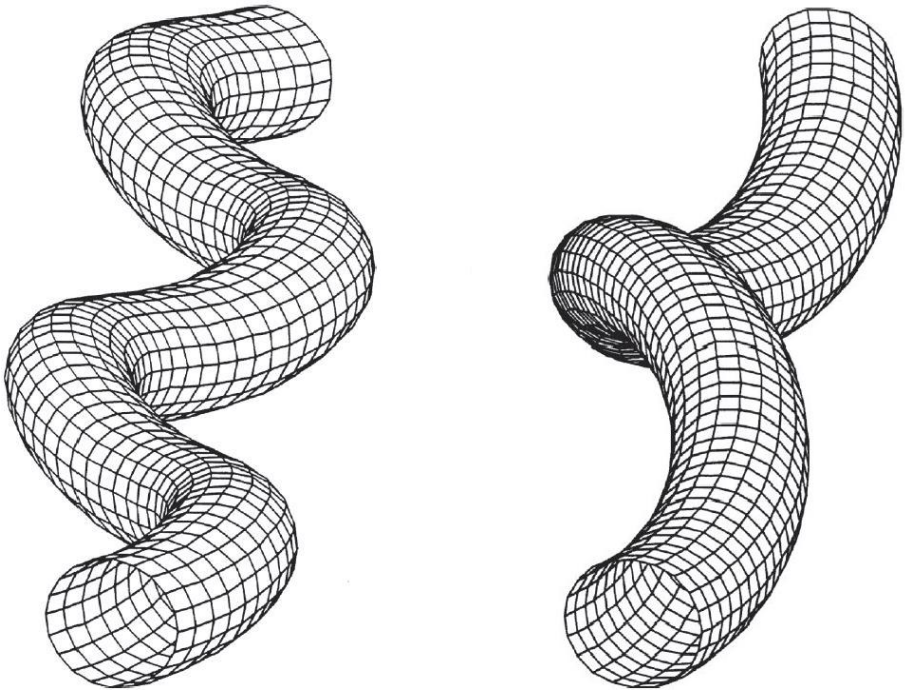

Fig. 3. To the left a lateral (sinusoidal) buckling configuration is illustrated, while a helical buckling configuration can be seen on the right (R. F. Mitchell, Tubing Buckling - The State of the Art 2006)

2.3.1. Vertical Wellbores

The first publicized analysis on helical buckling was based on equilibrium and energy methods (Lubinksi, Althouse and Logan 1962). The LBL (F_{lat}) is given by (Lubinski 1950):

$$F_{lat} = 1.94\sqrt[3]{EIw_e^2} \tag{5}$$

where the product of the modulus of elasticity and the area moment of inertia, EI, is the bending stiffness of the rod. Further increasing axial load will transform the pipe into a helical shape. The HBL (F_{hel}) can be expressed as (Bellarby 2009):

$$F_{hel} = 4.05\sqrt[3]{EIw_e^2} = 2.09F_{lat} \tag{6}$$

2.3.2. Deviated and Horizontal Wellbores

Dawson and Paslay (1984) modelled the LBL for a tubular in an inclined wellbore:

$$F_{lat} = 2\sqrt{\frac{EIwsin\theta}{\Delta r}} \tag{7}$$

Here, θ is the angle between the wellbore and a vertical line and Δr is the radial clearance, which is defined as the difference between the inside radius of the constraining tubular and the outside radius of the inner tubular. The HBL was later derived by Chen (1989) as:

$$F_{hel} = 2\sqrt{2}\sqrt{\frac{EIwsin\theta}{\Delta r}} = \sqrt{2}F_{lat} \tag{8}$$

Eq. 7 and 8 are valid for horizontal wellbores by setting θ = 90°. The factor multiplied by F_{lat} has been discussed by numerous authors ((Kyllingstad 1995), (Miska, et al. 1996), (Wu and Juvkam-Wold 1993)) and various suggestions have been proposed, although the factor is commonly agreed to be $\sqrt{2}$. Mitchell (1997) observed that the factor was almost $2\sqrt{2}$ during loading, and $\sqrt{2}$ during unloading. In other words, the load needed to initiate helical buckling from a lateral buckled state is higher than the load needed to initiate lateral buckling from a helical buckled state.

Miska and Cunha (1995) and He (1995) published papers on the effect of torque on helical buckling, where they all arrived at the same relationship:

$$T_{hel} = 2.09\sqrt[4]{\frac{(EI)^3 wsin\theta}{\Delta r}} \tag{9}$$

Here, T_{hel} is the torque required to initiate helical buckling when no compressional force is acting on the cylinder. In the paper by Miska and Cunha (1995), they concluded that torque reduces the HBL and the pitch, and this reduction was in the range of 3-6% for their example cases. In these theoretical cases the HBL was calculated when the torque was 0 and 10,000 ft·lbs. The calculations were done for wellbore inclinations between 10 and 90 degrees, and it was shown that the influence of torque decreases with increasing inclination. Radial clearance also affected the results, wherein a larger clearance increased the influence of torque.

2.3.3. Displacement

The tubular will experience two different types of shortening due to the axial compressional load. The first is because of Hooke's law, and the real axial force must be used (Lubinksi, Althouse and Logan 1962):

$$\Delta L_1 = -\frac{LF}{EA_s} \tag{10}$$

where ΔL_1 is the shortening due to Hooke's law effect, L is the total length of the tubular in compression, and F is the compressional force which acts on the bottom of the tubular. The second type of shortening is related to the helical shape of the buckled tubular. As with all buckling related equations, the effective force must be used. Lubinski (1962) proved that when part of the vertical tubular is in compression, this shortening can be written as:

$$\Delta L_2 = -\frac{\Delta r^2 F_{hel^+}^2}{8EIw_e} \tag{11}$$

where F_{hel^+} is a compressional force greater than the HBL acting on the bottom of the tubular. Shortening is defined as negative in this thesis, which explains the negative sign in Eq. 9 and 10. Mitchell (2006) later derived the equation for the same shortening, only in a horizontal well:

$$\Delta L_2 = -\frac{\Delta r^2 L F_{hel^+}}{4EI} \tag{12}$$

For an inclined well, the expression is (R. F. Mitchell, Tubing Buckling - The State of the Art 2006):

$$\Delta L_2 = -\frac{\Delta r^2}{8EIwcos\theta}\left(F_{hel^+,2}^2 - F_{hel^+,1}^2\right) \tag{13}$$

Here, $F_{hel^+,1}$ and $F_{hel^+,2}$ refers to the load at the top and bottom of the helix, respectively.

2.3.4. Lock-up

For a straight pipe, the friction force between the inner and the constraining tubular is:

$$F_f = \mu w_e sin\theta L \tag{14}$$

Eq. 14 is the same as Eq. 1, which can be seen by replacing $wsin\theta L$ with N. When the pipe is laterally buckled, the normal contact force has been found to not deviate significantly from the self-weight of the pipe (R. F. Mitchell, Tubing Buckling - The State of the Art 2006), and the friction force can therefore be approximated by Eq. 13.

Once the tubing is helically buckled, the contact force will consist of the normal force and an additional force generated by the confinement of the buckled cylinder. This additional normal force can be expressed as (R. F. Mitchell 1986):

$$\Delta N = \frac{\Delta r F_{hel^+}^2}{4EI} \tag{15}$$

It follows from Eq. 14 that after the onset of helical buckling, the additional contact force will increase by the square of the axial load, which leads to a rapidly growing frictional force. This will eventually result in lock-up of the tubular, which happens when bit weight cannot be increased due to frictional forces resisting any increase in axial compressional force (Wu and Juvkam-Wold 1993).

2.3.5. Yielding due to Buckling

The buckled configuration of a tubular will result in a bending stress that is tensile on the outer convex portion of the curve and compressive on the inner concave portion of the curve. By assuming that the tubular begins to deform permanently (see Section 2.4.2) when the effective compressive stress

reaches the yield strength (σ_y) of the pipe, the minimum load that will cause yielding (F_y) of a buckled tubular is (Maurer Engineering Inc. 1993):

$$F_y = \frac{\sigma_y}{\frac{1}{A_s} + \frac{r_o \Delta r}{2I}} \tag{16}$$

2.4. Deformation

Materials exposed to either a change in temperature or an applied load will deform. This thesis will only look at deformation caused by applied loads. The amount of deformation depends on the magnitude of the force and the shape and type of material that is exposed. To exclude the effect of cross-sectional area, stress is often used instead of force (Callister and Rethwisch 2011). Eq. 17 shows the relationship between stress (σ) and force:

$$\sigma = \frac{F}{A_0} \tag{17}$$

Here, F is the force applied perpendicular to the cross section of the specimen, and A_0 is the original cross-sectional area before the force is applied.

Deformation is often expressed as engineering strain (ε), which is a dimensionless parameter that is defined as (Callister and Rethwisch 2011):

$$\varepsilon = \frac{l_i - l_0}{l_0} = \frac{\Delta l}{l_0} \tag{18}$$

where l_i is the instantaneous length of the specimen, and l_0 is the length before any force is applied. Strain can also be expressed in length units as a total elongation or shortening.

2.4.1. Elastic Deformation

Deformation in which stress and strain are proportional is called elastic deformation, and can be expressed as:

$$\sigma = E\varepsilon \tag{19}$$

This proportionality is known as Hook's law, and the straight part of the graph in Fig. 4 represents this linear relationship. The modulus of elasticity (E), or Young's modulus, can be calculated as the slope of this straight line, and most steels have an elastic modulus of around 206.8 GPa (Bellarby 2009). However, this straight-line assumption is only an approximation, and for some corrosion resistant alloys, like production tubings, the relationship is non-linear throughout (Bellarby 2009). Elastic

deformation is not permanent, so when the applied force is released, the specimen will return to its original shape while releasing the energy that was stored up as elastic deformation energy.

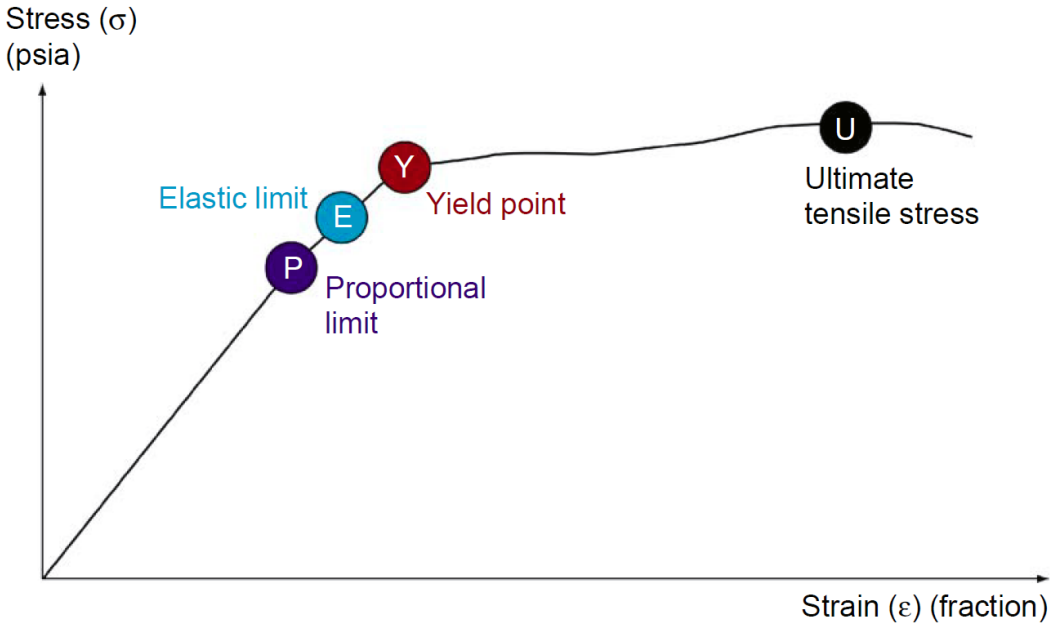

Fig. 4. Typical plot of stress versus strain for alloyed metal (Bellarby 2009).

2.4.2. Plastic Deformation

When a material exceeds the elastic limit in Fig. 4, permanent deformation usually occurs. This permanent deformation is called plastic deformation, and does not pose a linear stress-strain relationship. The elastic limit is usually close to the yield point, which is where a small increase in stress starts to cause a large increase in strain (Bellarby 2009). This is often difficult to measure, and the API (API Spec 5CT 2005) has therefore defined the API yield strength for different grades of steel (see Section 2.4.3) as the minimum stress required to elongate the material a certain percentage.

Stress can be increased until the ultimate tensile stress is reached. This is the maximum tensile stress the material can handle, and after this point the material will start to unload while strain increases until the material ultimately fails. For many low-grade tubulars, like the K-55 listed in Table 1, the difference between yield point and ultimate tensile stress is often large. These expandable tubulars can be used to an advantage where a large deformation of the tubing is required.

When the material is loaded in the plastic region and the stress is then removed, the material will follow the slope of the modulus of elasticity as it unloads. This means that the material will show permanent deformation. If the material is subsequently loaded, the yield strength may be altered from its initial value due to work hardening (essentially cold working) (Bellarby 2009). All steel grades follow the same slope when loaded below the yield point (Bellarby 2009).

2.4.3. API Material Specifications

The different steel grades used to qualify oilfield tubulars consists of a combination of letters and numbers, as seen in Table 1. The numbers specify the minimum API yield stress in ksi (1,000 psi) of

the specific grade. It should be noted that the API yield stress is above the yield point of a material, and that it is defined as the stress that causes a certain elongation (second column in Table 1). For API grades, the letters are usually arbitrary, but may have significance in some cases such as for L80 and N80, which are for sour and non-sour service, respectively. While all API grades uses a single letter prefix, proprietary grades use double letters. These letters do have significance, but each manufacturer have their own specifications (Bellarby 2009). The API steel grades in Table 1 only specifies tensile strength, and the tubulars are often alloyed to achieve higher corrosion resistance. An example is the L80 13 Cr tubing, which is similar to N80 grade, but with 13 % chromium, and this tubing is common in wells on the NCS (Belayneh 2016).

Table 1. API grades and strengths as defined by API Spec 5CT (2005) (Bellarby 2009)**.**

Grade	Elongation Under Load [%]	Yield Stress [ksi]		Minimum Tensile Strength [ksi]
		Minimum	Maximum	
H40	0.5	40	80	60
J55	0.5	55	80	75
K55	0.5	55	80	95
N80	0.5	80	110	100
M65	0.5	65	85	85
L80	0.5	80	95	95
C90	0.5	90	105	100
C95	0.5	95	110	105
T95	0.5	95	110	105
P110	0.6	110	140	125
Q125	0.65	125	150	135

2.5. Absorber Deformation

Energy-absorbing structures have been extensively used in vehicle design to minimize human injuries when a collision occurs by converting kinetic energy into plastic deformation energy (Salehghaffari, Tajdari and Mokhtarnezhad 2009). Various geometries have been investigated for this use, and metallic thin-walled cylindrical tubes has been considered as one of the most efficient means of energy absorption (Salehghaffari, Tajdari and Mokhtarnezhad 2009). Here, "thin-walled" is one of two categories in which circular cylinders are generally divided into:

- Thin-walled, if $t < \frac{1}{10}r$
- Thick-walled, if $t > \frac{1}{10}r$

Only cylindrical tubes will be investigated in this thesis, where the absorbers are placed vertically inside a test chamber and loaded axially. The preferred mode of collapse for these tubes is a controlled manner of deformation called progressive collapse, where the entire body of the member is deformed plastically by absorbing a major part of the impact energy (Hsu and Jones 2002). The different collapse modes observed in such experiments will be reviewed, and the effect of cylinder geometry will be investigated.

2.5.1. Load Types and Classification of Collapse Modes

There are mainly two types of loads which are used in the research of energy absorbers, namely, static and dynamic loads ((Andrews, England and Ghani 1983), (Ghani 1982), (Hsu and Jones 2002) (Salehghaffari, Tajdari and Mokhtarnezhad 2009)). As static loading may be difficult to reproduce in an experiment, quasi-static loading is typically used, which is defined by using such small displacement rates that any inertia effects can be disregarded.

Andrews et al. (1983) performed an experimental investigation of the collapse modes of quasi-static axial loading of aluminum alloy tubes of different geometries. From the axial crushing of 189 tubes, the following collapse modes were obtained (Andrews, England and Ghani 1983):

a) *Concertina (see Fig. 5*):
Axisymmetric and sequential folding starting at one end of the tube.

b) *Diamond (see Fig. 5*):
Non-axisymmetric, but sequential folding accompanying a change in the cross-section shape of the tube.

c) *Euler (see Fig. 5*):
Bending of tube as a strut.

d) *Concertina and 2-lobe and/or 3-lobe diamond:*
Folding first in the concertina mode and then changing to diamond configuration; 2 lobe: square cross-section pattern; 3 lobe: hexagonal cross-section pattern.

e) *Axisymmetric/concertina:*
Simultaneous collapse along the length of the tube, axisymmetric single or multiple barrelling of tube.

f) *2-lobe diamond:*
Simultaneous collapse along length of tube in the form of the 2-lobe diamond configuration.

g) *Tilting of tube axis:*
Shearing of tube on the platen surface in the form of transverse displacement at one end.

Fig. 5. Collapse modes of cylindrical aluminum tubes, from left to right; Euler, concertina, and diamond (Ghani 1982).

The collapse modes were plotted in a classification chart of t/D versus L/D, and clear regions within which a certain collapse mode could be expected was indicated. The authors concluded that absolute size does not affect the collapse mode of a cylindrical tube, and that initial proportions is the main source of influence (Andrews, England and Ghani 1983). The D/t and L/D values on the classification chart stretches from 3.84 to 50, and from 0 to 9, respectively. For D/t values of 16.6 (equal to the tubing in Chapter 6), all tubes having an L/D ratio above 6 failed by Euler collapse. Lower L/D ratios gave, among others, concertina and diamond modes of collapse, but each of them dominates different regions of the classification chart. The load-displacement curve for a mixed concertina and diamond mode tube is shown in Fig. 6, where a gradual increase in the peak loads during each concertina fold is seen, indicating progressive stiffening (Andrews, England and Ghani 1983). It should also be noted that the initial peak often is higher than the following peaks for a small number of lobes. The aluminum tubes used in the experiment had a yield strength of 34.2 MPa defined at 0.1% strain.

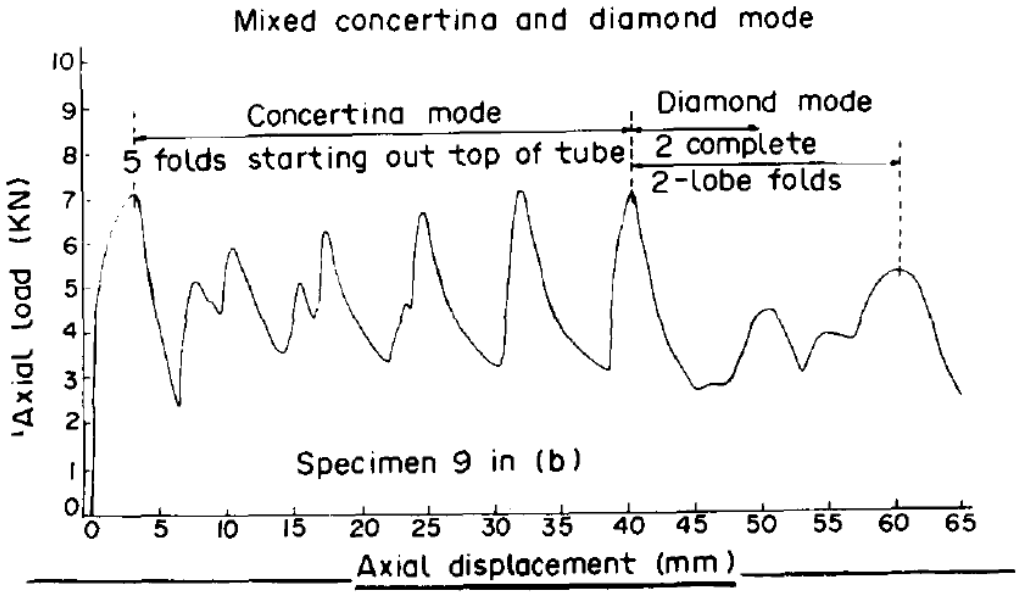

Fig. 6. Axial load-displacement curve for a mixed concertina and diamond collapse mode (Andrews, England and Ghani 1983).

Hsu and Jones (2002) performed quasi-static and dynamic tests on austenitic stainless steel cylinders. The steel had an average reported yield strength of 484 MPa, defined at 0.2% strain and assuming a Young's modulus of 197 GPa, and an ultimate tensile stress of 745 MPa. The quasi-static tests used a displacement rate less than or equal to 2 mm/min, and the dynamic test were performed in two drop hammer rigs, where a flat plate is given an initial velocity before accelerating towards the test specimen in free fall. The steel tubes had D/t ratios of 7.7, 22, and 47, categorizing them as thin-walled, intermediate, and thick-walled cylinders. For the cylinders not failing by Euler collapse, an axisymmetric wrinkle was first formed at either end, before progressive diamond collapse dominated the rest of the compaction. The authors created a best-fit curve for the critical length-to-width aspect ratio resulting in Euler buckling for the quasi-static test:

$$\left(\frac{L}{D}\right)_{cr} = 4e^{0.0138\left(\frac{D}{t}\right)} \tag{20}$$

where L is the length of the specimen, D is the outer diameter, and t is the thickness. From Eq. 20 it can be seen that the longer the length, the more susceptible is a cylinder to Euler buckling due to the

inability of the lateral inertia to stabilize the crushing process (Hsu and Jones 2002). An equation for the best-fit curve for the dynamic test results was also created:

$$\left(\frac{L}{D}\right)_{cr} = 4e^{0.0266\left(\frac{D}{t}\right)} \tag{21}$$

2.5.2. Variations in Cylinder Geometry

Several studies have been conducted to investigate the use of different methods to encourage an axisymmetric collapse mode during crushing of absorbers (Salehghaffari, Tajdari and Mokhtarnezhad 2009). A study done by Salehghaffari et al. (2009) used thick-walled mild steel cylinders with wide external grooves for absorber research, where both quasi-static and dynamic tests were performed. While the structure was subjected to axial compression, plastic folds were shaped within each grooved space, and the thick-walled portions of the tube controlled and stabilized the crushing process (Salehghaffari, Tajdari and Mokhtarnezhad 2009), as seen in Fig. 7. Several tests were conducted with different geometries. The test results seen to the right in Fig. 7 were initially a tube with an initial OD and ID of 60 mm and 52 mm, respectively, at the thick-walled part, and a wall thickness of 1.5 mm at the grooved sections. The width of each groove was 19.2 mm, and the space between each groove was 8 mm. All the test specimens had an initial length of 144 mm, and material testing revealed an elastic modulus of 210 GPa.

To compare the energy absorption between quasi-static and dynamic tests, the drop-hammer starting position was calculated as to generate the same energy as that absorbed during a quasi-static test where all grooves were completely plastically deformed. However, the impact energy from the dynamic test was not sufficient to fully deform all the grooves, which was explained by the material strain rate sensitivity, which increases the energy absorption capacity during high strain rates (Salehghaffari, Tajdari and Mokhtarnezhad 2009).

Fig. 7. To the left, a test specimen with wide external grooves before compaction. To the right, a specimen after compaction, from experiment at the top and from numerical simulation at the bottom (Salehghaffari, Tajdari and Mokhtarnezhad 2009).

During the axisymmetric compaction of the grooves, a single concertina fold was developed in each groove, as can be seen to the right in Fig. 7. Based on this observation, the authors created a simple collapse model of the absorber, shown in Fig. 8. The model shows the formation of three circumferential plastic hinges within each groove, and the metal between “Hinge 2” and “Hinge 3” experiences stretching. The required plastic energy in the formation of one concertina fold is therefore the sum of the energy absorbed by the three assumed-stationary circumferential plastic hinges and the energy absorbed by stretching the material, which can be expressed as (Salehghaffari, Tajdari and Mokhtarnezhad 2009):

$$E_D = \left(\frac{\pi t^2 \sigma_y}{\sqrt{3}}\right)(D\pi + \lambda) + \frac{2k\lambda^{n+2}}{(n+2)\left(\sqrt{3}\right)^{n+1} R^n} \tag{22}$$

where λ is the width of each groove, k is the strength coefficient in the flow stress equation, and n is the strain hardening exponent. The total required energy for plastic deformation of all grooves is Eq. 22 multiplied by the number of grooves in the specimen.

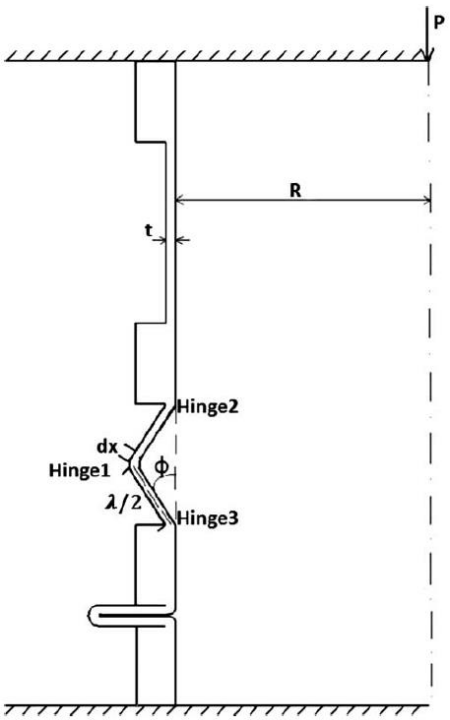

Fig. 8. Collapse model of an externally grooved thick-walled tube (Salehghaffari, Tajdari and Mokhtarnezhad 2009).

In one of the numerical simulation tests, where the only difference between that specimen and that in Fig. 7 was a groove width of 9 mm instead of 19.2 mm, only two plastic hinges formed. This was the result of the groove space being too short for the middle plastic hinge to form, leading to the formation of wrinkles instead of an axisymmetric collapse mode. The result was plastic deformation in the bottom of the cylinder of both a grooved space and the thick-walled section in connection with that grooved space, which completely destroyed the crushing stability of the structure (Salehghaffari, Tajdari and Mokhtarnezhad 2009). Results from other numerical simulations performed in this study indicated that the critical values of groove lengths for the formation of concertina folds vary with the values of groove thickness (Salehghaffari, Tajdari and Mokhtarnezhad 2009).

Chapter 3

Permanent Plug and Abandonment

A development well is usually abandoned when it is no longer profitable. This can be related to the cost of operating the well versus the amount of hydrocarbons that are produced, or be a result of a damaged wellbore or formation that is too expensive to fix. Permanently abandoning a well consists of isolating formation fluids within the wellbore in order to prevent leakage to surface or unwanted leakage between formations (Oil & Gas UK 2012). Cement is often used as plugging material and together with other well barrier elements (WBE) it forms a well barrier. A well barrier is defined as an envelope of WBE that prevents unwanted flow within a wellbore (NORSOK D-010 2013). This chapter presents standards and procedures related to PP&A.

3.1. Guidelines

Different standards exist as guidelines for petroleum activities. Two of these are NORSOK D-010 and Oil & Gas UK – Guidelines for the suspension and abandonment of wells, used in the Norwegian and British sector, respectively. None of these guidelines create any obligations, and only serve as to provide minimum criteria for best practice. The word *shall* is used to express these criteria and requirements. Some of the well integrity references from these guidelines that are relevant for this thesis will be described in this section.

3.1.1. Barriers

For redundancy purposes, NORSOK D-010 (2013) has defined a minimum number of well barriers that shall be present at all times during well activities. Table 2 relates the number of required well barriers to any source of inflow present during any activity.

Table 2. Number of well barriers based on source of inflow. A "normally pressured formation" is defined as a formation where the pore pressure is equal to the regional hydrostatic pressure (NORSOK D-010 2013).

Minimum number of well barriers	Source of inflow
One well barrier	a) Undesirable cross flow between formation zones b) Normally pressured formation with no hydrocarbon and no potential to flow to surface c) Abnormally pressured hydrocarbon formation with no potential to flow to surface (e.g. tar formation without hydrocarbon vapor)
Two well barriers	d) Hydrocarbon bearing formations e) Abnormally pressured formation with potential to flow to surface

NORSOK D-010 (2013) defines permanent abandonment as a well status where the well will not be re-entered, and where the wellbore is sealed with an eternal perspective. Temporary abandonment, on the contrary, shall be performed so that it is possible to re-enter the temporary abandoned well in a safe manner. The two abandonment methods also differ in which WBE that can be used to create well barriers. All permanent well barriers are required to be placed adjacent to an impermeable formation. Table 3 describes the different well barriers that should exist within a well after a PP&A operation has ceased.

Table 3. Different well barriers used in permanent plug and abandonment, their function, and positioning requirements (NORSOK D-010 2013)**.**

Name	Function	Depth position
Primary well barrier	To isolate a source of inflow, formation with normal pressure or over-pressured/ impermeable formation from surface/seabed.	The base of the well barriers shall be positioned at a depth were formation integrity is higher than potential pressure below.
Secondary well barrier	Back-up to the primary well barrier, against a source of inflow.	As above.
Crossflow well barrier	To prevent flow between formations (where crossflow is not acceptable). May also function as primary well barrier for the reservoir below.	As above.
Open hole to surface well barrier	To permanently isolate flow conduits from exposed formation(s) to surface after casing(s) are cut and retrieved and contain environmentally harmful fluids. The exposed formation can be over-pressured with no source of inflow. No hydrocarbons present.	No depth requirement with respect to formation integrity.

NORSOK D-010 (2013) provides the following recommendations for plugging materials used for PP&A:

- Provide long term integrity
- Impermeable

- Non-shrinking
- Able to withstand mechanical loads/impact
- Resistant to chemical/substances
- Ensure bonding to steel
- Not harmful to the steel tubulars integrity

Cement is widely used as plugging material, and fulfills several of the recommended properties listed above. Mechanical plugs, however, do not comply with NORSOK D-010 (2013) if used as WBE in permanent abandonment, and may only be used as a foundation for a plug of a suitable material. The well barrier is required to seal both vertically and horizontally, and cover the whole cross section of the well, as depicted in Fig. 9 (NORSOK D-010 2013).

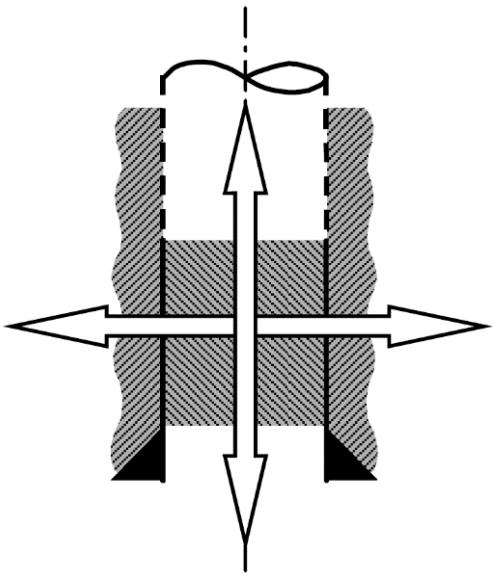

Fig. 9. A well barrier is required to seal both vertically and horizontally and include all annuli (NORSOK D-010 2013).

Many wells have control lines and cables attached to the tubing in order to control downhole equipment and receive electrical signals from the wellbore. NORSOK D-010 (2013) states: "Control lines and cables shall not form part of the permanent well barriers." The same requirement is found in the British guidelines: "Cables and control lines should not form part of permanent barriers, since they may be a potential leak path." (Oil & Gas UK 2012). The control lines are often connected to the production tubing with clamps and are difficult to remove, and the tubing is therefore often pulled before establishing permanent well barriers.

3.1.2. Length Requirements

Both Oil & Gas UK and NORSOK provides recommended lengths of quality cement that are regarded as sufficient for providing an eternal seal downhole. External cement is placed on the outside of the inner casing, while an internal plug is placed inside the inner casing. NORSOK D-010 (2013) requires 100 m of cement in an open or cased hole to qualify as a permanent WBE, while in a cased hole it is sufficient with 50 m of cement if a mechanical or cement plug is used as foundation. For the external plug, a minimum of 50 m is required, while 30 m is sufficient if logging verifies the cement. The

internal plug is required to cover the interval of the verified external plug. In the British sector, a minimum cement length of 100 ft (30.5 m) is recommended in cased hole, open hole, and in the annulus, but at least one permanent plug is required to be placed in cased hole (Oil & Gas UK 2012). As in NORSOK, the internal and external plugs are required to overlap over the length interval. Both standards allow combination barriers, which are two barriers fused into one, and where the length requirements are added ((NORSOK D-010 2013), (Oil & Gas UK 2012)).

As an example, Fig. 10 shows a combination barrier. The lower plug must be at least 100 m as it is not set on a foundation. Since the secondary barrier is placed immediately upon the primary barrier, the primary barrier acts as a foundation for the upper plug, which reduces the required cement length for the secondary barrier to 50 m.

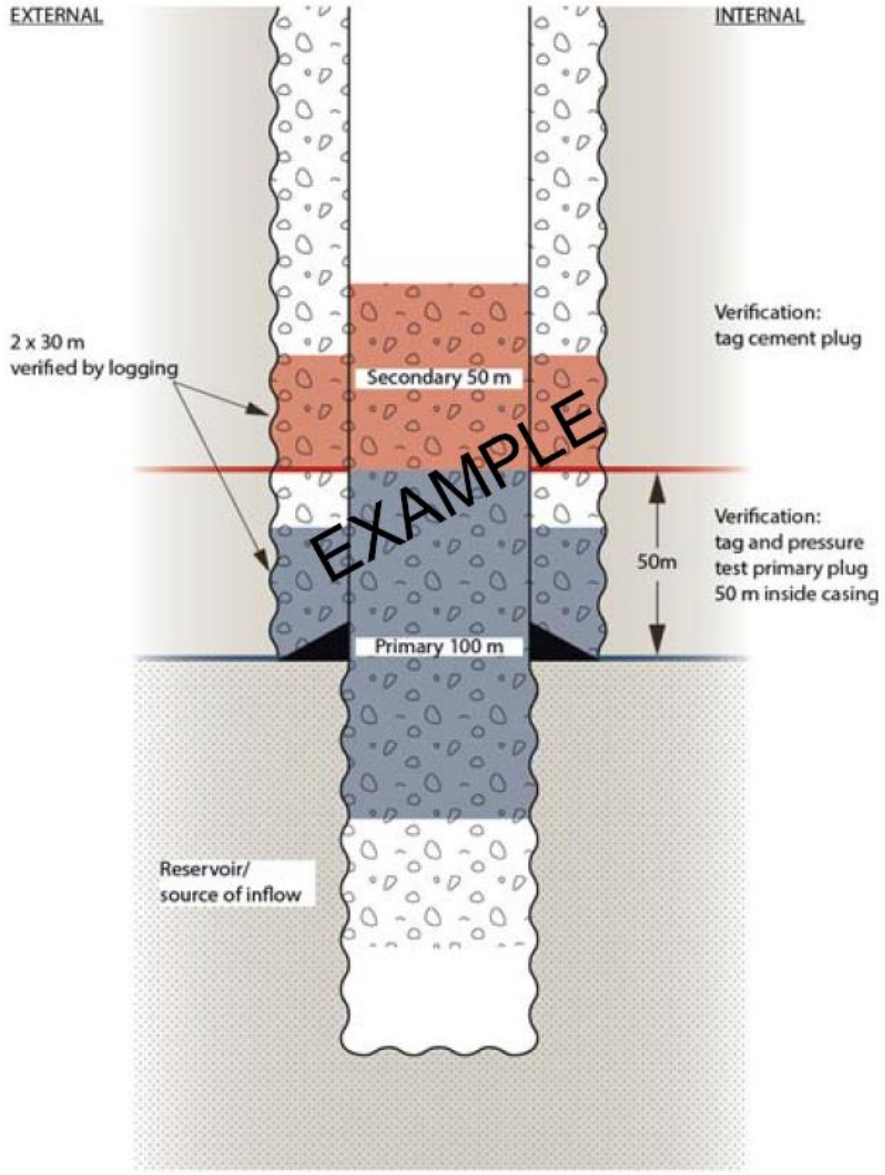

Fig. 10. Example from NORSOK D-010 (2013) that shows a combination barrier.

3.1.3. Verification

The verification of cement as a WBE depends on whether it is an internal or external barrier. In the case of an internal barrier, an open hole cement plug will only need to be tagged, while a cased hole plug will also need to be pressure tested. The pressure test shall (NORSOK D-010 2013):

a) be 70 bar above estimated leak off pressure below casing/potential leak path, or 35 bar for surface casing plugs; and

b) not exceed the casing pressure test and the casing burst rating corrected for casing wear.

If a cased hole plug is set on a pressure tested foundation, the plug does not need to be verified by pressure testing. Neither does an external cement WBE. As mentioned in Section 3.1.2, the length requirement of external cement WBE is dependent on the verification method. The two options that exist are to either use cementing reports and annulus pressure as verification, or to log the cemented interval to verify the sealing capacity of the WBE.

3.2. Vessels Used for Permanent Plug & Abandonment

Platform wells and subsea wells are different with regards to the type of vessels that can be used during abandonment. Platform wells are connected to fixed installations, and P&A of such wells typically involves skidding the derrick to the relevant well (Mehari 2014). On subsea wells, the abandonment operations are usually conducted from semi-submersible rigs, jack-up rigs, drill ships, and RLWI vessels. All of these, with the exception of RLWI vessels, have full drilling capacities, and can perform all PP&A operations. A comparison of rental prices between several of these vessels are presented in Table 4. It should be noted that these numbers are from 2015, and the market have significantly changed since then.

Table 4. Comparison of rental prices from 2015 for different vessels, some of them relative to water depth (WD) (Khalifeh 2016).

Vessel	Rental price [1,000 $/day]
Jack-up (> 100 m WD)	220-300
Semi-submersible (> 1000 m WD)	220-320
Semi-submersible (< 1000 m WD)	200-250
Drill ship	270-320
RLWI vessel	150-250

Riserless Light Well Intervention vessels perform well intervention and P&A operations without the use of a riser, as the name implies. They are of monohull constructions and are routinely used for wireline operations. In 2015, riserless coiled tubing drilling operations were also conducted from an RLWI vessel (Subsea world news 2016). See Fig. 11 for the necessary equipment to perform wireline and coiled tubing operations.

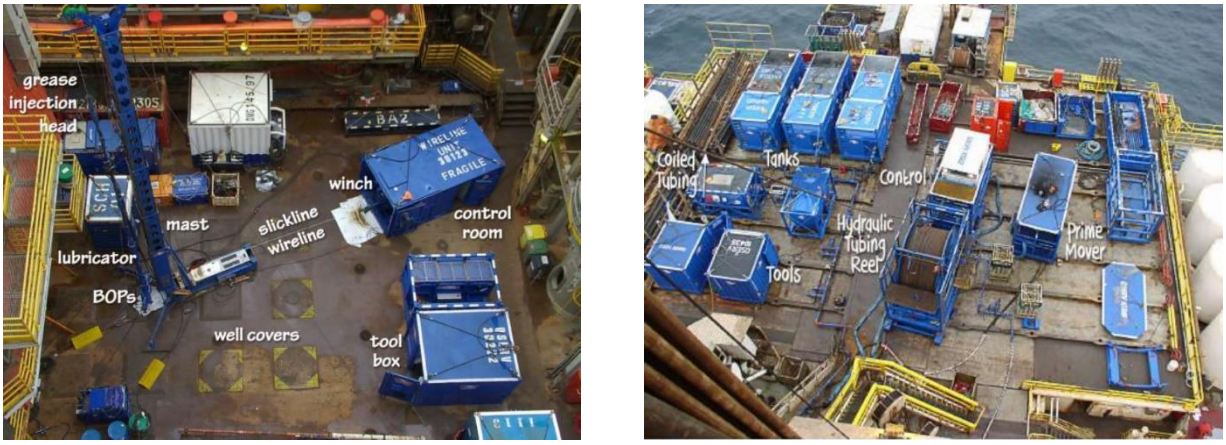

Fig. 11. The left picture shows common wireline components, while to the right a coiled tubing setup is shown (Oilfield Innovations 2016b).

3.3. Procedure

As stated by Oil & Gas UK (2011), the abandonment of any well can be divided into three distinct phases. Each phase reflects the required equipment and the work-scope in that part of the abandonment program. This is done to simplify the cost estimation of PP&A for either a single well or a batch. The phases are (Oil & Gas UK 2011):

- **Phase 1 – Reservoir Abandonment**
  - Primary and secondary permanent barriers set to isolate all reservoir producing or injecting zones. The tubing may be left in place, partly, or fully retrieved. Complete when the reservoir is fully isolated from the wellbore.

- **Phase 2 - Intermediate Abandonment**
  - Includes: isolating liners, milling and retrieving casing, and setting barriers to intermediate hydrocarbon or water-bearing permeable zones and potentially installing near-surface cement. The tubing may be partly retrieved, if not done in Phase 1. Complete when no further plugging is required.

- **Phase 3 - Wellhead and Conductor Removal**
  - Includes; retrieval of wellhead, conductor, shallow cuts of casing string, and cement filling of craters. Complete when no further operations required on the well.

To further ease the cost estimation of PP&A programs, a complexity classification is often used to describe each phase. Oil & Gas UK (2011) provides a numbering system that indicates the complexity of the work, which again sets requirements for the type of vessel or rig that is needed to perform the work in that phase. This can be used as a basis for cost estimation analysis. Oil & Gas UK (2011) presents the following classifications:

TYPE 0: No work required - A phase or phases of abandonment work may already have been completed.

TYPE 1: Simple Rigless Abandonment - Using wireline, pumping, crane, jacks. Subsea wells will use RLWI.

TYPE 2: Complex Rigless Abandonment - Using coiled tubing, hydraulic workover unit, wireline, pumping, crane, jacks. Subsea will use Heavy Duty Well Intervention Vessel with Riser.

TYPE 3: Simple Rig-based Abandonment - Requiring retrieval of tubing and casing.

TYPE 4: Complex Rig-based Abandonment - May have poor access and poor cement requiring retrieval of tubing and casing, milling, and cement repairs.

The abandonment procedure will depend on many factors, such as the governing regulatory body, the well design, operator's internal regulations, and current technology. The abandonment program will therefore vary from case to case. To highlight the main steps, a general procedure requiring a drilling rig will be presented (Birkeland 2011):

- **Get equipment and derrick ready**
  - Skid derrick in place. Necessary equipment must be ready or planned to arrive at the correct time.

- **Kill the well**
  - The well needs to be killed before entering if a drill pipe is to be used (not considering snubbing). This is done by replacing the well fluid with a heavier fluid so that the well pressure exceeds the formation pressure (overbalance). When the well is in overbalance, the Christmas tree (XMT) can be replaced by a blowout preventer (BOP).

- **Pull tubing**
  - The tubing is pulled, sometimes along with the lower completion.

- **Plug reservoir**
  - The reservoir is plugged, and unwanted cross-flow between formations is hindered by additional plugs. See Table 3 for more details.

- **Log, cut and place additional plugs**
  - Logging of cement behind casing(s) is done to asset the isolation capabilities. It can be challenging to log several annuli, and therefore section milling is often performed. Different technologies also exist to place cement behind casing without using section milling, such as "perforate, wash and cement". Required intermediate and surface plugs are placed.

- **Removal of top of surface casing, conductor, and wellhead**
  - NORSOK D-010 (2013) states: "For permanent abandonment wells, the wellhead and casings shall be removed below the seabed at a depth which ensures no stick up in the future. Required cutting depth shall be sufficient to prevent conflict with other marine activities."

Chapter 4

Downhole Tubing Disposal

Oilfield Innovations owns the patented method of Downhole Tubing Disposal (DTD), where a tubing is weakened prior to compaction downhole. One proposed method of performing this is by slicing the tubing longitudinally so that the strength of the cylinder is reduced, before a piston will compact the tubing into the liquid space of the wellbore. The motivation behind the development of the method was the high cost of PP&A operations, combined with old conservative procedures (Oilfield Innovations 2016b).

The objective of Oilfield Innovations is to trade the controlling interest of the method with an interested party, which could be an operator or a service company (Oilfield Innovations 2016b). As the principle behind the method is fairly simple, the final owner of the method may attune the procedure to accommodate the equipment they have at their disposal. In addition, the method may be tailored to a specific operator's needs. For this reason, a deep analysis of the procedure will not be performed in this thesis, and instead a short review of the method proposed by Oilfield Innovations will be presented.

4.1. Equipment

Except for the vertical cutting tool designed by Oilfield Innovations, seen in Fig. 12, only field-proven equipment is used for the procedure. Currently, longitudinal cutting of tubulars downhole is mostly performed in relation with cement operations, where the cuts provide access to the annuli behind the cut casing. The tools are therefore not designed to weaken the casing or tubing. The process of cutting the tubing downhole will not be further evaluated, but a tool called Gator Perforator is presented in Appendix C.

Other necessary tools include a piston packer and a bridge plug. The idea of using an inflatable packer as a piston is not field-proven. Packers use different technology to stay in place, as they usually are intended to, such as slips. By removing this interaction between the packer and the casing, there is nothing that resists the packer from being pushed downwards, except the friction between the rubber element of the packer and the casing wall. Oilfield Innovations have proposed the use of SlikPak™ Plus, and further information regarding this packer can be found in Appendix A. All equipment used for DTD can be run on wireline and coiled tubing.

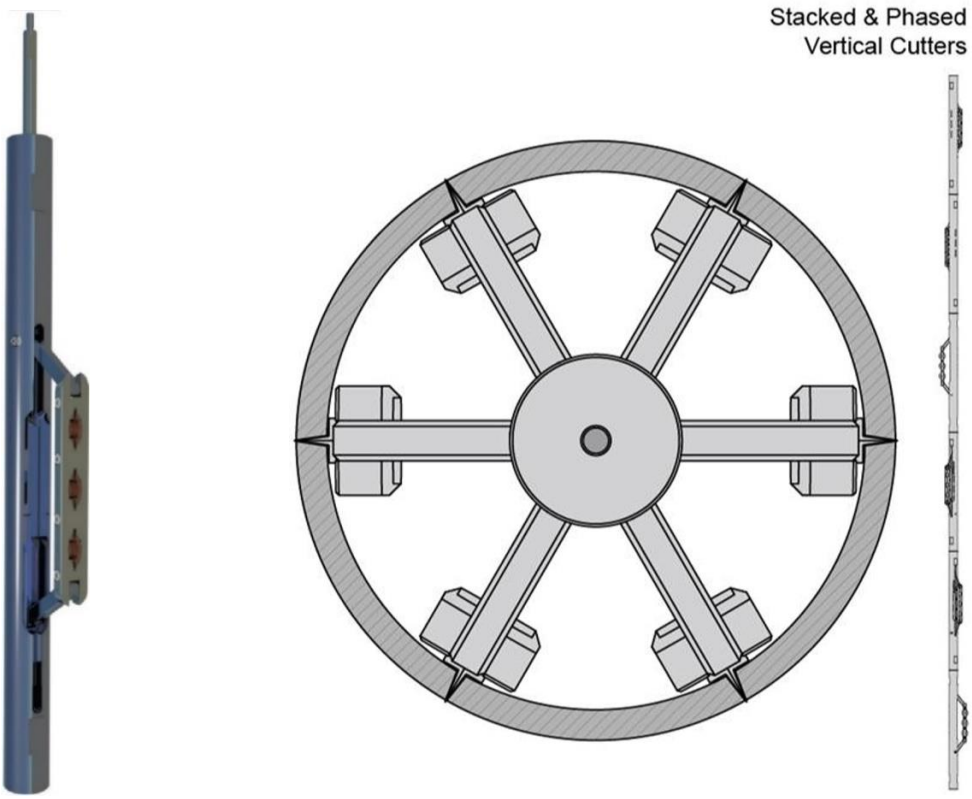

Fig. 12. To the left, the longitudinal cutting tool designed by Oilfield Innovations. To the right, a phased stack of cutting tools is shown which could reduce the cutting time significantly (Oilfield Innovations 2016b).

4.2. Generalized steps

The idea behind tubing compaction is simple, and it can be described as crushing a damaged tubing by applying a piston force. In this thesis, crushing is defined as bending and folding of a tube, contrary to buckling. The patent of DTD incorporates all types of weakening of the tubing, both mechanical and chemical. Further development of the method could therefore result in a completely different procedure than the one presented in this thesis. Oilfield Innovations (2016a) have proposed a general procedure for DTD, which will give an overview of the process as it is currently planned to be conducted. By referring to Fig. 13 and Fig. 14, the procedure can be generalized as follows (Oilfield Innovations 2016a):

1. Fig. 13a:
   Perform wireline gauge run to confirm well status. The drift diameter must allow the tool string with packer (not inflated) to reach the desired depth.

2. Fig. 13b:
   Punch tubing to allow for circulation of cleaning fluids between tubing and casing.

3. Fig. 13c:
   Pump cleaning fluids to clean inside of casing wall, as represented by long arrows, before optionally punching casing through tubing to plan for piston stopping depth (perforations at bottom of figure). Bleed-off perforations need to be placed if a travelling valve arrangement is not to be used, so that the fluid below the piston can be displaced as the piston moves downwards. The stopping depth perforations can be used to bleed off pressure.

4. Fig. 13d:
   Use a wireline cutting tool to vertically split the tubing. The cutting tool may be raised and lowered while springs force it against the tubing wall to penetrate the steel. The number of cuts, their placement, and their length is predetermined, and may vary from case to case. The tubing may also be cut in sections, leaving uncut tubing in between.

5. Fig. 13e:
   Optional: When only part of the to-be-compacted tubing is split, the tubing can be severed just above the vertical split (solid part of right tubing wall). This may allow the upper part of the severed tubing to be pushed alongside the lower part. In this case, the length of the to-be-compacted undamaged tubing should not exceed the length of the split part, since the undamaged tubing may not be crushed. Using this option will not affect the rest of the procedure.

6. Fig. 13e:
   Place a bridge plug (block with diagonal stripes) inside the uncut part of the tubing. It is important to include the length of the following piston packer when calculating the placement of the bridge plug. This is because the piston packer will not be crushed, and will stick out from the tubing once compaction is finished.

7. Fig. 13f:
   Sever the tubing right above the bridge plug. When referring to "the severed part of the tubing" further in this thesis, reference is made to this cut, and not the optionally horizontal cut mentioned in step 5.

8. Fig. 14g:
   Use wireline to determine the location of the tubing after it has been severed.

9. Two cases exist; where the piston packer is inside the casing and where it is inside the tubing (totally or partially).

   a. Fig. 14h:
      Inside the casing: Inflate the piston packer to an appropriate pressure.

   b. Fig. 14i:
      Inside the tubing: Either the tubing can be lifted, or the piston packer can be pushed out of the tubing by applying sufficient pressure behind the packer (as indicated by arrow). When the casing fully confines the piston packer, increase the piston pressure appropriately, as the radial clearance is now increased.

10. Fig. 14j:
    To initiate tubing compaction, increase pressure behind piston by pumping fluid down the tubing. No returns should be taken. The piston pressure is determined by the hydrostatic pressure from the fluid(s) above the packer and the back-pressure from the pump. To reduce leakage around the piston, a specially designed viscous fluid may be placed right above the piston. As the piston packer moves downwards, fluid below the packer is displaced and pushed through bleed-off perforations in the casing and then into the formation.

11. Keep increasing the pressure until:

    a. Maximum allowable pressure is reached, and wait to see if further compaction takes place. If that is the case, repeat this step. Maximum allowable pressure can be determined by pump capacity or burst rating of casing.

    b. Fig. 14k:
    The pressure bleeds off at the (optional) casing perforations used to facilitate piston stopping depth.

12. Fig. 14l:
    After tubing compaction has ceased, run wireline to tag the piston packer. The packer will be used as a foundation for a cement plug.

13. If the unobstructed length of casing is sufficient, phase 1 of the PP&A program can be completed by optionally logging the cement bond behind the casing and fixing any related problems, before placing primary and secondary reservoir barriers. By using the piston packer as a foundation, the required cement length is 50 m for the primary barrier (see Section 3.1.2). If the unobstructed casing length is not sufficient, the procedure can be repeated further up in the hole, taking into account the requirement for an impermeable formation adjacent to the well barrier, as mentioned in Section 3.1.1.

14. Tag top of cement using wireline, and optionally perform other tests to confirm well barrier integrity.

Whether the proposed method is executable will not be further discussed, but the thesis will be based on mechanical weakening in the form of cutting.

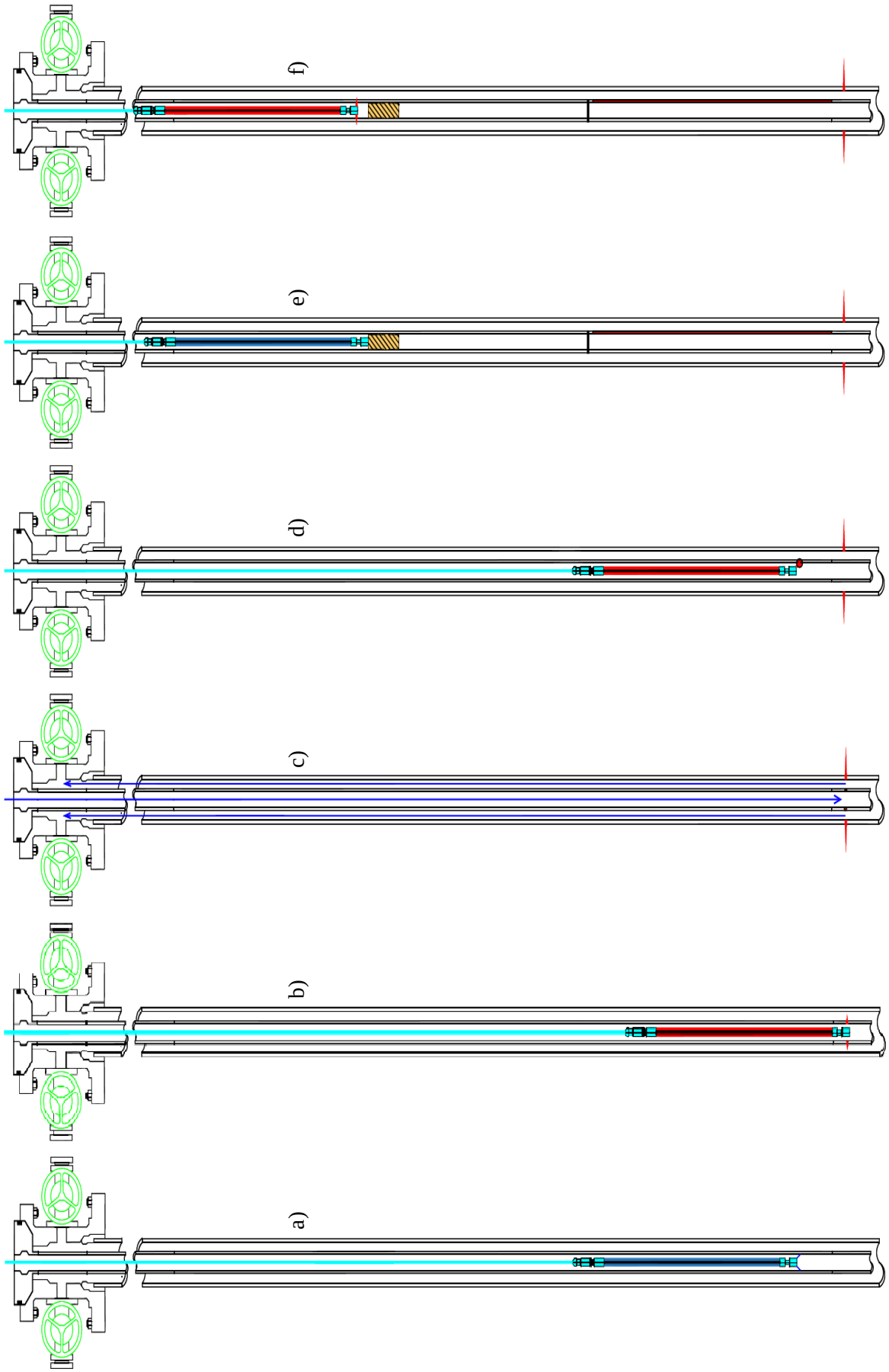

Fig. 13. a) through f) illustrate a generalized procedure of Downhole Tubing Disposal (Oilfield Innovations 2016a).

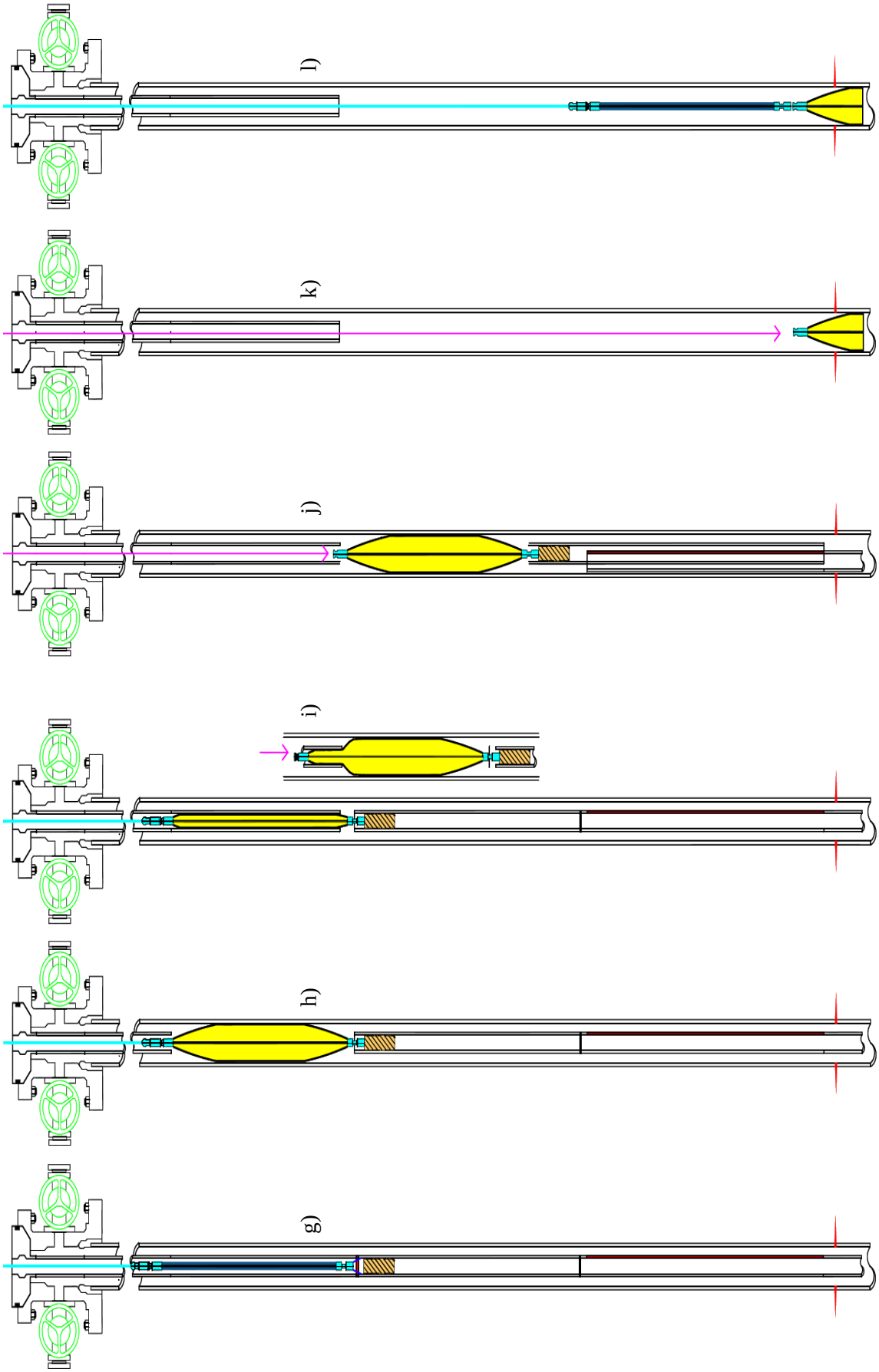

Fig. 14. g) through l) illustrate a generalized procedure of Downhole Tubing Disposal (Oilfield Innovations 2016).

Chapter 5

First Full-Scale Experiment

A full-scale experiment of tubing compaction was performed in Peach Valley, Delta Colorado, US, in July 2013 (Oilfield Innovations 2013). The objectives of the experiment were to test if a tubing can be compacted within a casing after being weakened, measure the necessary force to do so, and to determine the effect of different cutting patterns. Since the experiment did not have any external funding, costs had to be reduced to an absolute minimum, which resulted in cheap equipment. This chapter is based upon the report from the first full-scale experiment.

5.1. Equipment and Setup

The equipment used in the experiment was as follows:

- Different positive displacement pumps
- Hoses to connect from water source to pump, and from pump to casing
- 5 ½" (139.70 mm) OD, 4.778" (121.36 mm) ID, 20 pounds per foot (ppf) (29.8 kg/m) L80 casing
- 2 3/8" (60.33 mm) OD, 1.995" (50.67 mm) ID, 4.7 ppf (7.0 kg/m) J55 tubing
- Two casing end caps, where one of them enabled connection between casing and the hose from the pump
- Cement wiper plugs fitted for 5 ½" casing
- 4,5" steel cylinder with plates welded on both sides to protect wiper plugs
- Manometer placed between pump and casing end cap

Three different pumps were used during the experiment, and all of them suffered from small displacement volumes at high pressures. This resulted in a slow pressure build-up during all tests. The maximum pressure during the experiment was 400 bar, which was delivered by a pneumatic pump. Fig. 15 shows the setup during the experiment, where two casings are laid out horizontally next to each other. Only one casing was used at a time. One casing end cap was connected to the "dry" side of the casing, which is the opposite side of where water was pumped in. This side of the casing was exposed to atmospheric pressure during the test. Another casing end cap was connected to the "wet" side of the casing, and was further connected to a manometer and the pump.

Fig. 15. The setup for the first full-scale compaction experiment (Oilfield Innovations 2013).

5.2. Procedure and Results

The experiment consisted of compressing 2 3/8" tubing into a horizontally laid "dry" (not filled with water in advance) 5 ½" casing. The tubing was cut in different ways, varying both in direction and number. The force used to compact the tubing came from a positive displacement pump and was transferred to the cement wiper plugs, and further onto a steel push plate. The steel push plate then pushed and compacted the tubing against the casing end cap at the "dry" end.

A total of six model runs were performed, but failure of the equipment during some of the test runs resulted in satisfactory results for only the last three. Each model run will be presented, along with the associated result.

Model run [1]
The first test was done without weakening the tubing on beforehand. The objective of this test was to investigate the frictional forces associated with the tubing, both normal friction and helical buckling friction. A total length of 106.00 m of tubing was placed inside the casing, and the pressure was raised to 165.5 bar before the cement wiper plug failed. A second cement wiper plug was used at a pressure of 193.1 bar before the test was ended and the tubing was pumped out. The frictional forces was not presented in the report.

Fig. 16. The tubing was helically buckled and plastically deformed (Oilfield Innovations 2013).

Model run [2]
Two tubing joints with a length of 19.35 m were placed inside the casing, connected to a 1 m centralizing stub, resulting in a total tubing length of 20.35 m. Three longitudinal cuts were made in

the tubing before placing it in the casing and applying a 275.8 bar piston pressure. The centralizing stub twisted and caused the piston to fail, which ended the model run. The test conductors believed that the twisted centralizing stub prevented axial force transference to the tubing. The final length of tubing was 17.19 m, which equals a compaction ratio of 15.5%. The compaction ratio is defined as the difference between the initial and final length divided by the initial length.

The crushed tubing showed two different types of compaction; side-by-side compaction and longitudinal compaction, as shown in Fig. 17. The longitudinal compaction pattern (named after its association with longitudinal cuts) was common to longitudinally cut tubing for each of the other model runs.

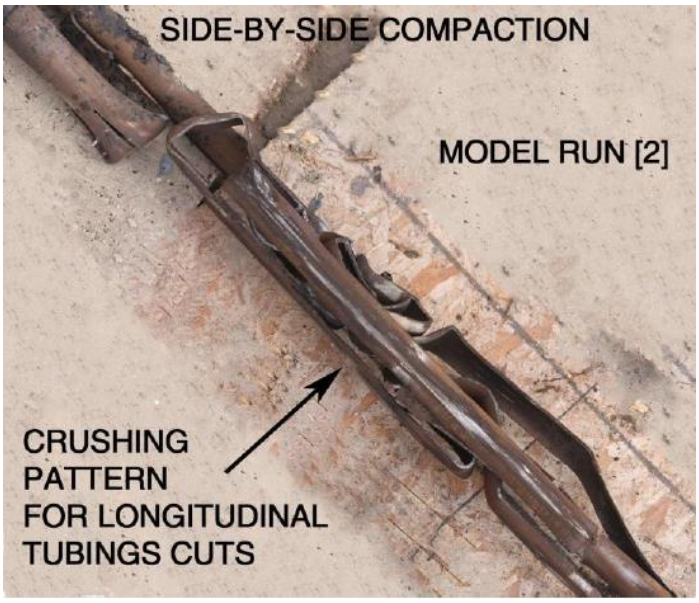

Fig. 17. Compacted tubing from model run [2], showing side-by-side (at the very top) and common longitudinal compaction patterns (Oilfield Innovations 2013).

Model run [3]

To remedy the twisting of the welded steel plate in model run [2], a wooden piston with steel plates attached was placed between a single tubing joint and the cement wiper plug. The length of the tubing joint was 9.69 m and six longitudinal cuts were placed along its length. Leakage around the piston at a pressure of 124.1 bar ended the test, where the wooden piston had failed due to point loading of the tubing. At this point, the crushing process resulted in a compaction ratio of 11.8%, wherein the tubing had been compressed to 8.57 m. As seen in Fig. 18, the longitudinal crushing pattern dominated the deformation.

Fig. 18. The failed wooden piston and the crushed tubing used in model run [3] (Oilfield Innovations 2013).

Model run [4]

An improved piston was constructed, made from 4.5" OD pipe, with a length of 50.8 cm. A tubing consisting of three joints, measuring 28.86 m, was then divided into three parts of nearly identical length. The bottom part measured 9.58 m and was weakened with six longitudinal cuts, while the part above measured 9.65 m and was weakened with three cuts. The top part was uncut and measured 9.63 m. The pressure slowly built up to a maximum of 399.9 bar. The tubing was crushed to an axial length of 15.62 m, giving a compaction ratio of 45.9%.

In order to measure the compacted length, the end-cap of the casing was removed and the crushed tubing, along with piston and plugs, was ejected. As also seen in model run [2], both side-by-side and longitudinal compaction patterns were observed, as shown in Fig. 19. The side-by-side compaction was associated with the uncut part of the tubing, while the longitudinal compaction was associated with the longitudinal cuts. The shape of the tubing in Fig. 19 clearly shows that the tubing has elastically expanded after being ejected from the casing. This elastic strain could mean that the compaction was greater than measured.

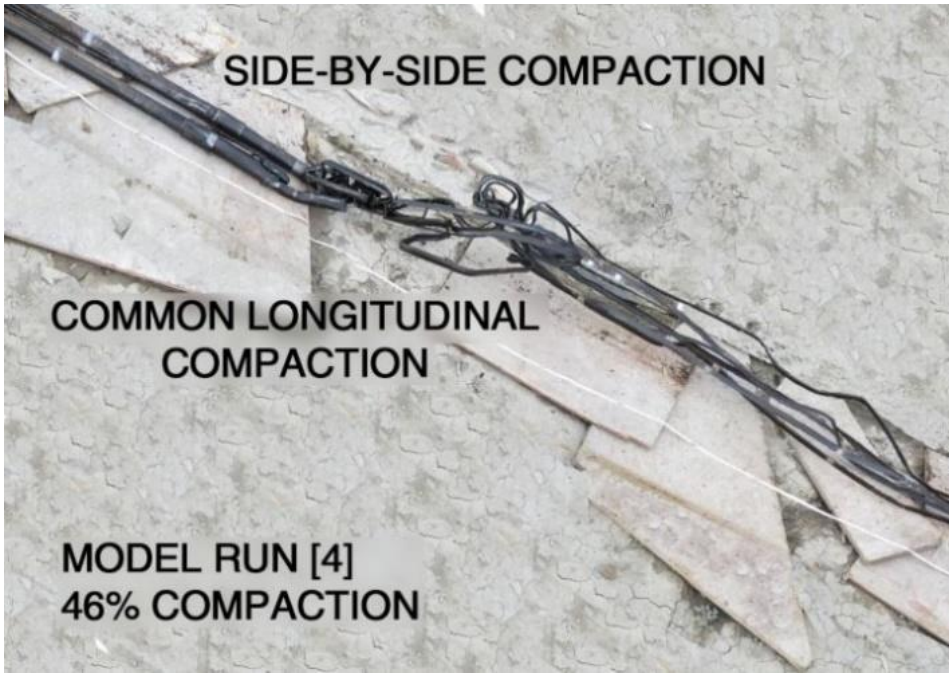

Fig. 19. The crushed tubing from model run [4] after ejection from the casing (Oilfield Innovations 2013).

Model run [5]
To reduce the uncertainty of the measured compaction, the crushed length was measured before ejecting the tubing by cutting a window in the casing. The original length was 9.63 m, and three longitudinal cuts were made along the whole joint. The pressure reached a maximum value of 289.6 bar before the test was stopped due to a failure in the cement wiper plug seal. With a compacted axial tubing length of 5.23 m, the compaction ratio was calculated as 45.6% before ejecting the crushed tubing.

The test conductors noted that there was a visible difference in the amount of crushing when comparing the bottom of the tubing to the part closest to the piston, while referring to the picture in Fig. 20. In the words of the report, "(…) the horizontal orientation of the casing caused significant crushing to occur close to the piston with less compaction at the lower end."

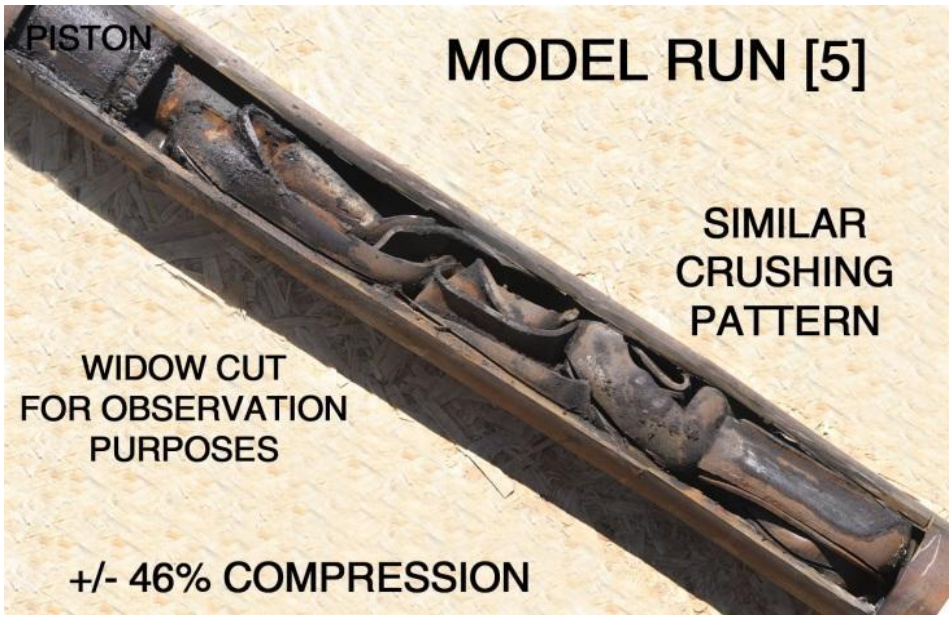

Fig. 20. The crushed tubing from model run [5] is seen through a window cut in the casing (Oilfield Innovations 2013).

Model run [6]
The last model run aimed to utilize the experience gained from the previous tests. Based upon the side-by-side and longitudinal compaction patterns seen in Fig. 19, the 9.63 m joint of tubing was weakened with six longitudinal cuts and transversely split into three approximate equal lengths. By using a pressure of 206.8 bar, notably lower than the two previous tests, the tubing compaction was measured as 45.6%. The ejected crushed tubing can be seen in Fig. 21.

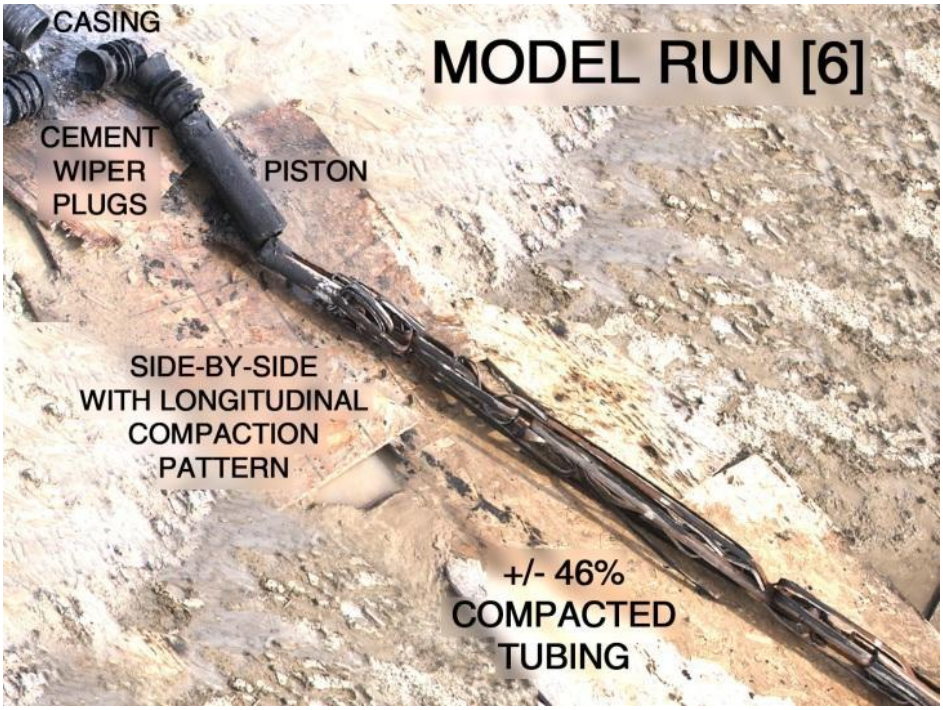

Fig. 21. The crushed tubing from model run [6] after ejection from the casing (Oilfield Innovations 2013).

The results from the experiment are presented in Table 5. The cutting geometry is not included. Note the apparently independent relationship between compaction and maximum piston force.

Table 5. The results from model runs [2] through [6] are presented. Tubular sizes were the same for all tests.

Model run	Original length [m]	Resulting axial length [m]	Compaction [%]	Maximum piston pressure [bar]	Equivalent piston force [kN]
[1]	106.00	Not applicable		193.1	223.3
[2]	20.35	17.19	15.5	275.8	319.0
[3]	9.69	8.57	11.8	124.1	143.6
[4]	28.86	15.62	45.9	399.9	462.6
[5]	9.63	5.23	45.6	289.6	335.0
[6]	9.63	5.24	45.6	206.8	239.3

5.3. Discussion

The experiment was conducted to test the theory of tubing compaction with a weakened tubing. The results show that splitting the tubing vertically reduced the strength of the tubular. It should be noted that the pressures presented in the report were obtained from an analog manometer, and should only be considered as approximate values. One could argue that the compaction ratios obtained from this experiment should represent the lowest possible compaction ratios of a real case with the same tubulars. Some of the arguments behind this statement are:

- *Horizontal layout:*
  A horizontal layout gives maximum friction with regards to the weight of the pipe, as seen from Eq. 13 by setting $\theta = 90°$. In addition, as force transferred from the piston is lost to

friction along the tubing, the maximum compression force is found near the piston. This will lead to the earliest tubing deformation near the piston (assuming homogenous strength of the tubular), which means that the piston must overcome an additional friction created by pushing the crushed tubing through the casing. This additional friction is the result of the elastic behavior of the tubing, since the tubing will behave somewhat like a compressed spring pushing against the casing wall. This can be seen in Fig. 19, where the tubing has expanded after being ejected from the casing.

Furthermore, like with constrained buckling in deviated or horizontal wellbores, additional force is required to lift the tubing laterally from the constraining casing during crushing. In a vertical setup, gravitation would increase the compressive force in the bottom of the tubing, and no force would resist lateral movement of the tubing.

- *Dry test:*
  The experiment was run "dry", meaning that liquid did not surround the tubing. In a real case, the casing will be cleaned before compaction, and the tubing will be enclosed by a liquid with lubricative properties. This will reduce friction, both for the packer and the tubing.

- *Quality and grade of equipment:*
  The type of pump used in the experiment is commonly found at hardware stores and provide substantially lower displacement rates compared to pumps used in the oilfield. As the pressure increased, the flowrate decreased, resulting in a slow increase in force. When the wiper plugs moved due to crushing, the piston pressure dropped, and the slowly increasing pressure prevented continuous compaction. An oilfield grade pump would provide a higher and more constant compressive force, which would in turn lead to a more continuous tubing compaction. As the static friction is higher that the kinetic friction (see Section 2.1), continuous compaction could lead to increased tubing displacement. The same could be said about the pressure limitation of the pump, as a higher pressure could result in increased compaction.

This experiment was mainly conducted to verify if tubing can be compacted within casing. Therefore, determination of the influence of important parameters was not the main concern. Apart from the deviation angle of the casing, two other important compaction parameters are:

- *Size of tubulars:*
  All the tests were performed using the same casing and tubing size. Therefore, there is no way of knowing the impact of tubular dimensions on compaction.

- *Number and direction of cuts:*
  The tubing was cut to weaken the cylinder and allow for easier compaction. Model run [4] consisted of an uncut part and two longitudinal cut parts, [5] consisted only of longitudinal cuts, and [6] also included transverse cuts. As the results from the tests were approximately the same, there is little way of knowing the impact of the cuts, even though different pressures were applied. This is because there is no indication of what pressure that initiated the compaction, or at what pressure the compaction stopped.

A second full-scale compaction experiment was planned which aimed to give more information regarding the influence of different parameters on the compaction of tubing, with special emphasis on the two mentioned above. This test will be described in the next chapter, and a more in-depth analysis of the different compaction parameters will be given in Section 6.6.

Chapter 6

Full-Scale Experiment in Norway

6.1. Introduction

The first full-scale tests reported in Chapter 5 confirmed that a relatively small tubing could indeed be compacted within a casing. Still, the question remains whether common tubing and casing sizes found on the NCS can also give promising compaction results. A second full-scale experiment has therefore been planned, which also aimed to give more data and test the influence of different compaction parameters. The launch date for the experiment is currently not set, and a final procedure have not been established. Thus, this chapter is largely based on the preliminary preparation report by Oilfield Innovations (2017). Conoco Phillips have donated an inventory of tubulars that will be used for the experiment, and may also provide funding for the experiment.

In the preliminary report, two casing sizes are planned for the experiment. These are 9 5/8" and 7 5/8" casings. However, manual measurements of the donated tubulars revealed that no 7 5/8" casings were present, and instead 7", 38 ppf casing joints had been donated. It is not certain which casing sizes that will be used in the experiment, and this thesis will be built upon the assumption that the 7" casing joints will be replaced by 7 5/8" casing joints prior to the experiment.

6.2. Test Site

The full-scale compaction experiment sets forward several requirements for the test site. The most important one of these is related to the topography. The site should provide straight, uninterrupted, flat ground (or be able to be leveled) of at least 200 m. This length will cover 112-122 m laid out casing (see Section 6.3.3 for casing length details), ±50 m of crushed tubing that will be ejected at one end, room for a 9 m tubing joint that will be pushed inside the casing at the other end (see Section 6.4.2 for tubing installation details), and the remaining length will accommodate for maneuvering vehicles and a safe margin. If the crushed tubing is too long to be pushed out and moved in one piece, it will have to be divided into manageable sections prior to handling. In addition to the length requirement, there should also be sufficient unobstructed space around the casing ends so that vehicles and personnel may work (use plasma cutter, maneuver forklift etc.). The test site should be either accessible by large vehicles such as semi-trailer trucks, or provide the possibility for offloading

tubulars and equipment from a dock. The former is believed to be the best, both in terms of transportation cost and complexity.

Other elements exist that are not required by the test site, but still provide significant benefits. The experiment will require large amounts of water, either fresh or saline. By having a local source of water, either through regional water grid or by proximity to a naturally source, such as the sea, it will not be necessary to transport the water to the test site. Since transportation can be costly and time consuming, the test site should be near where the tubulars are donated from, and preferably also where the necessary equipment can be obtained. There should also be some kind of shelter nearby to provide comfort in case of bad weather, and also a toilet, but both of these can easily be installed.

A yard situated on an island called Rennesøy, 30 minutes north of Stavanger, was selected as test site for the experiment. The area is used to store oilfield tubulars and is also a production site for gravel, which means that there are already large vehicles entering the site on a regular basis. As seen in Fig. 22, the yard provides easy access to water, and there are several buildings there which among others contain a metal work shop and a toilet. The area where the assembled casing will be placed is sufficiently leveled, and obstructing objects will be moved prior to the experiment so that all space requirements will be fulfilled. A lot of equipment is already in place, including two large water tanks, marked in Fig. 22 with the number "1", forklifts, cranes, high-pressure pumps, plasma cutting equipment, a winch, and chain tongs. There is also a large amount of scrap metal that can be used to construct tools that would otherwise have to be rented, and welding equipment necessary to create casing end caps (see Appendix B) is accessible.

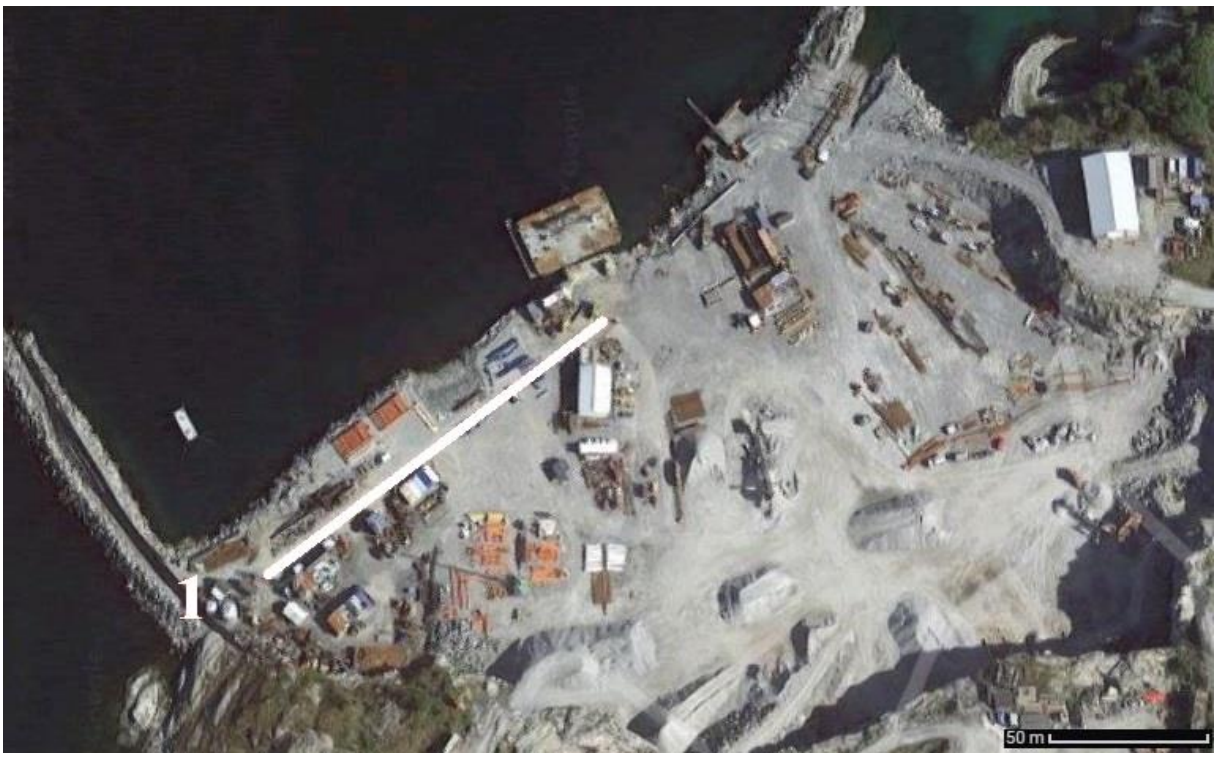

Fig. 22. A satellite image of the test site. The edited straight line represents where the casing will be laid out. The number "1" shows where two large water tanks are located (from Google Earth).

6.3. Equipment

First, some of the most important installation tools mentioned in the preliminary procedure report by Oilfield Innovations (2017) will be presented. These are all suggestions and may be adapted according to budget, timeframe, and planned setup. The equipment that constitutes the experimental layout is presented in greater detail, as some of this equipment is mandatory for the test.

6.3.1. Tools

Forklift
A forklift can be used to lift the pipes and inject the tubing into the casing. The maximum anticipated weight during installation is the weight of a 9 5/8", 47 ppf casing joint, where a joint of 12,2 m weighs 853 kg.

Rollers and wooden blocks
When connecting two tubulars, one joint will be rotated while the other is stationary. To prevent damage to the tubulars and reduce friction, the rotated joints are placed upon rollers, such as the ones in Fig. 23. After the joints have been sufficiently tightened, the rollers will be replaced by wooden blocks, to reduce the required number of rollers.

Fig. 23. Rollers made at the test site.

Chain tongs
Chain tongs, as depicted in Fig. 24, are used to tighten threaded connections. Two tongs are normally used as opposing pairs to prevent the tubulars from rotating in the same direction. Before make-up, pipe dope is added to the tool joints to protect against metal-to-metal wear damage and reduce friction, as well as to provide sufficient sealing.

Fig. 24. A handheld chain tong used for tightening threaded connections, such as connecting casing joints[2].

Plasma cutter

By sending a superheated electrically ionized gas, called plasma, through the work material, plasma cutters can penetrate several inches of electrically conductive materials. An example of a plasma cutter in action is shown in Fig. 25. The depth of penetration should be equal to or greater than 7 mm of steel, which is the wall thickness of the 4 ½" tubing.

Fig. 25. Handheld plasma cutter cutting through steel[3].

6.3.2. Setup Equipment

All the equipment that is part of the experimental setup is listed in Table 6, which is slightly modified from the one presented in the preliminary report. Elements are identified with specific piping and instrumentation diagram (P&ID) numbers, which can also be found in Fig. 26. The P&IDs of the pipework state an OD of 2" (50.8 mm), but the only requirement for the pipework is that it is able to withhold the anticipated test pressure of the specific pipework. It should be noted that Fig. 26 represents the setup of the experiment prior to tubing compaction inside the 9 5/8" casing. When performing compaction inside the 7 5/8" casing, the tubing will be placed inside this casing, and the 9 5/8" casing will have no tubing inside. Also, some of the pipework will be switched when changing the constraining casing, represented in Fig. 26 by "ABILITY TO SWITCH" in the top right corner.

[2] Image from http://www.gearench.com/products/machine-tongs.asp?sub=chain-wrenches&sname=CHAIN%20WRENCHES

[3] Image from http://www.plazmasolutions.net/plasma-hand-cutting-machine.html#plasma-hand-cutting-machine

Table 6. List of equipment used for the setup and compaction process. P&ID numbers refer to Fig. 26 (Oilfield Innovations 2017).

#	P&ID Number	Description
1.	9.625”-FF-A1-01	One API 9 5/8” (244.5 mm) OD casing pin end cap reducer (see Appendix B) to the diameter of valve (VV-02) and pipework (2”-FF-A3-02 and 2”-FF-B2-02) of sufficient grade and wall thickness to withstand a pressure greater than or equal to 345 bar.
2.	9.625”-FF-A1-02	At least 112 m and preferably 122 m of coupled API 9 5/8” OD casing joints (see Section 6.3.3) of sufficient grade and wall thickness to withstand a pressure greater than or equal to 345 bar. Preferably premium couplings with flush ID to minimize piston packer damage.
3.	9.625”-FF-A1-03	One API 9 5/8” OD casing box end cap reducer (see Appendix B) to the diameter of valve (VV-03) and pipework (2”-FF-A3-03) of sufficient grade and wall thickness to withstand a pressure greater than or equal to 345 bar.
4.	7.625”-FF-A2-01	One API 7 5/8” (193.7 mm) OD casing pin end cap reducer (see Appendix B) to the diameter of valve (VV-04) and pipework (2”-FF-A3-02 and 2”-FF-B2-02) of sufficient grade and wall thickness to withstand a pressure greater than or equal to 345 bar.
5.	7.626”-FF-A2-02	At least 112 m and preferably 122 m of coupled API 7 5/8” OD casing joints (see Section 6.3.3) of sufficient grade and wall thickness to withstand a pressure greater than or equal to 345 bar. Preferably premium couplings with flush ID to minimize piston packer damage.
6.	7.625”-FF-A2-03	One API 7 5/8” OD casing box end cap reducer (see Appendix B) to the diameter of valve (VV-03) and pipework (2”-FF-A3-03) of sufficient grade and wall thickness to withstand a pressure greater than or equal to 345 bar.
7.	4.5”-TC-C1-01	At least 50 m of coupled API 4 ½” (114.3 mm) OD tubing of any condition (e.g. used), any grade, and any wall thickness. Short plasma cuts are planned. A total of 400 m of 4 ½” coupled tubing is required for three test runs.
8.	4.5”-TC-C1-02	At least 50 m of coupled API 4 ½” OD tubing of any condition (e.g. used), any grade, and any wall thickness. Long plasma cuts are planned. A total of 400 m of 4 ½” coupled tubing is required for three test runs.
9.	4.5”-TC-C2-01	Same as #7 above, where the only difference in labelling is due to the difference in constraining casing string.
10.	4.5”-TC-C2-02	Same as #8 above, where the only difference in labelling is due to the difference in constraining casing string.
11.	VV-02 and VV-04	Two valves capable of withstanding a pressure of at least 345 bar.
12.	PP-01, CV-01, CV-02, FR-01, PI-01, PSV-01 and associated pipework 2”-FF-A3-01	One positive displacement piston pump (PP-01), and associated pipework (2”-FF-A3-01), capable of 100 L/min at a pressure of at least 345 bar, with associated pump valves (CV-01 and CV-02). The pump must be equipped with a flow rate stroke counter (FR-01), pressure gauge (PI-01), and pressure safety valve (PSV-01) or pressure relief valve to prevent over-pressuring the pipework.

13.	WT-01, LG-01 and VV-01	One valve (VV-01) usable to contain water within an open water tank (WT-01) equipped with a level indicator (LG-01).
14.	2”-FF-A3-02	A series of pipework capable of withstanding at least 345 bar, used to connect the pressure safety valve (PSV-01) to the casing end cap (9.625”-FF-A1-01 and 7.625”-FF-A2-01) valves (VV-02 and VV-04). It should be possible to connect the pipework to both valves, so that the experiment may be run with both casing strings.
15.	2”-FF-A3-02 and VV-03	A series of pipework (2”-FF-A3-02) and a valve (VV-03) capable of withstanding at least 345 bar, used to connect casing pin endcap (9.625”-FF-A1-03) to the corresponding casing pin end cap (7.625”-FF-A1-03). The high-pressure piping is used between the two casing strings to allow pressure testing of both casing strings at the same time.
16.	2”-FF-B2-01	A series of hoses and/or pipework compatible with the low-pressure side of the piston pump (PP-01) capable of withstanding at least 7 bar to connect the water tank (WT-01) to the pump (PP-01).
17.	2”-FF-B2-02	A series of hoses and/or pipework capable of transporting water between casing box end caps (9.625”-FF-A1-01 and 7.625”-FF-A2-01) and valves (VV-02 and VV-04) to the open water tank without significant leakages.
18.	DR-01	A data recorder capable of digitally recording flow rate (FR-01), pressure (PI-01), and tank level (LG-01) at least every second.
19.	PISTON-1	A constructed piston with seals, a cement wiper plug, or an inflatable packer sized for 9 5/8” API casing. See Section 6.3.4.
20.	PISTON-2	A constructed piston with seals, a cement wiper plug, or an inflatable packer sized for 7 5/8” API casing. See Section 6.3.4.

Long and short plasma cuts in the tubing are mentioned in Table 6. This refers to the cut tubing in Fig. 26, which is illustrated with both short slots and long spacing and long slots and short spacing. Since Table 6 and Fig. 26 are based on a preliminary plan for the experiment, the cutting patterns are only proposals. The illustrated cutting patterns will therefore not be assumed to be the final cutting patterns for any of the test runs in this experiment. Table 6 also specifies the total length of coupled 4.5” tubing. This length is based upon one rig-up debug test run and three normal test runs. The final number of test runs, and therefore required length of coupled tubing, will depend on the cost of the experiment and the budget, and can therefore change.

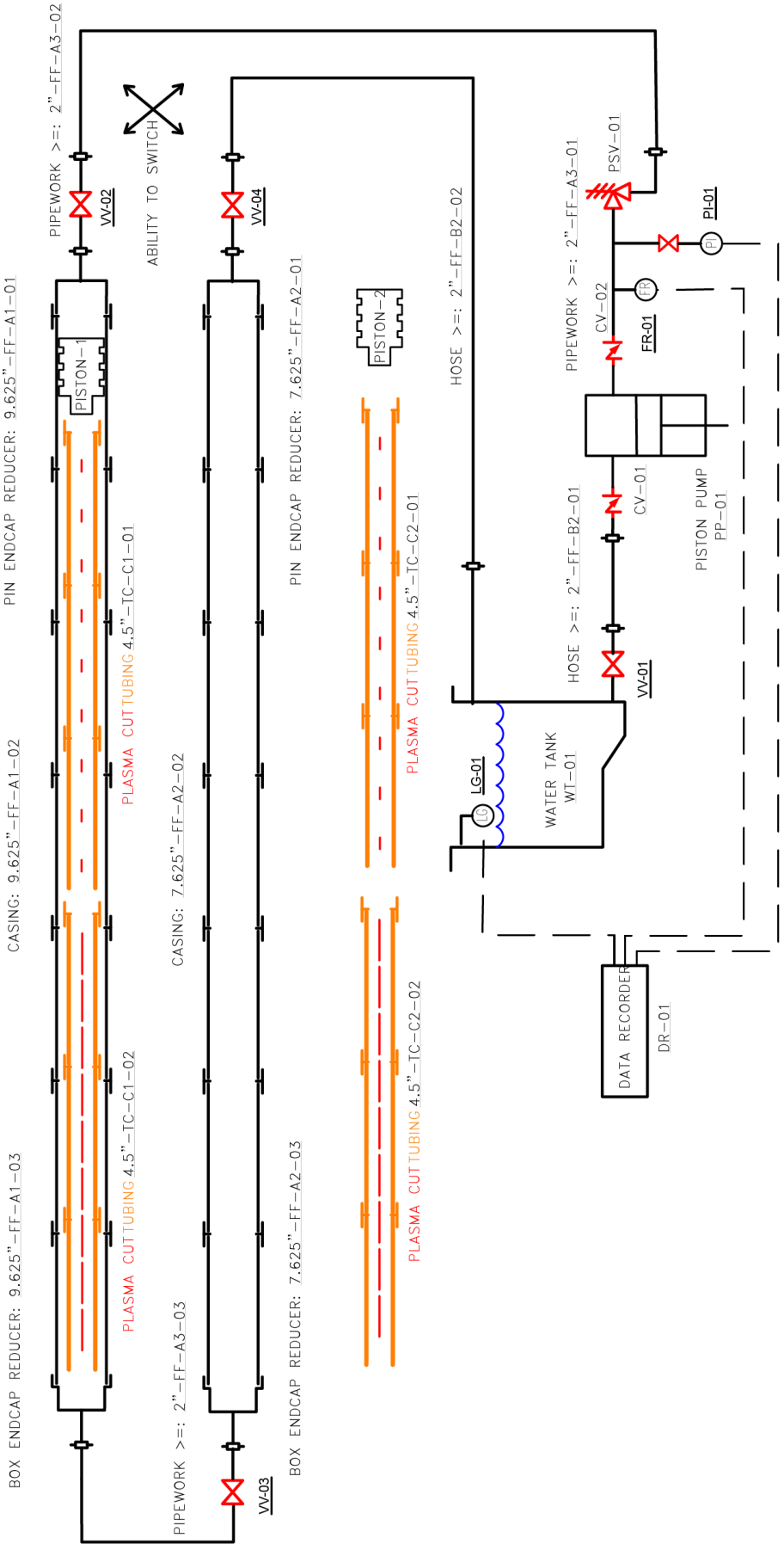

Fig. 26. Piping and instrumentation diagram for the full-scale compaction experiment (Oilfield Innovations 2017).

6.3.3. Tubulars

The requirement for the casings are, as stated in Table 6, that they can withstand the maximum test pressure of 345 bar. This requirement relates both to the specified thickness of the casings and the degradation due to wear. ConocoPhillips have donated an inventory of used tubulars, but as stated in Section 6.1, the 7" casing does not match with what was planned for the experiment. The tubulars presented in Table 7 are therefore what was initially planned for the experiment. ConocoPhillips have stated that they are able to donate more tubulars if the need should arise. The steel grade is believed to be L80, but this could not be verified.

Table 7. Tubulars planned to be used in the experiment.

Tubular OD [in] (mm)	Tubular ID [in] (mm)	Weight [ppf] (kg/m)
9 5/8 (244.5)	8.681 (220.5)	47 (69.9)
7 5/8 (193.7)	6.625 (168.3)	39 (58.0)
4 ½ (114.3)	3.958 (100.5)	12.6 (18.8)

Based on the results from the first full-scale compaction experiment discussed in Chapter 5, a compaction of around 50% is expected (Oilfield Innovations 2017). The method of DTD aims to create 50 m of unobstructed casing so that a 50 m cement plug can be placed downhole during PP&A. To test this, the initial length of the assembled tubing should be 100 m. The required length of casing is dependent on the type of piston and push plug that is used. A packer may be around 10 m in length, while a cement wiper plug may be around 0.75 m, according to Oilfield Innovations (2017). According to TAM International (2012), the SlikPak™ Plus can have a total assembly length of 5.79 m, but the packer element itself is much shorter. However, it will still be assumed that the packer length is around 10 m. The push plate may be around 0.5 m (see Section 6.3.4) (Oilfield Innovations 2017). To account for possible variations in tubing lengths, an additional 10% is added to the required casing length (Oilfield Innovations 2017). Two scenarios for the approximate required length of the 9 5/8" and 7 5/8" casings exist (if a self-constructed piston is used, the required casing length will depend on the length of this piston):

- *Packer as piston:*
  Length of 9 5/8" and 7 5/8": (100 m + 10 m + 0.5 m) × 1.10 ≈ 122 m

- *Cement wiper plug:*
  Length of 9 5/8" and 7 5/8": (100 m + 0.75 m + 0.5 m) × 1.10 ≈ 112 m

It should also be noted that four casing end caps will need to be constructed from casing joints, two from each of the casing types.

6.3.4. Piston

The piston is arguably the most critical component in the experiment, especially if a packer is used. The currently proposed method of DTD cannot be confirmed until a piston that is deployable downhole through tubing has been verified. An inflatable packer (see Fig. 27) can travel through the tubing before being inflated inside the casing, which is a necessary characteristic of a real case piston.

However, it should be noted that packers provided by TAM currently do not have the capacity to travel through the 4 ½" tubing and inflate with sufficient seal inside the 9 5/8" casing, this can only be done for the 7 5/8" casing[4]. This is not an issue for the experiment, since no through-tubing operations will be performed. There are many reasons to conduct the test without the use of a packer, if difficulties in acquiring or using the packer should arise. Two of the proposed alternative pistons are cement viper plugs, seen in Fig. 27, and a self-constructed piston, where both will use rubber as sealing element, just as the packer.

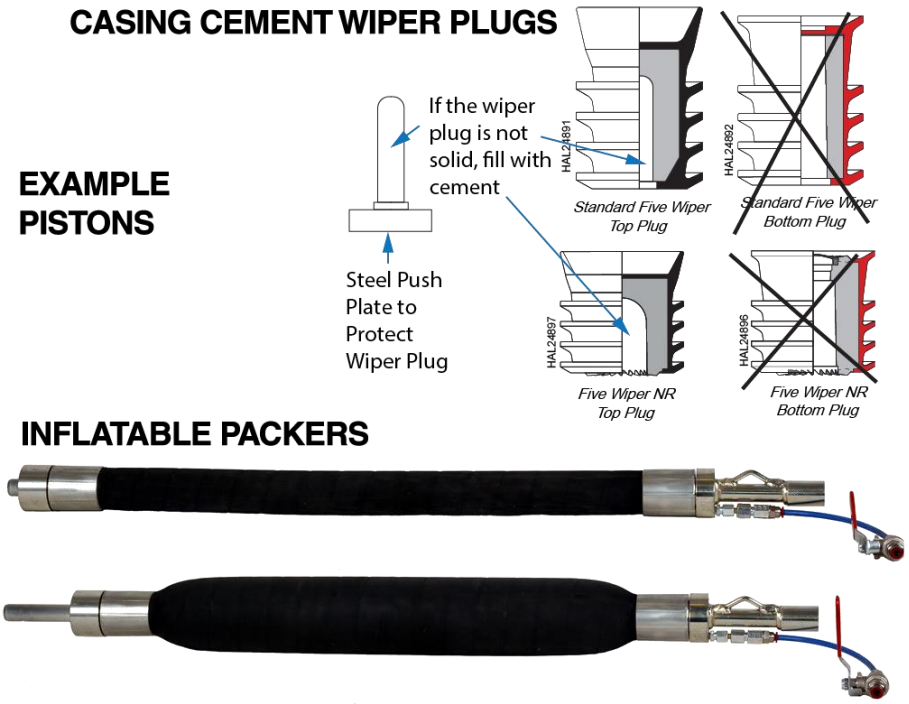

Fig. 27. The function of an inflatable packer is shown at the bottom, and wiper plugs with a steel push plate are illustrated at the top (Oilfield Innovations 2017).

Inflatable packers can be used for water shut-off, mechanical integrity testing, and act as a retrievable bridge plug during workover and recompletions, among other uses (TAM International 2012). The SlikPak™ Plus comes with different uninflated element ODs, which are designed to work in different hole sizes and with different differential pressures. For this experiment, the element should be capable of sealing inside a 9 5/8" and a 7 5/8" casing (if the same packer is used for both casings), and should be rated for pressures around 345 bar, which is the planned maximum pressure for these tests. TAM, who are planning to donate at least one inflatable packer for the experiment, recommend a 5 ½" OD fully covered packer to be used, which fulfills both requirements[4].

To minimize the damage on the piston, whether it is a packer or a cement wiper plug, a push plate will be placed between the piston and the tubing. This push plate will be made from steel and serves the purpose of protecting the piston against the tubing, which may have sharp edges and an uneven surface after cutting and during compaction. The push plate should be cylindrical, and there should be made one for each of the casing sizes, so that the radial clearance can be minimized. If a hollow cement wiper plug is used as piston, it will be reinforced with cement (see Fig. 27) so that it may withstand the forces that will develop during the experiment. Also, only top wiper plugs will be used, as their

[4] From oral correspondence with TAM employees.

design is more suitable for the task compared to bottom plugs (bottom plugs have a rupturable diaphragm). The wear on the piston during the experiment is unknown, and it is therefore advised to have several pistons ready for use.

6.4. Experimental Arrangement

The experimental arrangement, which includes everything that is done prior to the start of the experiment, can be performed in many ways. A detailed procedure will therefore not be given, but some possible issues will however be addressed. It should be noted that it is generally a good idea to collect as much data as possible about the test specimens prior to such experiments, especially regarding the cutting patterns and length of the tubing before compaction.

6.4.1. Setup

The finished setup is illustrated in Fig. 26. The 9 5/8” casing will be connected to the 7 5/8” casing to minimize the required number of pipes. As mentioned in Section 6.3.2, it should be possible to switch the pipework so that the test can be done on both casings. No further comments will be made on the setup since the plans may change before the experiment begins.

6.4.2. Cutting of Tubing Joints and Placement Inside Casing

The tubing joints should be cut in a way that allows them to be placed inside the casing. If the tubing is assembled before cutting, the required unobstructed length of the test site would need to accommodate for this. It may also arise problems regarding handling the tubing after cutting, so that it may be difficult to inject it into the casing. To avoid this, the relevant tubing joints could be cut before assembling, leaving the tool joints and a couple of additional centimeters uncut so that the joints may be assembled (see Fig. 28). If longitudinal cuts are planned along the whole axis of the joint, a short length of uncut tubular could increase the ease of handling. When the tubing joints are ready to be placed inside the casing, the following procedure can be used:

1. Place a joint of tubing so that only the tool joint is inside the casing, while the rest is supported by rollers. Make the final cutting pattern, only leaving the tool joint furthest from the casing uncut.

2. Push the tubing joint inside the casing to that only the uncut tool joint is extruding.

3. Place the next joint of tubing in front of the previous, supported by rollers, in a height that allows for the two joints to be connected. Connect the two joints.

4. Before pushing (or pulling from the other side of the casing) the two joints inside the casing, make the remaining cuts so that the planned cutting pattern is achieved. Do not cut the tool joint of the outermost tubing joint, as this will be performed in the next iteration.

5. Push the tubing inside the casing until the tool joint of the outermost joint hangs freely outside the casing.

6. Repeat steps 3-5 until the planned tubing length is inside the casing.

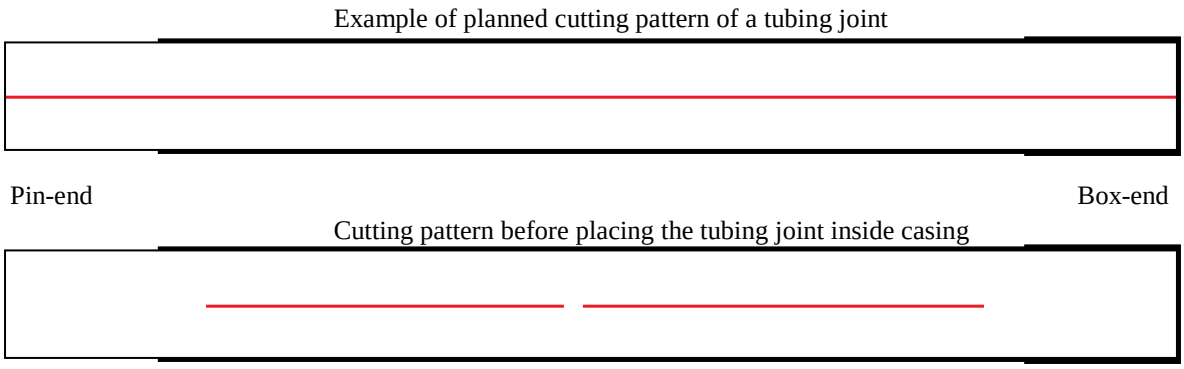

Fig. 28. Illustration of how tubing can be cut prior to placement inside casing.

Not all joints should be cut straight away, as the results from the first test(s) may give information regarding the optimal cutting method. Oilfield Innovations have proposed some cutting patterns, but as the document is relatively old, they will not be discussed in this thesis.

6.4.3. Fill casing with water

To simulate the downhole conditions, the casing will be filled with liquid during compaction. This may pose some problems since the tubing and piston must be placed inside the casing prior to filling. Two different ways of solving this are presented below.

Method 1:
Oilfield Innovations have proposed a design of the casing end caps, presented in Appendix B. Their solution consists of making several ports radially around the center of the end caps, and weld threaded connections to each of the ports so that they can be closed. When the tubing and piston are inside the casing, and everything else is ready, the casing will be filled with water from the tubing side of the piston. The top port in the casing end cap on this side is opened, and water is pumped through the empty casing. When water pours out of the casing end cap port, pumping is commenced and the port is closed. Now the tubing side of the piston should be filled with water. The same procedure is used to fill the other side of the piston. Since the ports in the casing end caps are not placed at the edge of the welded plate, the casing will not be completely filled with water.

Method 2:
A different method can be used to reduce the amount of air inside the casing. After the casing is connected, two holes are made at the top of the casing, one in each end. One should be aware that sharp edges inside the casing can occur during the creation of these holes, and this may damage the piston. This should be investigated before moving forward with the experiment. Threaded connections are then welded to the holes. The casing is filled with water in the same way as for “Method 1”, and the only difference is that pumping is commenced when water pours out of the hole at the top of the casing. The hole is then closed, and the experiment can start. Using this method removes the need for the ports in the casing end caps.

6.5. Test Procedure

Before starting the compaction experiment, all parameters that may influence the results should be recorded and noted. Some of these can be outside temperature, water temperature, and amount of friction reducing additives in the water (if this is used). The maximum allowable pump pressure should also be determined, based on the burst pressure of the casing, pipework ratings, and casing end cap tests. In this thesis, it is assumed that the upper pressure limit is 345 bar, as is indicated in the preliminary procedure report (Oilfield Innovations 2017). Section 6.5 is based on the information provided in this report.

6.5.1. Measure Leakage and Friction

The first part of the experiment will determine the leakage around the piston, and the frictional force required to start moving and to maintain movement of the piston. In addition, if a packer is used the optimal inflation pressure will also be determined. During these tests, the setup will be visually inspected to ensure that no unacceptable leakage in the pipework occurs.

To measure the friction of and leakage around the piston, the first test run will be conducted without a tubing inside the casing. The piston and push plate will be pushed through the casing while pressure and pump volumes are recorded. From these data, the frictional forces required to initiate movement of the piston, and the force required to maintain motion, are calculated. When the piston is at the end of the casing, the pressure will begin to rise. If a purposely built piston or a cement wiper plug is used, these pressures can damage the piston, and the pumping may therefore be stopped immediately if this damage is to be avoided. If an inflatable packer is used, leakage around the piston is measured for different pressures up to the maximum test pressure of 345 bar. If it is not possible to achieve this pressure because of the leakage, the leakage rate associated with the maximum pressure is recorded. The optimal inflation pressure should also be investigated if a packer is used. According to Oilfield Innovation, the inflation pressure should ensure that the leakage around the piston at the maximum test pressure does not exceed half of the pump rate (Oilfield Innovations 2017). The inflation pressure should therefore be adjusted so that this can be achieved, but should also take into consideration any damage that this may cause on the packer. All the parameters measured in this test, and especially the leakage around the packer, can be investigated without using the full length of the casing.

6.5.2. Compaction Procedure

Oilfield Innovations (2017) have suggested the following procedure, and it will be the same for both the 7 5/8” and the 9 5/8” casing:

1. Slowly bring the pump pressure up to 70 bar.

2. Vary the pump rate to keep the pressure between 70 bar and 280 bar while compacting. One should try to keep the compaction going, as the static friction coefficient is higher than the dynamic.

3. When pressures start to exceed 280 bar, reduce the pump rate to ensure that the pressure rating of the system is not exceeded.

4. Stop pumping when the system reaches 345 bar. Wait a few minutes, and if further compaction occurs and pressure decreases from movement, pressurize the system to 345 bar and wait a few minutes again. Monitor the returns to the tank throughout the compaction. If pressure falls or does not increase with returns to the tank, the piston may have failed and pumping should be stopped if a custom piston or cement wiper plug is used. If a packer is used, compare the leakage rate to that measured in the friction and leakage test to determine when to stop the test.

5. Do one of the following:

    - Stop pumping and hold 345 bar for approximately two minutes if the piston is not leaking.
    - Continue pumping at the maximum pressure attained for two minutes if a packer is used.
    - Stop pumping and bleed down pressure if a cement wiper plug is used.

6. If not already done, safely bleed pressure from the pump side of the piston, and ensure that there is no pressure in the rest of the system.

7. Remove the high-pressure piping from the casing end cap farthest from the pump, and disconnect the casing end cap. Slowly start pumping to force the compacted tubing, push plate, and piston out of the casing.

8. Measure the length of the compacted tubing (tools exist that can be used to measure the compacted tubing while still inside the casing, which should be considered for a more precise measurement).

6.6. Discussion of the Experiment

Since there are no results from this experiment, assumptions which the discussion is based on will be presented. Subsequently, different compaction parameters are discussed. Parts of this discussion will be based on the small-scale experiment which is presented in Chapter 7.

6.6.1. Assumptions

Some important assumptions throughout this discussion are:

- *Casing is filled 100% with water:*
  The goal is to completely fill the casing with water. However, the selected filling method will govern the actual water level inside the casing. The impact of some air inside the casing is not believed to be significant. Air behind the piston will be compressed by the fluid pressure and will most likely leak around the piston to the tubing side. Air on the tubing side of the

piston may reduce the lubrication between the crushed tubing and casing, but as compaction increases, the water level will increase, which means that this effect should be minimal.

- *Packer inflation pressure is the same for all tests:*
  Assuming that an inflatable packer is used as piston, the most appropriate inflation pressure will be investigated. It is assumed that once this pressure is determined, it will be the same for all the tests for that casing.

- *Leakage and friction is the same for all the tests:*
  This assumption somewhat builds upon the previous assumption. Regardless of the piston used, it is assumed that all the tests will have the same leakage and friction associated with the piston. This is believed to be the most important assumption, as an increased leakage will result in less force on the piston. The pistons should be visually inspected before each test to see if there is any damage that may cause unacceptable leakage.

- *Casing is 100% horizontal:*
  The test site is most likely not 100% leveled. However, a small inclination angle is not believed to have a significant impact on the results.

6.6.2. Compaction Variables

Without any physical results from the full-scale experiment, a theoretical approach to the impact of different compaction variables is given. In Chapter 7, a small-scale experiment is presented where the aim was to investigate the influence of cutting patterns and radial clearance, two of the most important compaction variables. Some of the results from the small-scale experiment will be used as reference during the discussion below.

Piston and push plate
The only objective of the piston is to transfer force from the fluid pressure to the push plate, which in turn pushes the tubing. The piston is not in direct contact with the tubing, so the only effect from the piston on the experiment should be the leakage around it and the friction it creates. The leakage around the piston at a given pressure is believed to be most dependent on the force between the rubber element and the casing. Leakage reduces the pressure behind the piston, which again reduces the axial force on the tubing. The leakage around the piston also has another effect. Instead of a direct contact between the casing and the rubber element of the piston, there will be water flowing around some parts of the piston, which will act as a lubricative and reduce the friction (See Section 2.1.2). The only effect of piston (and push plate) friction on the compaction process should be the reduction in compressive force transferred to the tubing, and wear on the rubber element. Still, in the case of the inflatable packer, these effects are of utter importance as they may determine the viability of using an inflatable packer as a piston.

The friction will depend on the type of piston that is used. Cement wiper plugs are made as to isolate the fluid behind them from the fluid in front of them. However, the pressures that will arise during the experiment are much higher than the differential pressures that wiper plugs usually are designed for. The Five Wiper Cementing Plugs from Halliburton (Halliburton 2009) require a 24.13 bar differential pressure to rupture the diaphragm and let the cement flow through it, which means that it is probably not designed for several hundreds of bars. Hence, one should expect leakage around the cement wiper

plug, and that the leakage will increase with the differential pressure. Cement wiper plugs are made to fit tightly in the constraining tubular, which in this case is a casing. The normal force, which is a governing factor for the friction, will therefore depend both on the weight of the cement wiper plug and the elastic energy that is built up in the rubber elements when the cement wiper plug is pushed into the casing. As cement wiper plugs are designed to be pushed through tubulars, the friction associated with this process is expected to be small.

For an inflatable packer, increasing the inflation pressure could result in less leakage around the piston, but the normal force would also be increased, which means more friction and wear. The ability to change the normal force between the piston and the casing is one of the major differences between a cement wiper plug and an inflatable packer. Nevertheless, tuning the leakage rate by changing the inflation pressure may be difficult, especially since the applied differential pressure affects the pressure inside the packer[5].

The push plate may have a significant impact on the friction in the experiment, depending on the radial clearance between the plate and the casing. If a part of the shredded tubing gets stuck in this radial clearance, high friction forces may develop. If the radial clearance is sufficiently small so that nothing is expected to get stuck, then the only effect of the push plate is the friction created from the weight of the plate, which should be negligible.

Tubing cuts

It is difficult to predict how the cuts in the tubing will influence the compaction. This is the compaction variable that provides the greatest number of possibilities, as illustrated in Fig. 29, and is arguably the most important manipulable compaction parameter. Chapter 7 presents a small-scale experiment where the influence of cutting patterns are investigated, which may serve as a guidance for the full-scale choice of cutting patterns.

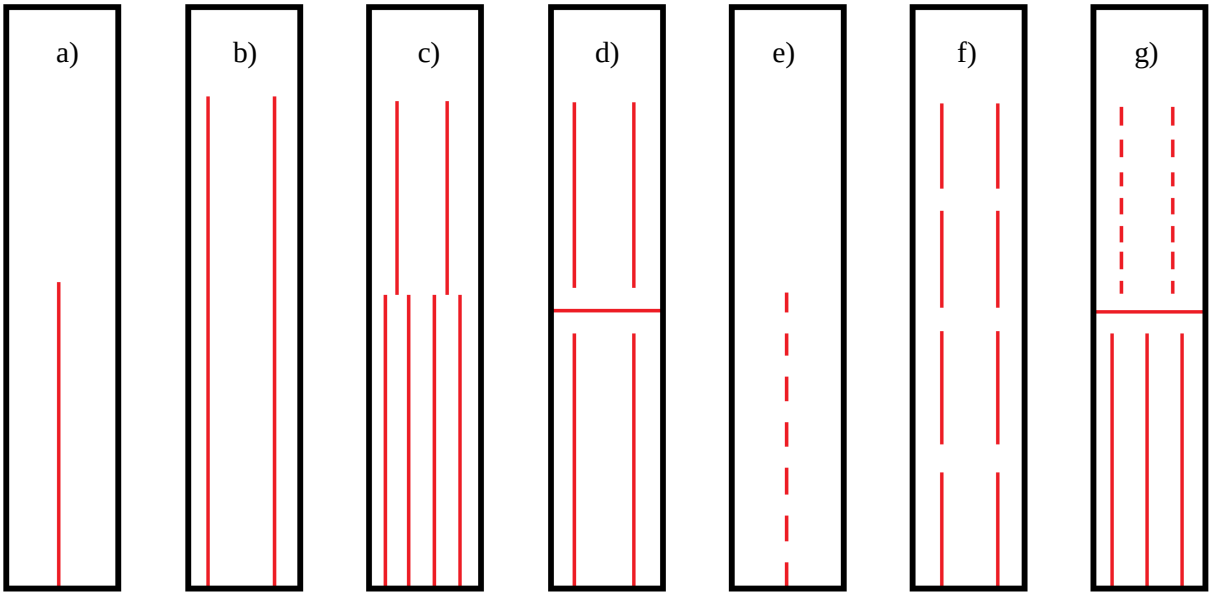

Fig. 29. a) through g) illustrate some of the different cutting selections that can be made and how they can be combined.

[5] From oral correspondence with TAM.

There are five main selections that can be made, and all of them can be combined in various ways:

- *Total length of cut pipe:*
  This describes the total length of the pipe that is longitudinally cut, either continuously (Fig. 29a) or by dashed cuts (Fig. 29e). It is possible to cut the pipe in sections, so that there is a long piece of uncut tubing in between cut tubing. The longitudinal cuts weaken the tubing, but it is not certain whether it is possible to crush whole tubing or if it will only undergo buckling with the pressure limitations in the experiment. Section 5.2 showed buckling of undamaged tubing, but with enough force it may be possible to crush whole tubing also, which was demonstrated in Section 7.3.4 during the small-scale experiment.

- *Number of cuts:*
  Fig. 29a through Fig. 29c illustrate some examples of different numbers of cuts. The number of cuts refers to the number of longitudinal cuts that are made along the circumference of the pipe, either dashed/slotted or continuous. To make it clearer, Fig. 29a and Fig. 29e have the same number of cuts, even though one is continuously cut and the other is slotted. Fig. 29b and Fig. 29c have the same total length of cut pipe, but in the latter this length is divided in two, where the lower portion consists of four cuts and the upper portion consists of two cuts.

  Increasing the number of longitudinal cuts, dashed or continuous, reduces the load capacity of the tubing (see Section 7.4). For continuous cuts, each strand can have its own individual geometry, and as they can move in separate directions, the degrees of freedom would increase with an increasing number of cuts. The stiffness and strength of each strand should decrease with an increasing number of strands. For an increasing number of longitudinal dashed cuts, each slot will be weaker, but does not have the same freedom of movement as a long tubing strand.

  Apart from resulting in a weaker tubing, an increased number of cuts could affect the friction during compaction. The results from the experiment in Chapter 7 showed lower friction when more than three longitudinal cuts were used, but the results were not conclusive. In addition, as was discussed under “Piston and push plate”, the strands could get stuck within the radial clearance between the push plate and casing. A greater number of cuts would imply smaller individual strands, which could more easily fit inside this radial clearance. This relationship was however not seen during the experiment in Chapter 7.

- *Cutting angle:*
  Cutting the tubing laterally, as in Fig. 29d, can make it easier for the tubing to compact side-by-side, which has been suggested by Oilfield Innovations (2016b), but a small radial clearance may prevent this. If the radial clearance is greater than the OD of the tubing, then it may be possible to perform DTD with minimal required force. To do this, the to-be-compacted tubing section would need to be severed in the middle before severing the tubing at the top of the section. This could make it possible for the upper tubing section to be placed next to the lower section, even without weakening the tubing first. This method could also work if the radial clearance is not greater than the OD of the tubing, which is a more common scenario, but then one would have to weaken at least the lower tubing section before attempting to compact them side-by-side. This method has been proposed by Oilfield Innovations (2016a), and is shown in Section 4.2. It is also possible to make diagonal cutting patterns, like a helix, along the tubing, but the effect of this is not known.

- *Dashed cuts:*
  Dashed cuts, as illustrated in Fig. 29e and Fig. 29f, can have different spacing and slot length. When the tubing is weakened with dashed cuts, the cross-sectional area is not divided into long individual strands in the same way as that expressed during the discussion of "*Number of cuts*". From the results in Section 7.3.7, a slotted tube could lead to less friction compared to a continuous cut tube with the same number of longitudinal cuts. The same results also show that dashed cuts make a smaller reduction in the load capacity of the tubing compared to continuous cuts.

  Dashed cuts may be the only viable option to weaken the tubing with current technology when considering the required time to weaken the tubing to an acceptable level. In the preliminary report for the experiment, Oilfield Innovations (2017) have therefore suggested making a dashed cutting pattern simulating what could be accomplished by using a Gator Perforator (see Appendix C) for the weakening process.

- *Thickness of cuts:*
  The thickness of the cuts depends on the method used to make them. For example, if a grinding machine is used, then the cut thickness would be close to the thickness of the grinding wheel. A greater thickness of the cuts would mean that more metal has been removed, which would result in a weaker structure. The total reduction of cross-sectional area of the tubing would therefore be directly linked to a reduction in load bearing capability of the tubing.

All the different cutting selections can be combined in various ways within the same tubing. Fig. 29g shows a tubing where 50% of the total cut length consist of three longitudinal cuts, and the other half consists of two dashed cuts with short spacing and cut length. The tubing is also severed in the transition between continuous and dashed cuts. Combining cutting methods such as this can be used to make the tubing behave a certain way during compaction, like making the bottom section of the tubing compact before the top section, which was proven in the small-scale experiment in Chapter 7.

Fluid present during compaction

The only fluid present in the casing during compaction is water, possibly mixed with a friction-reducing additive. Water has a relative low viscosity, and is therefore able to flow more easily around the piston compared to a more viscous fluid. This may increase the leakage, which was discussed under "Piston and push plate" earlier in this section. Water will also reduce the effective weight of the tubing inside the casing. This reduces the buckling load compared to a dry test, but this effect is believed to have little impact on the compaction. A friction reducing additive may cause measurable friction reduction during the compaction process. One such additive is the RX-72TL (Ramex n.d.), which is designed to reduce metal-to-metal friction such as in coiled tubing operations. The additive could reduce both packer-casing friction and tubing-casing friction during crushing. However, in the latter case the additive may just be squeezed out due to the large forces, which would result in metal-to-metal contact and dry friction, as stated in Section 2.1.2. In the case of packer-casing friction, friction reducing additives are believed to have a big impact. TAM operates with different friction factors depending on the fluid present in the well. In a water wet scenario, 0.035 is used, while in an oil wet scenario, 0.017 is used[6]. Having oil instead of water present in the well reduces the packer associated friction by half according to these numbers, and an additive specifically designed to reduce friction could be even more effective.

[6] From written correspondence with TAM.

Tubular dimensions

The main elements affecting the strength of a steel cylinder is the chemical composition, the method of manufacture, heat treatment, and the geometry of the cylinder (Callister and Rethwisch 2011). The latter will be discussed further in terms of radial clearance and tubing length. The influence of the casing ID will also be emphasized.

- *Radial clearance:*
  Radial clearance, together with the thickness of the tubing, determine how much liquid space that is available for the tubing to be compacted into, which is believed to have a significant impact on the compaction result (see Section 7.4.1). It also determines the maximum possible angle between the axial compressive force vector and the tubing, as shown in Fig. 30. A larger angle results in an increased bending moment on the tubing, and the necessary force to bend and fold the pipe is reduced, as will be discussed in Section 7.4.1.

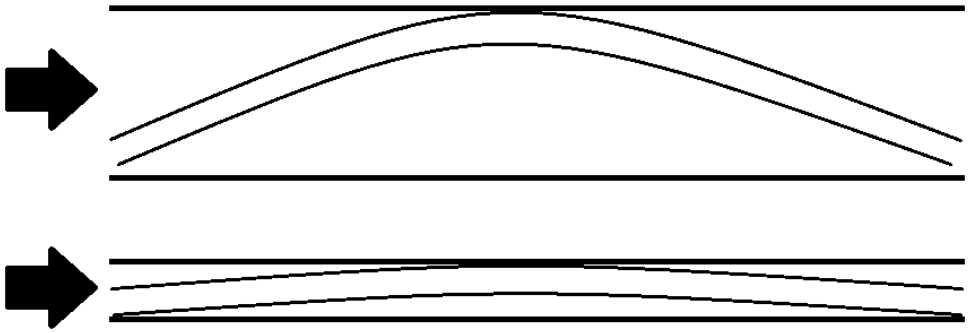

Fig. 30. An increased radial clearance results in a greater angle between the compressive force vector and the tubing at the point of contact during loading, leading to longer moment arms and therefore lower forces associated with bending and folding.

- *Tubing length:*
  The weight of the tubing is a linear function of its length. An increased length will therefore result in an increased normal force, and hence greater friction. Once the tubing has been crushed to some degree, and the tubing is pushing against the casing wall by stored up elastic energy, the friction will increase. This additional friction will become greater when there is more tubing pushing against the casing.

- *Casing ID:*
  An increased casing ID would lead to an increased internal casing wall area, but also an increased compaction ratio, as seen during the small-scale experiment in Section 7.4.1. These results also show much higher friction for a smaller constraining tube compared to a larger one. Another benefit from having a greater casing ID is the increased available piston force for a given piston pressure.

Tubing condition

The condition of the tubing will affect its strength, where a new tubing will generally be stronger than a used tubing of the same grade. One of the main reasons for this reduction in strength is corrosion, which attacks the inner surface of the tubing. Another reason is through-tubing intervention, which may cause wear inside the tubing. The outer side of the tubing is normally surrounded by a packer fluid, which is designed to protect against corrosion.

Casing wall roughness

A rusty casing may have a rougher inner surface than a corrosion free casing. The redox reaction resulting in rust may create pits on the metal surface, and may also leave flaky iron oxide products. The pits may interlock with asperities on the tubing wall, and energy is consumed as the tubing breaks free. This will increase friction. The effect of the friable iron oxide flakes may be insignificant to the tubing friction since they are easily crushed. However, as the surface of the piston is softer and more evenly divided on the casing wall compared to the metal tubing, the piston may "ride" on top of the rust flakes as is moves inside the casing, reducing the friction like a car braking on gravel. This effect would be reduced as the inside of the casing is wiped during the tests.

Pressure

One of the arguments behind the claim that the results from the first experiment presented in Section 5.3 represent pessimistic compaction values, was that the pressure build-up rate was very slow. This prevented continuous compaction, which means that the static coefficient of friction mainly governed the frictional forces. In this experiment, a much stronger pump is planned to be used, which can both give a more rapid and steady built-up rate, as well as achieve higher pressure values.

Inclination

As mentioned in Section 5.3, a horizontal layout gives maximum friction and minimum gravitational assistance. It also gives a higher axial compressive force on the tubing closest to the piston, which may cause the crushed tubing to get stuck. For further discussion, see Section 8.2.1.

Chapter 7

Small-Scale Experiment

7.1. Introduction

When it was certain that the full-scale compaction experiment at Rennesøy would not be completed within the time frame of this thesis, a small-scale compaction experiment was planned and executed by the author of this thesis. This chapter will present the experiment and discuss the results.

The main objectives of the experiment were to look at the effect of different cutting patterns and the impact of different radial clearances on the compaction process. A thick-walled steel pipe was used to represent the tubing, and the constraining tubulars were chosen as to scale with the 9 5/8" and 7 5/8" casings planned for the full-scale compaction experiment presented in Chapter 6.

7.2. Equipment

The experiment was conducted at a laboratory at the University of Stavanger, and the following equipment was used:

- *Hydraulic press with software:*
  The hydraulic press could deliver a maximum force of 250 kN and was controlled through the software package testXpert by Zwick. Several parameters could be digitally recorded, and for this experiment, the outputs from the software were applied force, stress, and elapsed time.

- *Angle grinder:*
  To minimize the reduction of cross-sectional area of the compaction tube, the thinnest available grinder wheel was selected, which had a thickness of 1 mm.

- *Steel tube:*
  Seamless cold drawn normalized steel tubes were used as test specimens for compaction, with the following properties (ThyssenKrupp 2012):

- Outer diameter: 25 mm
- Inner diameter: 21 mm
- Steel grade: E235
- Minimum yield strength: 235 MPa
- Tensile strength: 340-480 MPa
- Modulus of elasticity: 210 GPa (20°C)

Fig. 31. One of the seamless cold drawn steel tubes used as compaction specimen during the experiment.

The compaction tube selection was based on its OD/t ratio, and was limited by available tubes of sufficient length as to provide enough test specimens for the experiment. The OD/t ratio for the 4 ½" tubing equals 16.6. The test tube had an OD/t ratio of 12.5, making it more thick-walled.

The steel tube was initially 530 cm long, and was cut into 13 specimens of 40 cm length each using an automatic saw. Each specimen was then prepared using an angle grinder with the cutting patterns presented in Section 7.3. The length of the compaction tubes was chosen to provide a sufficient number of test specimens while still being long enough to get acceptable results regarding crushing and friction forces.

- *Four different constraining tubulars:*

Table 8. Material and dimensions of the different constraining tubulars, which were all prepared to a length of 45 cm.

Material	Outer Diameter [mm]	Inner Diameter [mm]
Steel	60.3	49.3
Steel	42.2	36.8
Aluminum	42.0	39.0
Aluminum	35.0	32.0

Limitations on available material restricted the selection of constraining tubulars, and the selection therefore contained two aluminum tubes. Tubular selections were based on the ratios between the casings and tubing planned for use in the full-scale compaction experiment presented in Chapter 6. The ratio between the casing IDs and the tubing OD is 2.15 for the 9 5/8" and 1.47 for the 7 5/8". The ratios between the constraining tubular IDs and specimen OD in this experiment are 1.97, 1.56, 1.47, and 1.28 for the 49.3 mm, 38.5 mm, 36.8 mm, and the 32.0 mm tubes, respectively. The constraining tubes were severed with the same automatic saw used for the compaction tubes, all to a length of 45 cm. The two different constraining steel tube sizes are shown in Fig. 32, which were the main tubes used in the experiment.

Fig. 32. The two different constraining steel tubes, the one on the left with an ID of 49.3 mm and the two others with an ID of 36.8 mm. The picture was taken after the experiment was finished, which is why the middle tube is deformed.

- *Extension rods:*
  The end of the piston connected to the hydraulic press could not fit inside any of the constraining tubulars used in the experiment. Extension rods were therefore placed on top of the compaction tubes so that the hydraulic press could transfer force to these rods, which again pushed and compacted the test specimens. The rods were chosen so to be much stronger than the specimens to avoid any buckling of the extension rods.

7.3. Test Procedure and Results

To scale the experiment with the full-scale experiment presented in Chapter 6, the piston force over tubing cross-sectional area was selected as scaling parameter. Using the maximum planned pressure for the full-scale test in Chapter 6 of 345 bar will result in a piston force of 1,317,395 N and 767,270 N for the 9 5/8" and 7 5/8" casing, respectively. This gives a stress on the tubing cross-sectional area of 5671 bar and 3303 bar for the two casings. The internal minimum yield pressure of a 9 5/8", 47 ppf, L80 casing is 473.7 bar (Tarpon Pipe and Supply n.d.). Using this pressure in the 9 5/8" casing gives a pressure on the cross-sectional area of the tubing equal to 7787 bar. The hydraulic press uses the piston force as input, so to achieve the same pressure on the test specimens as on the tubing in the previous calculations, the tubing pressures would need to be converted to piston force. A pressure of 5671 bar and 7787 bar on the cross-sectional area of the test specimen equals a piston force of 81,953 N and 112,532 N, respectively, while a pressure of 3303 bar yields a piston force of 47,733 N.

Before the tests on the steel pipe described in Section 7.2 were conducted, two tests were performed on a copper tube, namely specimen T1 and T2. The hydraulic press used during these tests could not record parameters digitally, and was operated using a pumping lever. The tests and associated results are presented in Appendix D. The test specimens were given names based on the chronological order in which they were tested in, following the capital letter "T", which resulted in the first steel tube specimen being labeled as T3. All figures of the test specimens, either pictures or illustrations, are oriented so that the left side of the figures was at the bottom during the tests (unless stated otherwise).

Using a hydraulic press with digital parameter readings, 13 tests were conducted with the equipment listed in Section 7.2. Extension rods were used to transfer force from the piston in the hydraulic press to the tube, seen in Fig. 33, and the constraining tubular was not fixed. For safety reasons, the constraining tubulars were placed within thick-walled steel cylinders which had no effect on the experiment other than ensuring that no metal pieces during a potential mechanical failure or overturn could do any harm to material or personnel. In Fig. 33, one of these protective cylinders is seen, but another one was added later to ensure increased safety, which also made it safe to remove the cardboard seen in the same figure. Because of stability issues with the extension rods they could not be very long, which resulted in multiple test runs for each test specimen where the extension rods were changed between each test run. All test runs were conducted with a constant increase in force[7], and force, strain, and time were recorded digitally. The stop criterion for each test run was based on both a maximum force and a maximum deformation, where the maximum deformation was determined by the distance between the piston and the constraining tube. Because of the shape of the piston, a short solid cylinder or rectangular prism was placed between the piston and the extension rod. The starting position for all tests was when the piston touched this solid cylinder or prism.

Section 7.3.1 through 7.3.11 present the tests performed on each specimen. First, a general overview of the test is given, followed by a figure showing the cutting pattern for that specimen. Subsequently, a summary of the test runs with references to the associated force-strain graphs are presented. As mentioned, multiple test runs were performed on each specimen. This was due to short extension rods, unknown errors, and a break criterion within the software controlling the hydraulic press, commonly used for concrete testing. This break criterion stopped the test if a certain strain criterion was fulfilled, and was not detected and deactivated until the testing of T5 was completed. The force-strain graphs for each specimen are presented in the chronological order in which they were performed, and because of the varying maximum force between the test runs, the axes are scaled differently between the different test runs. The results from the first two steel specimens are presented in Appendix E since these results could not be used in the discussion. For specimen T4, this was due to the constraining aluminum tube buckling in Euler mode, which also led to the decision to not use aluminum tubes further. Sources of error will be discussed in Section 7.4.3.

[7] The applied rate of force was varied during the experiment, but from T6 and onwards, a rate between 20 and 25 kN/min was used. Lower rates were used during ejection of the crushed tubing.

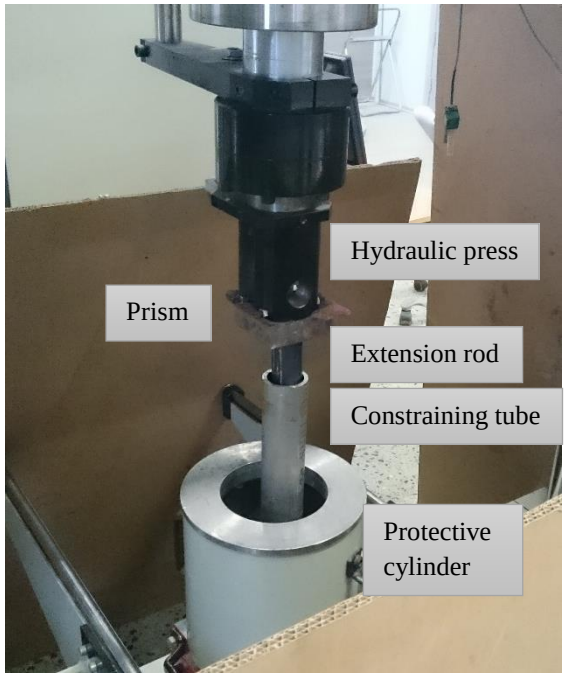

Fig. 33. The test setup with extension rod, protective cylinder, constraining tube, prism, and hydraulic press.

The cutting patterns presented in this section were made with an angle grinder, which caused slight variations of a few millimeters between each specimen (see Fig. 34 for examples of cut specimens). However, the aim during the cutting procedure was as follows:

- Leave 10 mm of uncut pipe on each end.
- Use equal radial spacing/phasing between cuts.
- Leave 10 mm of uncut pipe between different cutting patterns.
- For the dashed cutting pattern, the slot length should be 60 mm and the spacing should be 5 mm.

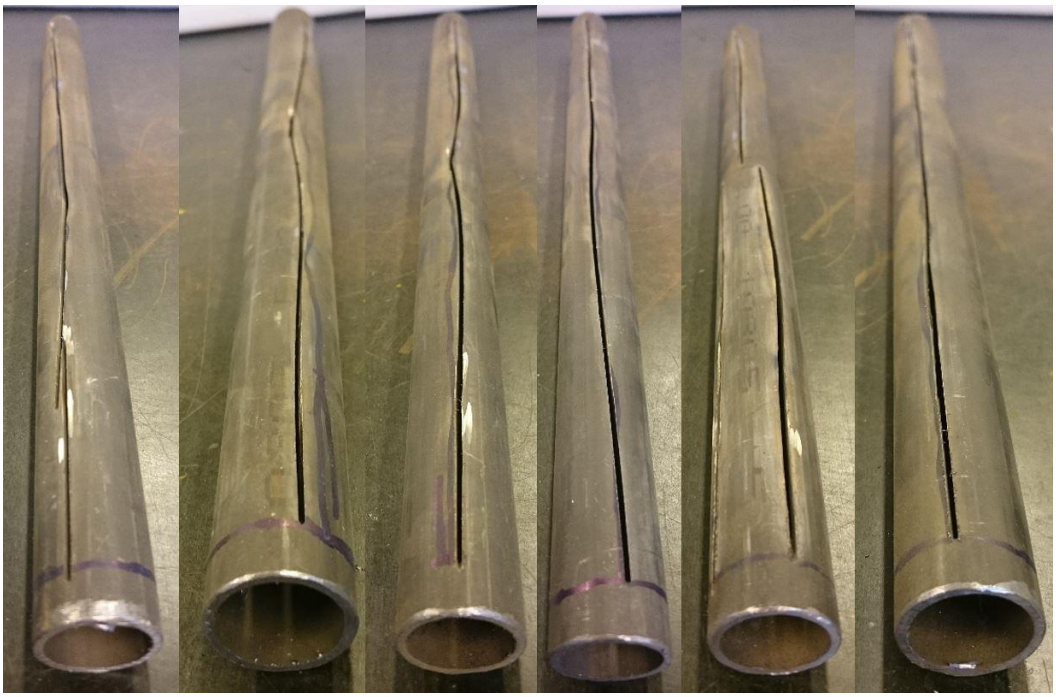

Fig. 34. Some of the longitudinal cuts in six different specimens.

7.3.1. Specimen T5, 4 cuts

Test specimen T5, seen in Fig. 35, was placed inside the 36.8 mm ID steel tube and loaded in 6 test runs to a maximum load of 98.80 kN. One of the test runs most likely stopped due to the break criterion that was activated, but this is not certain since the software did not give any outputs regarding the reason of the stopped tests. The constraining tube had been deformed plastically by the inner tube, but not buckled. The crushed tube was ejected with the manual hydraulic press operated with a pumping lever.

Fig. 35. Cutting of specimen T5, where the uncut parts at the ends were approximately 10 mm long. This means that the cuts were around 380 mm long.

The test results from specimen T5 can be seen in Fig. 36. During the first test run, seen in Fig. 41a, the force steadily increased until it reached a peak load of 14.89 kN, where it suddenly dropped. Large deformations followed as the inner tube was crushed. The second test run, seen in Fig. 36b, continued with non-linear compaction at approximately the same load as where the first test run stopped. The peak load during the second test run was 11.80 kN, and the spike in the end of this test run was caused by the prism touching the constraining tube and will therefore not be included in the calculated total strain. Test run 3, seen in Fig. 36c, had a generally increasing force while large deformations took place, and ended with a peak load of 60.33 kN. The high force during the end of this test run should lead one to expect similar forces during the start of plastic deformation in the next test run, seen in Fig. 36d. Instead, a plateau is reached at around 11-12 kN, and large deformations take place. This low recorded force may be caused by the extension rod landing on an extruding metal piece of the test specimen, as seen to the right in Fig. 37 (the shortest extruding piece), since it would not require much force to push the extension rod further down next to this metal piece without compacting the specimen further. At around 25 mm strain, the force starts to rapidly build up, which can be explained by the extension rod touching the compacted area of the test specimen and starting to load it further. The graph in Fig. 36e shows the strain decreasing in the end, which is most likely due to this test being stopped manually and therefore the machine unloaded while still recording force and strain. The decrease in strain is most likely due to elastic deformation. The last test run, seen in Fig. 36f, most likely resumed the crushing at the end of the previous test run since the loads are approximately the same.

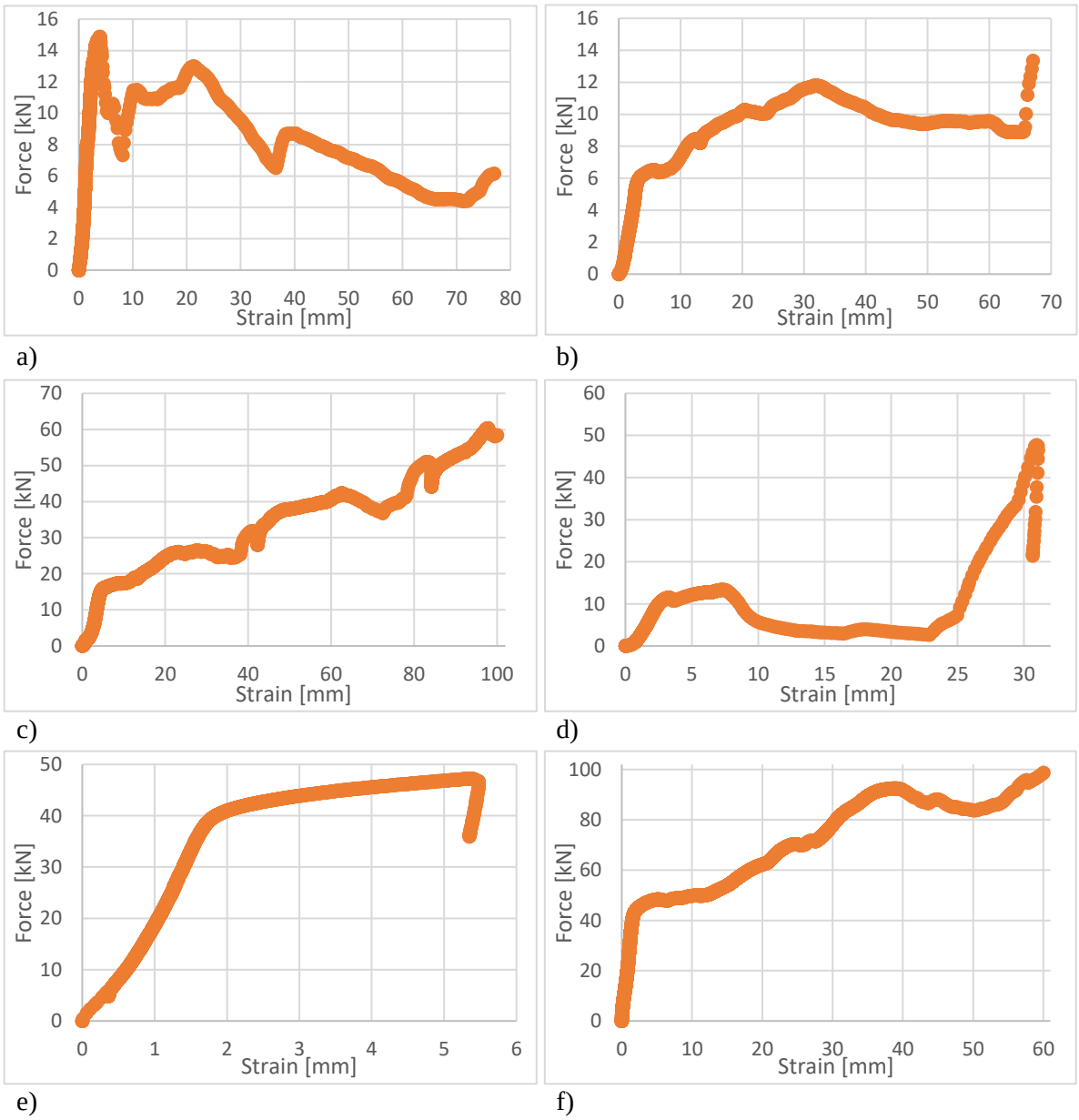

Fig. 36. Test results from loading of specimen T5.

The cumulative strain from the test runs seen in Fig. 36 is equal to 338.37 mm. Manual measurement determined a crushed specimen length of 97.5 mm, which equals a strain of 302.5 mm. This big difference in measurements may have its root in Fig. 36d. By removing the strain up until 24.97 mm, which is where the force starts to build up rapidly, the total strain becomes 313.4 mm. The graphs in Fig. 36 will be assumed to represent the correct permanent strains, after removing the assumed invalid part of the fourth test run. With this assumption, the total strain after reaching a load of 48 kN and 82 kN was 227.46 mm and 284.89 mm, respectively.

The lengths of all the crushed tubes during the experiment were measured using a fractional caliper, where both the shortest and longest lengths were measured. The whole bottom ends of the tubes were flat, while the top often had a flat area created by the extension rod and some pieces extruding further out on the edges, which had not been placed directly beneath the extension rod during loading. This effect can be seen to the right in Fig. 37. Only the shortest lengths will be presented in this thesis, as these are believed to best represent the crushed lengths.

The constraining tube was visually inspected after the final test run, revealing plastic deformation in the bottom of the tube, where the most severe deformation is shown to the left in Fig. 37. The top of the deformed area was located around 12 cm from the bottom. It is believed that this deformation was created during the last test run, and because of its location, it is not believed to have made a significant impact on the test results. The crushing pattern of specimen T5, seen to the right in Fig. 37, is similar to the longitudinal crushing pattern seen in the first full-scale experiment in Section 5.2, only with a much greater compaction. This was also the case for all the other test specimens that were cut, and will not be commented further in Section 7.3. A long piece of metal extrudes from the edge of the crushed specimen, seen to the right in Fig. 37, which may have caused additional friction. Inspection of the test specimen after the first test run revealed that compaction initiated in the top of the constraining tube. The same compaction process was observed for all the other test specimens that did not have mixed cutting patterns, and this will therefore not be commented further for these specimens in Section 7.3.

Fig. 37. To the left, the constraining tube is seen after the final test run. To the right, specimen T5 is pictured after crushing and ejection. Note the long metal piece extruding on the edge of the upper part of the crushed specimen.

During ejection of specimen T5 from the constraining tube, the force was displayed on an analog manometer in terms of tons. The highest recorded measurement during this process was approximately 4.2 tons, seen in Fig. 38, which is equal to 41.2 kN. Compared to the ejection forces for the other specimens, this is a considerably large force. A thin extension rod was used during the ejection, so the long extruding metal piece seen to the right in Fig. 37 should not have caused any additional friction during this process. However, the deformed area in the bottom of the constraining tube could have affected the required ejection force, since the specimen would have to deform the end of the constraining tube in order to be ejected. This deformation was seen on the end of the middle tube in Fig. 32. Regardless of this, the results will still be used in the discussion.

Fig. 38. Maximum frictional force during ejection of specimen T5 using the manual pumping press.

7.3.2. Specimen T6, 5 cuts

Test specimen T6, seen in Fig. 39, was placed inside the 49.3 mm ID steel tube and loaded in 6 test runs to a maximum load of 100.01 kN. During two of the test runs, the hydraulic press stopped abruptly. At this point, the break detection setting was believed to be deactivated, so the reason behind these errors is not known. The crushed tube was ejected from the constraining tube using the same method as with specimen T3 and T5.

Fig. 39. Cutting pattern of specimen T6, where the uncut ends were roughly 10 mm long and the cuts were around 380 mm long.

The test results from specimen T6 can be seen in Fig. 40. From the first test run in Fig. 40a, it can be seen that plastic deformation apparently initiated at around 3.69 kN, before the force further increased until a peak load of 4.47 kN was reached. A small decrease in force took place before roughly the same peak again was reached, followed by a sharp and rapid drop in force during what is assumed to be crushing of the inner tube. The first and second test run stopped abruptly without any known error. Test run 2 and 3, seen in Fig. 40b and c, respectively, showed large deformations at forces below 4.2 kN, and the latter ended with a sharp peak caused by the prism touching the constraining tube. The deformation during this sharp peak is not included in the presented results. In the fourth test run, seen in Fig. 40d, the force built up towards a peak load of 7.64 kN, after which the force quickly dropped and started to build up again during large strains. The graphs in Fig. 40e and f show large deformations during a relatively steady increase in force.

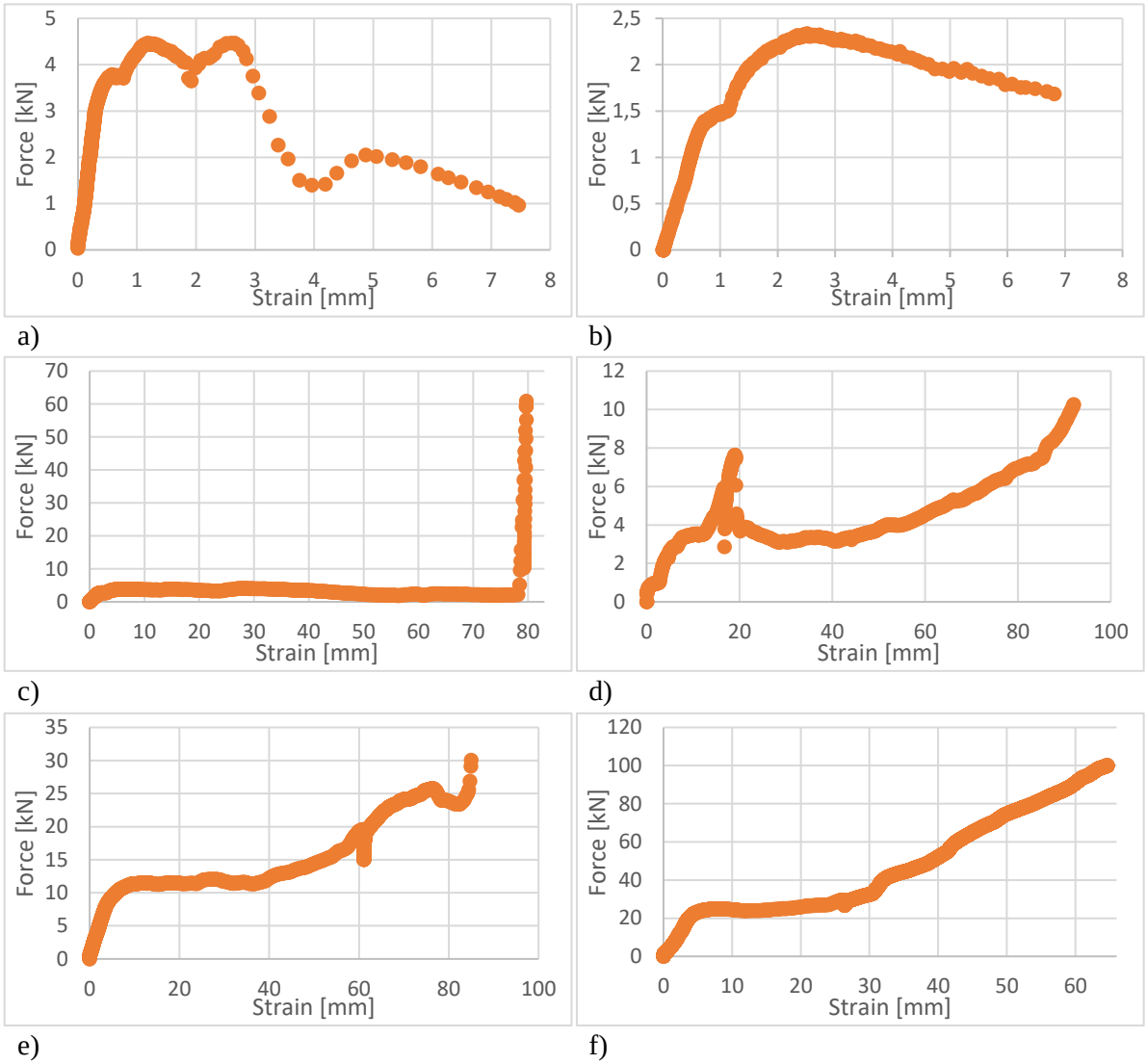

Fig. 40. Test results from loading of specimen T6.

The total strain from the graphs in Fig. 40 is equal to 333.70 mm. Manual measurement of test specimen T6 after crushing, seen in Fig. 41, showed a crushed length of 72.0 mm, resulting in a strain of 328.0 mm. These results are close to one another, and it will therefore be assumed that the deformations seen in Fig. 40 are correct and related to permanent deformations. Assuming this, the total strains after reaching a load of 48 kN and 82 kN are equal to 307.50 mm and 324.59 mm, respectively.

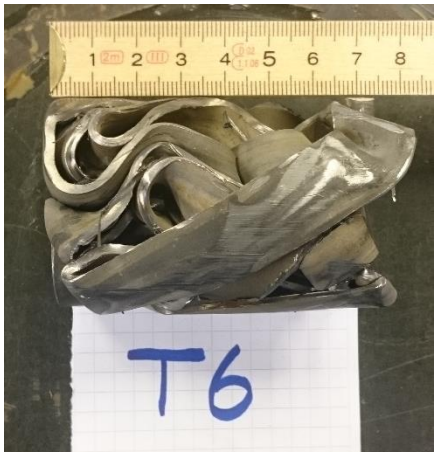

Fig. 41. Specimen T6 after crushing and ejection from the constraining tube.

During ejection of the crushed specimen from the constraining tube, the force was so low that no recordings could be made from the manual pump press.

7.3.3. Specimen T7, 3 cuts

Test specimen T7, seen in Fig. 42, was placed inside the 49.3 mm ID steel tube and loaded in 4 test runs to a maximum load of 82.00 kN. The press abruptly stopped during one test run for an unknown reason. The crushed tube was ejected using the digital hydraulic press after some new equipment was found that ensured stability during this process.

Fig. 42. Cutting pattern of specimen T7, were the uncut ends were approximately 10 mm long and the cuts were around 380 mm long.

The test results from specimen T7 can be seen in Fig. 43. During the first test run, seen in Fig. 43a, the load increased steadily, but with a short fall at around 9.7 kN, until it reached 18.72 kN. Here a sharp drop in the force occurred, before the force continued to grow towards a peak value of 21.22 kN. Subsequently, the force dropped during what is assumed to be crushing of the inner tube. The first test run ended with a load of 4.64 kN, and it can be seen in Fig. 43b that the initially straight line from the start of the second test run dips when it reaches 4.35 kN, which can be assumed to be a continuation of the deformation which commenced in the first test run. The second test run reached a plateau ranging between 7.0 kN and 7.6 kN, and after some deformation, a new plateau was reached ranging between 7.8 kN and 8.9 kN. The graph in Fig. 43c shows large deformations below 30 kN, and the load at the end of Fig. 43c is approximately the same load as where the curve in Fig. 43d starts to flatten out, which may indicate continuation of plastic deformation.

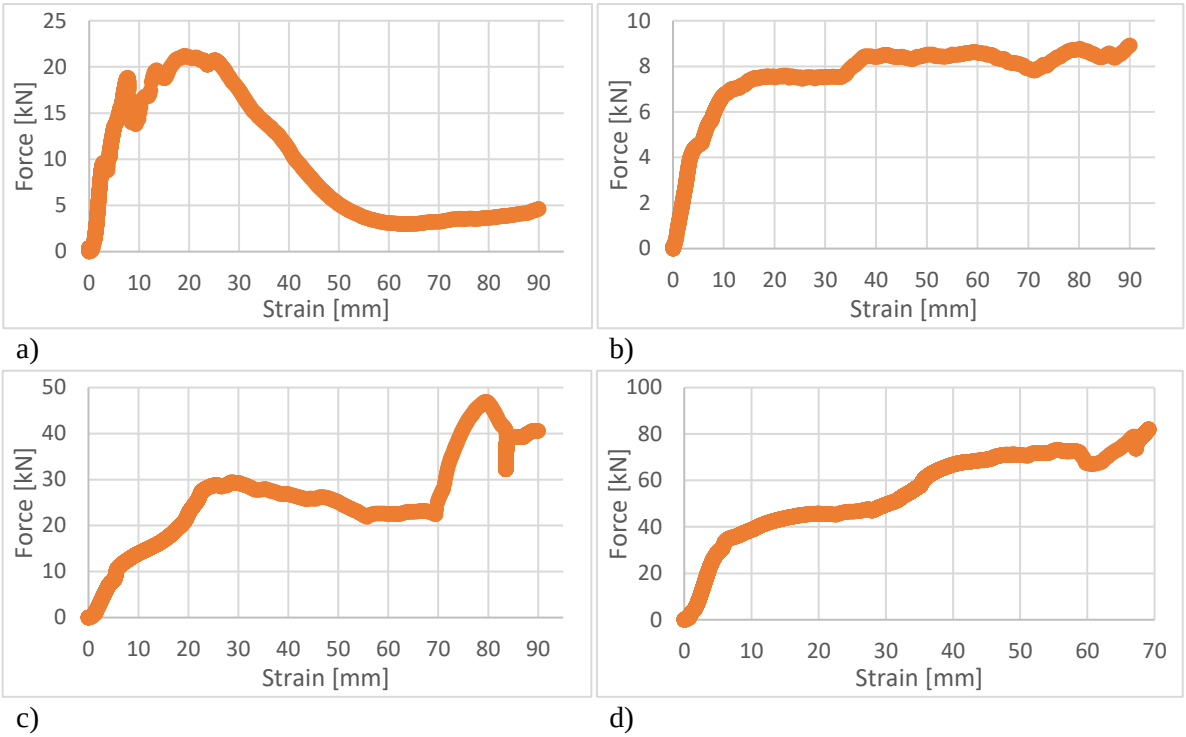

Fig. 43. Test results from loading of specimen T7.

All the strain seen in Fig. 43 sums up to a total of 338.89 mm. Manual measurement of specimen T7 after crushing showed a length of 75.4 mm, which equals a strain of 324.6 mm. The difference between these two results are relatively large, but it will still be assumed that the digital results from these tests represent the correct plastic deformations at the given loads. This means that the total strain when the load reached 48 kN was 298.45 mm.

Fig. 44. Specimen T7 after crushing and ejection from the constraining tube.

As mentioned, new equipment made it possible to measure the friction when pushing the crushed tube out of the constraining tube. As seen in Fig. 45, the force required to initiate the ejection was 15.54 kN, and this was also the largest force during the process. The sudden spike at the end of the curve was caused by the prism touching the constraining tube. The ejection process required several test runs for most of the specimens, but only the first graphs will be presented since the applied force in these test runs was always the largest.

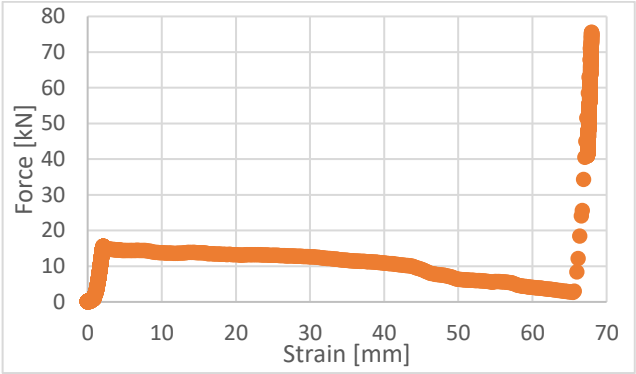

Fig. 45. Frictional force as specimen T7 was pushed out from the constraining tube.

7.3.4. Specimen T8, no cuts

Test specimen T8, seen in Fig. 46, was placed inside the 49.3 mm ID steel tube and loaded in 5 test runs to a maximum load of 82.00 kN. This tube was uncut so that it could be used as a reference for the other test specimens. An unknown error caused one test run to stop abruptly. The crushed tube was ejected using the digital hydraulic press.

Fig. 46. Specimen T8 was not damaged.

The test results from specimen T8 can be seen in Fig. 47. The force-deformation curve is close to linear in the first test run, seen in Fig. 47a, until a peak load of 41.07 kN was reached. The force then dropped as deformation continued, before again increasing and reaching a plateau with a maximum value of 50.34 kN. At the end of the first test run, the force rapidly increased due to the prism touching the constraining tube, and this deformation will therefore not be included in the results. The second test run, seen in Fig. 47b, stopped abruptly due to an unknown error, and the low force required for deformation seems suspicious considering the first test run ended with a force of 29.06 kN. The curve in Fig. 47c starts to flatten out at around 25.6 kN, and the deformation at this point may be an extension of the deformation at the end of the first test run. The graph in Fig. 47c ends at 45.50 kN and the curve in Fig. 47d starts to deviate from its linear characteristic at around 45.3 kN, which suggests that the deformation after this point is likely linked to the deformation at the end of the third test run. The fourth test run ended with a decreasing load, which may be the reason the last test run, seen in Fig. 47e, reached a plateau around 10 kN below the end of the previous test run.

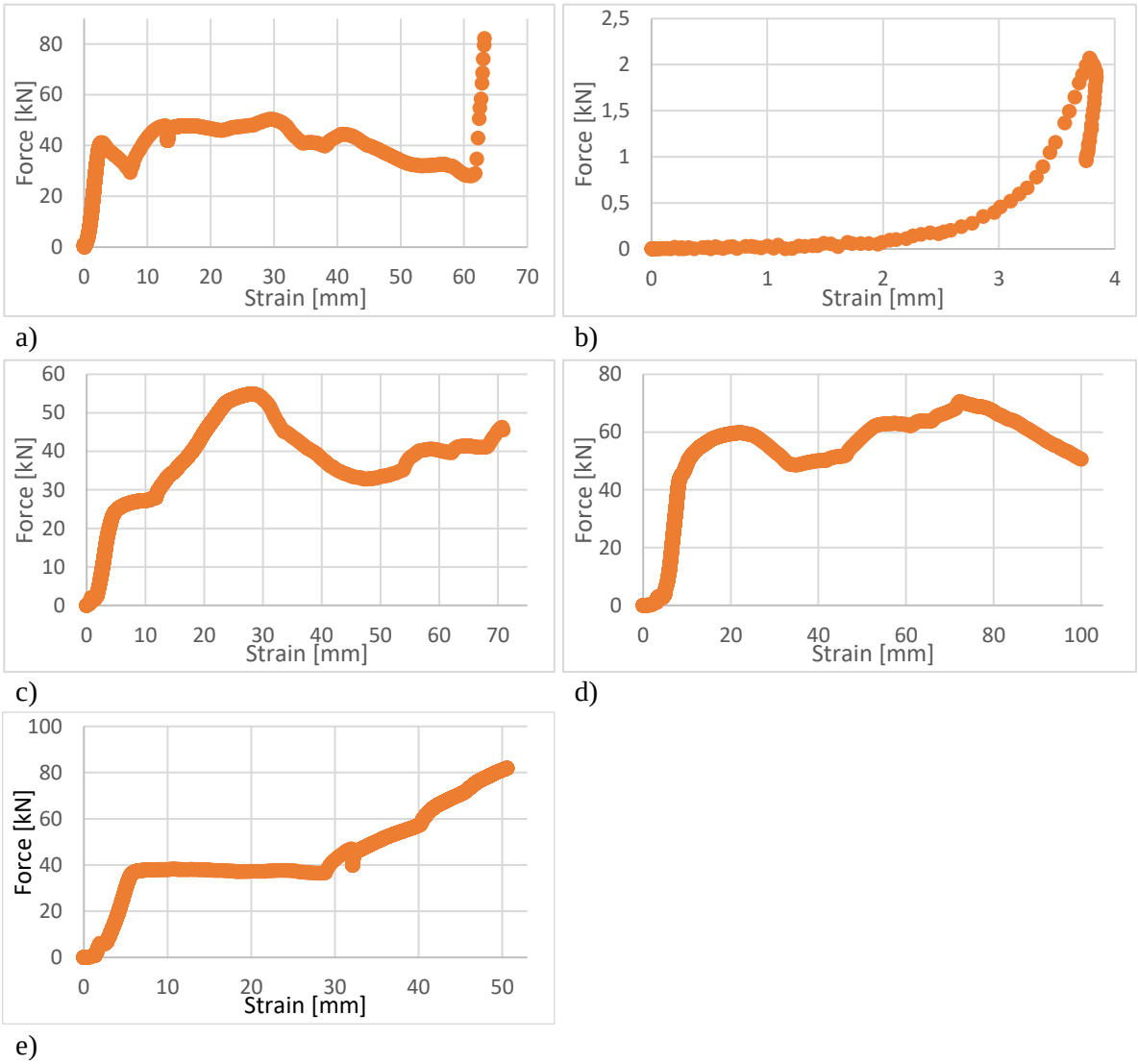

Fig. 47. Test results from loading of specimen T8.

The cumulative strain in Fig. 47 is 286.47 mm. Manual measurement of specimen T8 after crushing, as seen in Fig. 48, revealed a length of 137.0 mm, which converts to a strain of 263.0 mm. However, some of the deformations in Fig. 47 may be incorrect, and removing these may give a more accurate estimation of the deformation. By subtracting the strain throughout the second test run and removing the strain at the very beginning of the curves in Fig. 47c, d, and e, a strain of 275.35 mm can be calculated. The reason for removing the start of these curves will be explained in Section 7.4.3. With the new, and arguably more accurate, deformation from Fig. 47, it will be assumed that the graphs now represent accurate plastic deformations during loading of specimen T8. With this assumption, the total strain after reaching a load of 48 kN was equal to 81.32 mm.

Only the upper part of specimen T8 was compacted during the test runs, as seen in Fig. 48. After the upper part was crushed, further increase in compressive load most likely distributed the force to the constraining wall in terms of radial stress and friction, which reduced the axial compressive force on the uncrushed part of the tube. This reduction was enough to stop further compaction of the test specimen. The crushing pattern of the specimen looks like a helix, which suggests that the tube was helically buckled before further increase in load caused failure, which initiated bending and folding of the tube.

Fig. 48. Specimen T8 after loading and ejection from the constraining tube.

The force required to initiate the ejection of specimen T8 was 8.08 kN, which is where the curve first starts to flatten out in Fig. 49, but the force continued to rise until reaching a maximum value of 11.49 kN. The sudden spike at the end of the curve was caused by the prism touching the constraining tube.

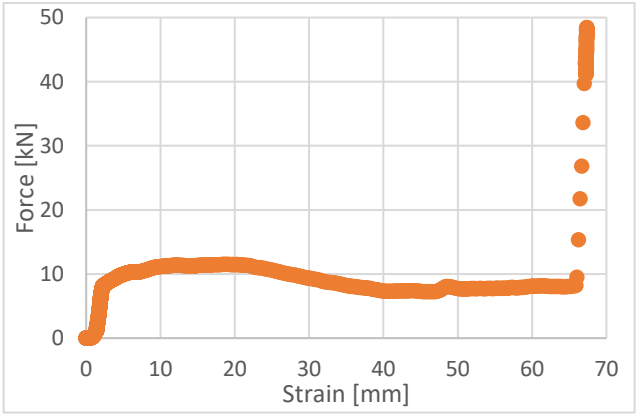

Fig. 49. Frictional force as specimen T8 was pushed out from the constraining tube.

7.3.5. Specimen T9, 4 cuts

Test specimen T9, seen in Fig. 50, was placed inside the 49.3 mm ID steel tube and loaded in 4 test runs to a maximum load of 82.01 kN. In an attempt to maximize the deformation during the first test run, a longer extension rod was used. During loading, the extension rod overturned, which may have been due to the inner tube not being centered within the constraining tube. The crushed tube was ejected using the digital hydraulic press.

Fig. 50. Cutting pattern of specimen T9. This specimen was similar to T5, but placed within a larger constraining tubular for comparison purposes. The uncut ends were around 10 mm long, and the cuts were roughly 380 mm long.

The test results from specimen T9 can be seen in Fig. 51. The first approximately linear part of the graph from the first test run, seen in Fig. 51a, reaches a maximum value of 5.39 kN before the force starts to drop. A high rate of deformation followed until a maximum load of 9.25 kN was reached, but at the end of this test run, the extension rod overturned, which may have caused some of the data points at the end of Fig. 51a to be invalid. The second test run, seen in Fig. 51b, started with an approximately linear curve until it flattened out before reaching a peak load of 5.88 kN. During a short plateau, some deformation took place before the force again started to increase until reaching a new peak of 9.13 kN. After some deformation with decreasing force, the force started to rapidly grow until reaching the last peak of the second test run equal to 15.47 kN. The graph of the second test run ends with a steep decline curve at a value of 8.80 kN, and this rapid decline in force may explain why the force in the start of the third test run, seen in Fig. 51c, starts to decline after reaching an initial peak of 5.15 kN. The sudden spike at the end of the third test run was due to the prism touching the constraining tube, and will therefore not be included in the results. The assumed crushing in Fig. 51d picks up at approximately the same place as where the previous test run ended.

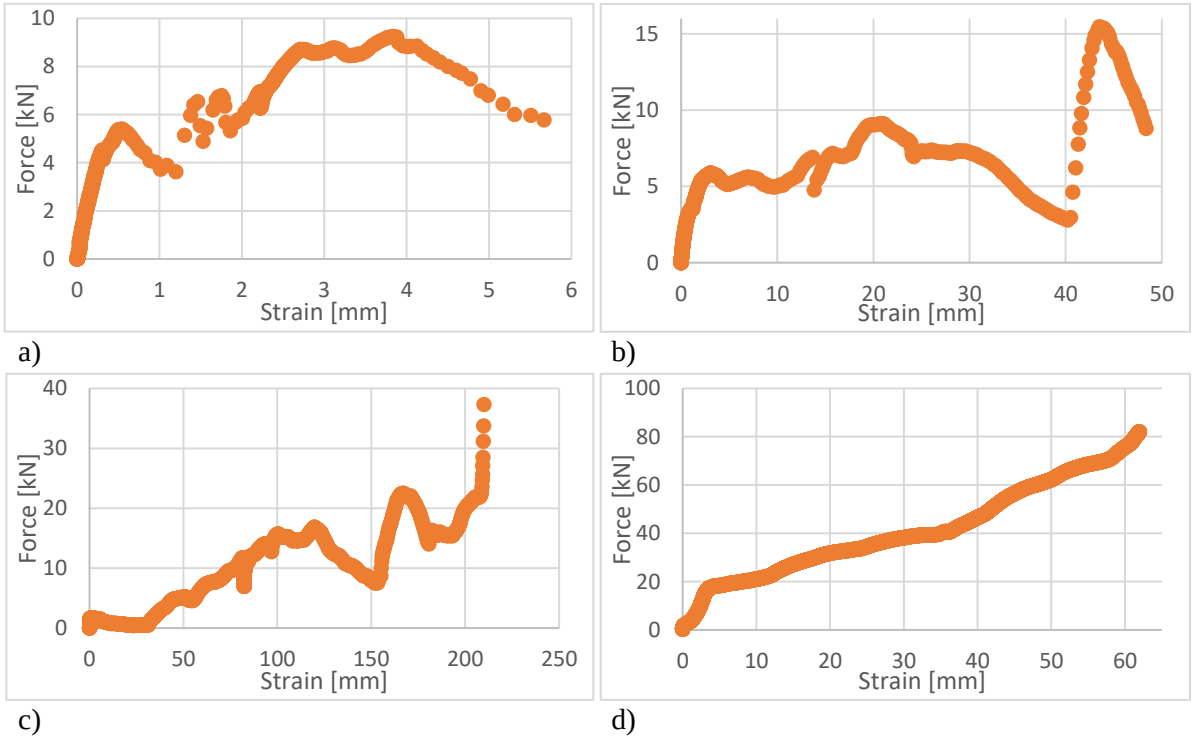

Fig. 51. Test results from loading of specimen T9.

The total strain from the graphs in Fig. 51 is 324.53 mm. Using a fractional caliper to measure specimen T9 after crushing, seen in Fig. 52, revealed a length of 72.9 mm, which equals a strain of 327.1 mm. The difference between the two measurements is very small, and the manual measurement is bigger than that of the hydraulic press. None of the data points from the first test run was removed, even though the extension rod overturned. The press automatically stopped when this happened, and since the overturning may have been caused by a rapid deformation of the inner tube, the data points are assumed to be valid. It will be assumed that the strain in Fig. 51 are correct and related to plastic deformations. With this assumption, the strain after reaching a load of 48 kN was 303.60 mm.

Fig. 52. Specimen T9 after loading and ejection from the constraining tube.

The maximum force used to push out test specimen T9 from the constraining tube was 5.00 kN, represented by the first peak in Fig. 53.

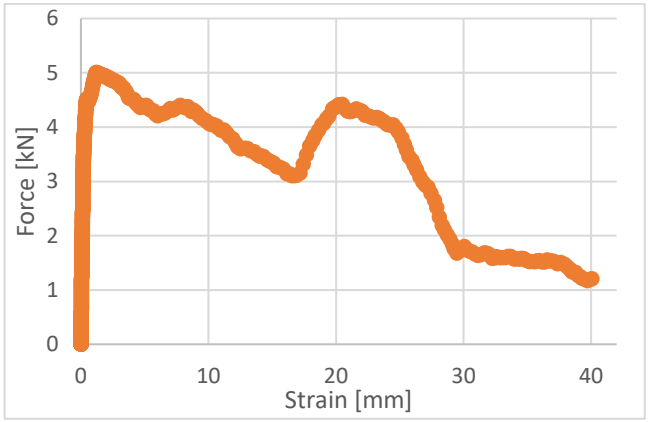

Fig. 53. Frictional force as specimen T9 was pushed out from the constraining tube.

7.3.6. Specimen T10, 4 and 3 cuts

Test specimen T10, seen in Fig. 54, was placed inside the 49.3 mm ID steel tube and loaded in 7 test runs to a maximum load of 82.01 kN. This cutting pattern was used to investigate if the lower part of the test tube could be crushed before initiating compaction in the upper part, and see how this could affect the force-deformation curves. In the first test run, a longer extension rod was again used to

reduce the number of test runs, and the inner tube was centered prior to loading. Unfortunately, the extension rod overturned again. Three instances of unknown errors where the press suddenly stopped also contributed to the high number of test runs. The crushed pipe was ejected using the digital hydraulic press.

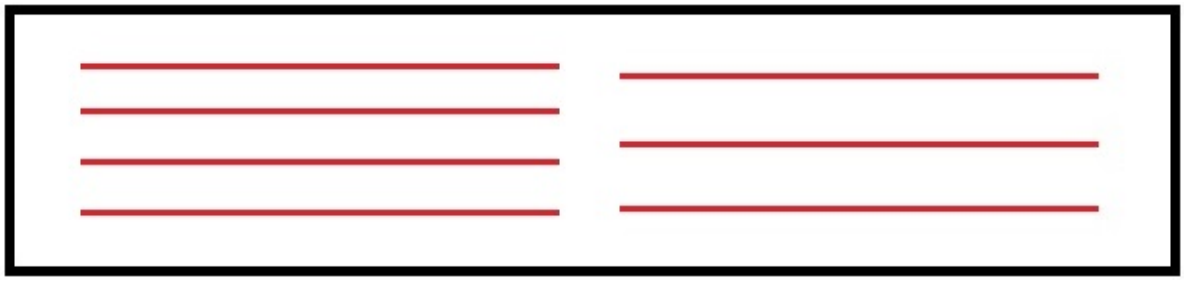

Fig. 54. Cutting pattern of specimen T10, where the uncut ends were approximately 10 mm long. The cuts were all roughly 185 mm long, while the longitudinal spacing between the cuts was around 10 mm.

The test results from specimen T10 can be seen in Fig. 55. During the first test run, seen in Fig. 55a, the force followed an approximately linear curve until reaching a peak load of 15.52 kN, followed by a rapid drop in force combined with some deformation. The extension rod overturned at the end of this test run, and is not certain whether some of the data points are invalid. The second test run, seen in Fig. 55b, is near-linear until the curve flattens out for a short deformation at around 6.1 kN before continuing to increase until reaching a peak load of 8.79 kN. After this, the force dropped as deformation continued until an unknown error caused the test to stop. The third test run, seen in Fig. 55c, seemed to run smoothly, but the results show a negative force during most of the deformation. This is not realistic, but since the second test run ended with a force of 0.91 kN and the third test run experienced the first drop in force after a peak load of 0.34 kN, one can assume that the force presented as negative during the third test run was between 0 kN and 1 kN. This will be discussed further in Section 7.4.3. The third test run ended with a force of 4.17 kN, which is relatively close to 7.46 kN where the fourth test run started to deviate from the straight line, as seen in Fig. 55d. The test runs represented by Fig. 55e and f both stopped abruptly without any known reason, and since the fourth test run terminated with a force of 72.27 kN while increasing, the deformation during the low forces in these test runs may not be valid. The last test run, seen in Fig. 55g, had a smooth increase in force while the inner tube was compacted.

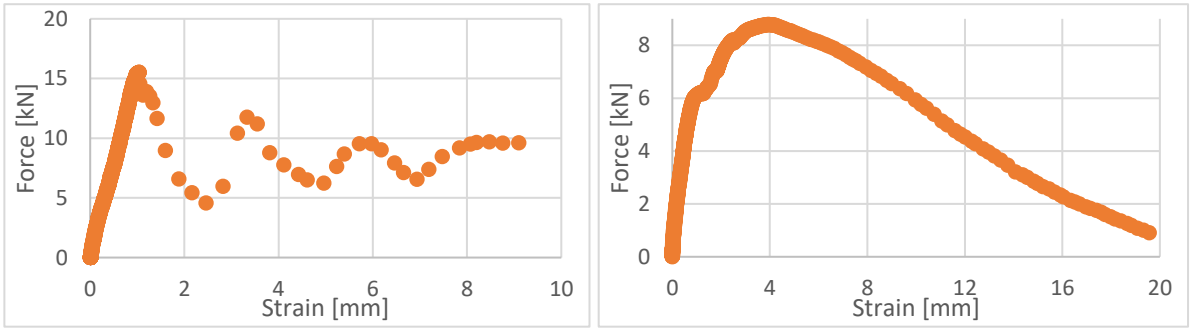

a) b)

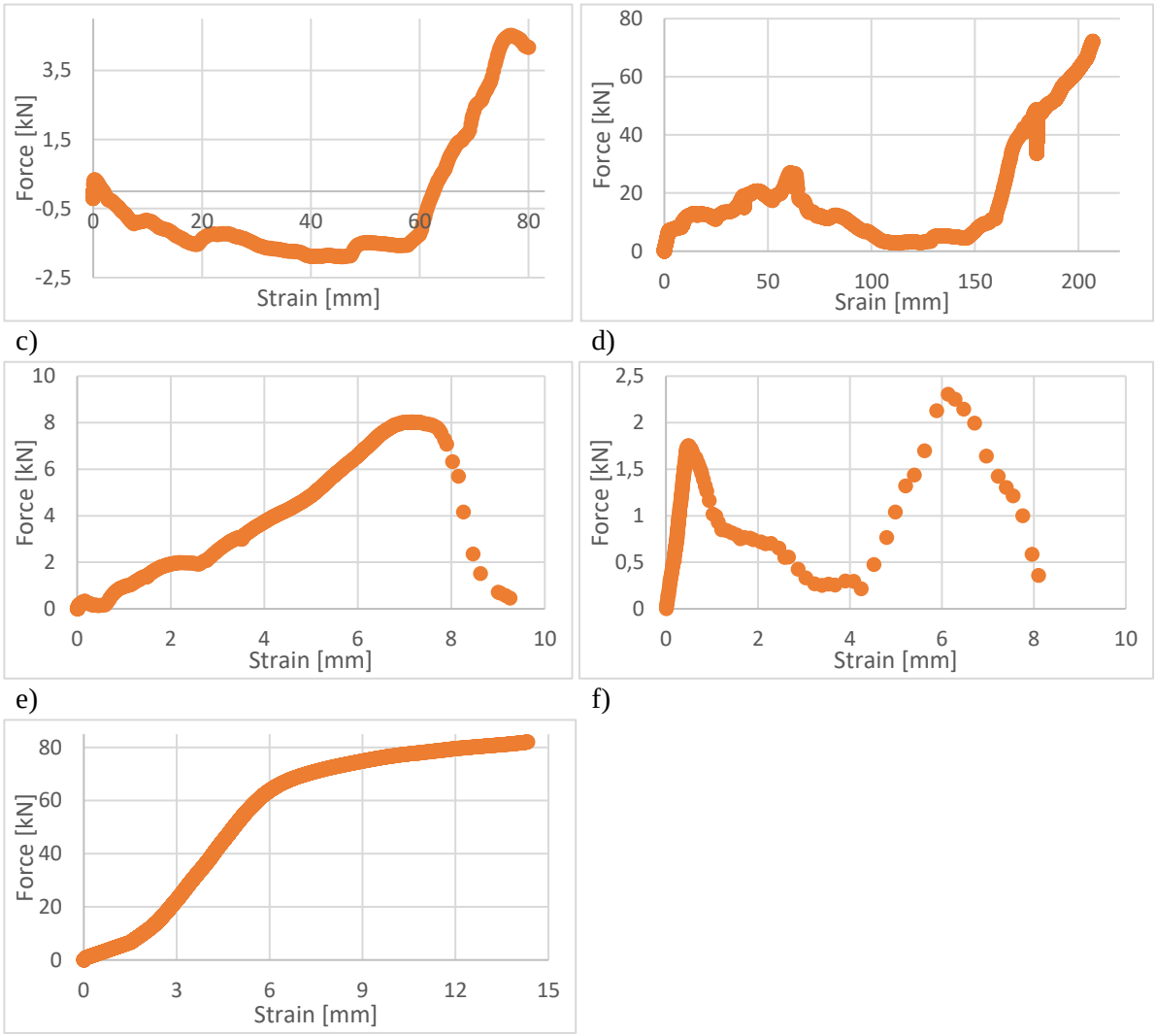

Fig. 55. Test results from loading of specimen T10.

The total strain from Fig. 55 is 347.31 mm. The manually measured length of specimen T10 after compaction, as seen to the left in Fig. 56, was 76.6 mm, which equals a strain of 323.4 mm. Since the overturning of the extension rod during loading of specimen T9 did not seem to produce additional, invalid deformation, none of the data points from the first test run will be removed. Since the load during the fourth test run exceeded 48 kN, the results from Fig. 55e and f will not affect the calculation of total strain at this load. The strains from the first four test runs are therefore assumed to be correct and related to plastic deformations, which results in a total strain of 291.10 mm after reaching a load of 48 kN.

This test run aimed to verify whether it was possible to make the bottom end of the test specimen compact before the top part. As seen in the middle and right picture in Fig. 56, the compaction did indeed start at the bottom where the specimen had been weakened with the most longitudinal cuts

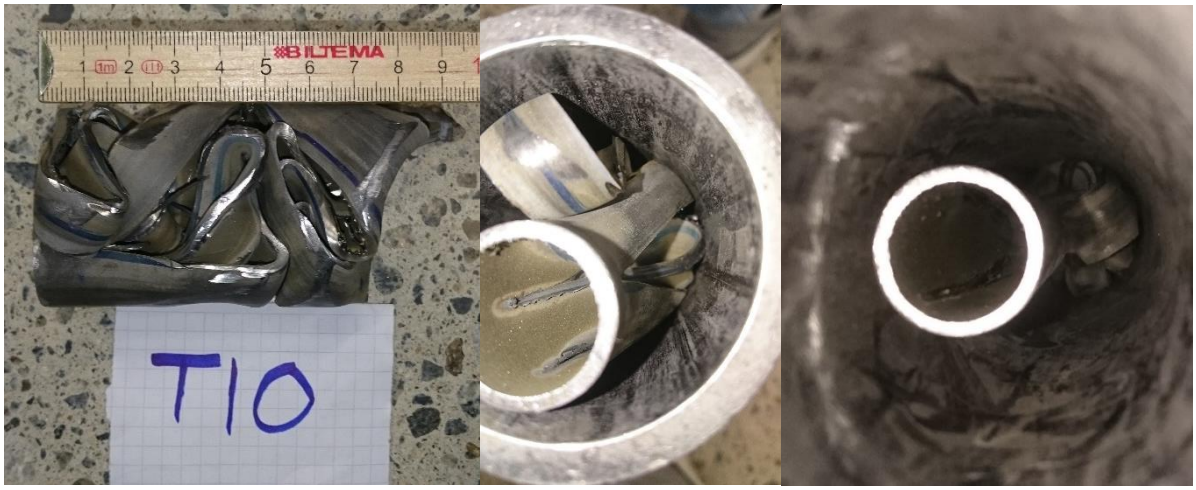

Fig. 56. To the left, specimen T10 is seen after loading and ejection from the constraining tube. In the middle and to the right, the test specimen is seen inside the constraining tube from the bottom and the top, respectively, after the third test run.

During ejection of specimen T10 from the constraining tube, the force reached a value of 1.94 kN, before dropping for a very short strain. The force quickly built up again, reaching a maximum value of 2.11 kN, followed by increasing strain while the force decreased.

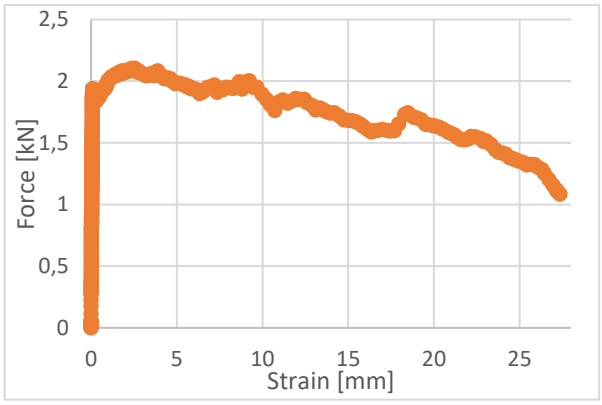

Fig. 57. Frictional force as specimen T10 was pushed out from the constraining tube.

7.3.7. Specimen T11, 4 dashed cuts

Test specimen T11, seen in Fig. 58, was placed inside the 49.3 mm ID steel tube and loaded in 3 test runs to a maximum load of 82.00 kN. The slot lengths were chosen arbitrary, but it is believed that both the slot lengths and the spacing could have a significant effect on the strength of the specimen. As an example, using long slots with very short spacing would approach the behavior of a continuous cut pipe, while short slots with long spacing should behave more like an uncut pipe. The press stopped abruptly without any known reason during one of the test runs. The crushed tube was ejected using the digital hydraulic press.

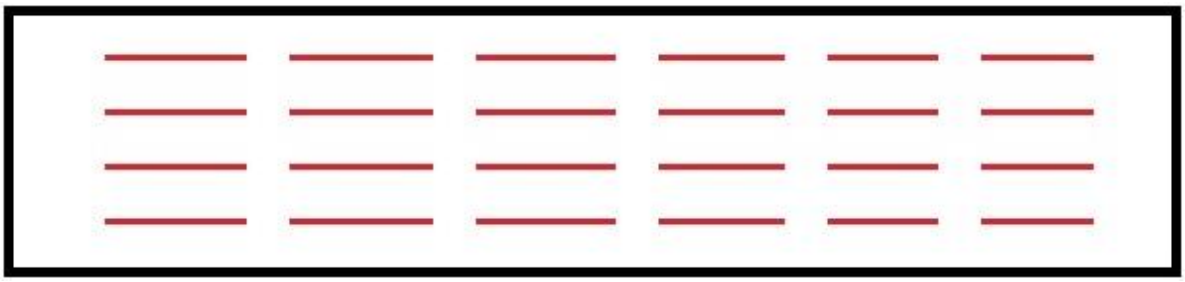

Fig. 58. Cutting pattern of specimen T11, where the uncut ends were approximately 10 mm long. The slots had a length of roughly 60 mm while the spacing was around 5 mm.

The test results from specimen T11 can be seen in Fig. 59. During the first test run, seen in Fig. 59a, the force-strain curve increased linearly until reaching a peak value of 29.18 kN, after which the force rapidly dropped while the inner tube deformed. The test run ended at a force of 1.14 kN while increasing due an unknown error. In the second test run, seen in Fig. 59b, the initially linear curve started to flatten out and decrease after a peak value of 1.87 kN, most likely resuming the compaction which terminated in the previous test. Like with the results from specimen T10, the graph from the second test run shows negative force values. This will be discussed in Section 7.4.3, but it will again be assumed that these negative values are just very low forces, most likely below the peak of 1.87 kN. After returning to positive values, the force rapidly built up to a new peak of 25.62 kN, followed by a decrease in force while strain continued. The third test run, seen in Fig. 59c, started to flatten out at approximately the same force as where the second test run ended.

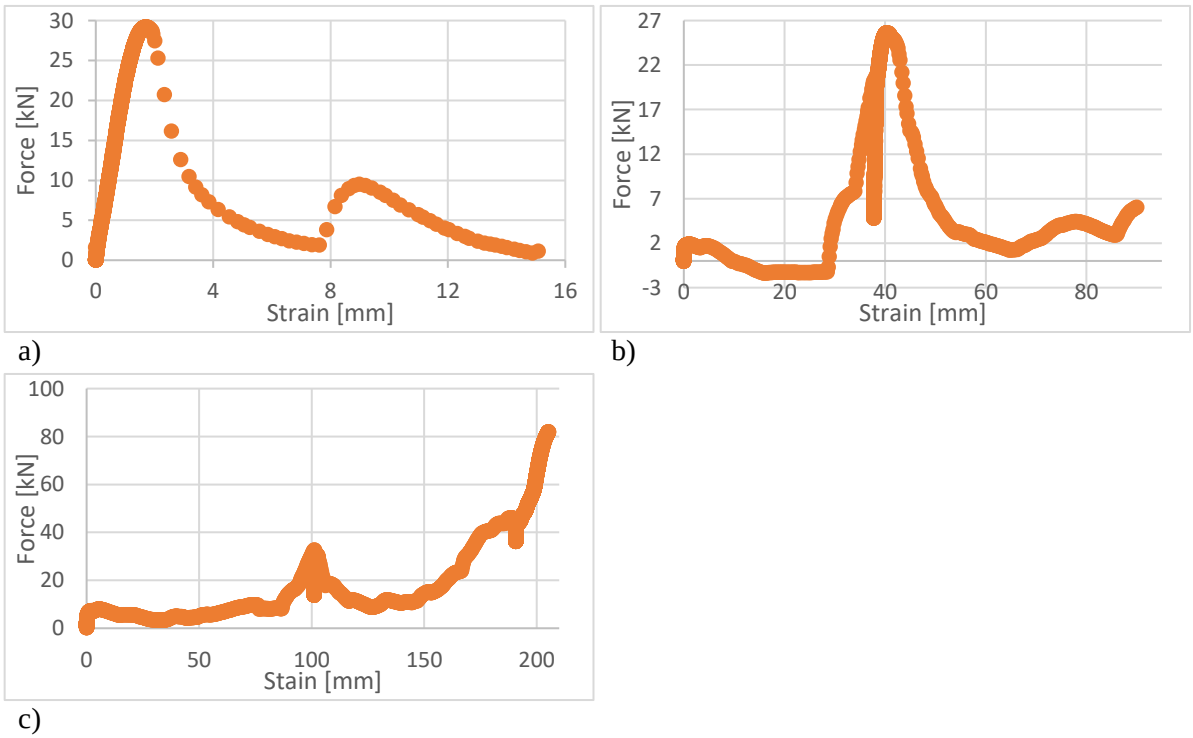

Fig. 59. Test results from loading of specimen T11.

The cumulative strain in Fig. 59 is 310.31 mm. Manual measurement of specimen T11 after crushing, as seen in Fig. 60, gave a length of 90.0 mm, which equals a strain of 310.0 mm. These results are almost identical, and it will be assumed that the strains seen in Fig. 59 are correct and related to permanent deformations. This assumption gives a total strain of 299.50 mm after reaching a load of 48 kN.

The crushing pattern of specimen T11, as seen in Fig. 60, was similar to the crushing pattern observed for the other specimens that were weakened. Some of the slot spacings had been ripped apart, creating longer slots.

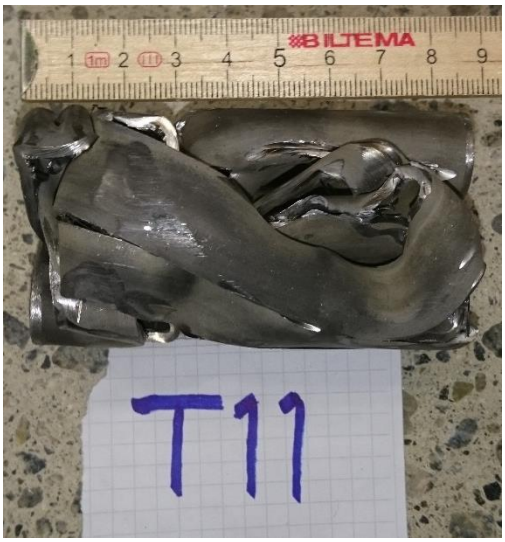

Fig. 60. Test specimen T11 after loading and ejection from the constraining tube.

When adjusting the piston so that it touched the prism before the start of each test run, a button was pressed that lowered the piston down. When the piston came in contact with the prism, the press applied a relatively small amount of force before unloading some of this force and then locking in place. However, this small amount of force was enough to start pushing specimen T11 out of the constraining tube, and no recordings of the applied force is therefore available. This suggests that the force can be assumed to be the lowest of all the ejection forces recorded with the digital hydraulic press.

7.3.8. Specimen T12, 1 cut

Test specimen T12, seen in Fig. 61, was placed inside the 49.3 mm ID steel tube and loaded in 5 test runs to a maximum load of 82.00 kN. In the first test run a last attempt was made to maximize the initial deformation by using a new extension rod which fit better inside the constraining tube than the previous ones. During loading, this extension rod started to slowly move sideways, and the test was stopped. The specimen was inspected and measured before continuing. In the second test run, the specimen was loaded to a predetermined maximum force of 48 kN. This loading did not initiate crushing, and since the tube had no frictional contact with the constraining tubular wall, the specimen was taken out for inspection. A new maximum force of 82 kN was selected since the results from the 48 kN load had already been documented. After the tests, the crushed tube was ejected using the digital hydraulic press.

Fig. 61. Cutting pattern of specimen T12, where the uncut ends were around 10 mm long and the cut was roughly 380 mm long.

The test results from specimen T12 can be seen in Fig. 62. The force seemed to increase logarithmically during the start of the first test run, as seen in Fig. 62a, until reaching a peak value of 20.43 kN. After this, the force decreased quickly, before again increasing to a new peak of 23.18 kN. The test run was stopped manually when the extension rod started to move laterally, and some of the data points may be linked to the movement of the extension rod rather than deformation of the test specimen. The second test run, seen in Fig. 62b, showed continuous increase in force during the compaction of the inner tube, and ended at a force of 48.01 kN while starting to flatten out. The same deformation most likely continued in the third test run, seen in Fig. 62c, reaching a peak load of 50.05 kN before the force dropped rapidly during a large strain. The curve in the start of the fourth test run, seen in Fig. 62d, deviates from linearity at around the same force as the previous test run ended with, which is also the case for the graph in Fig. 62e.

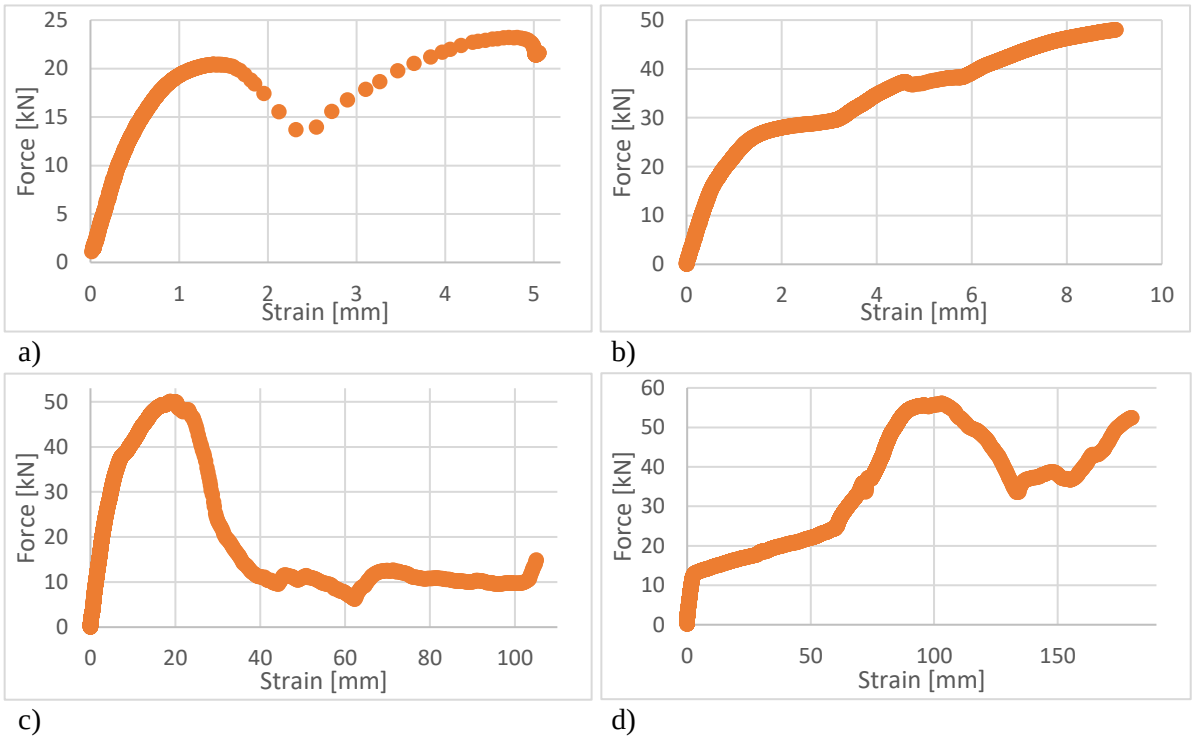

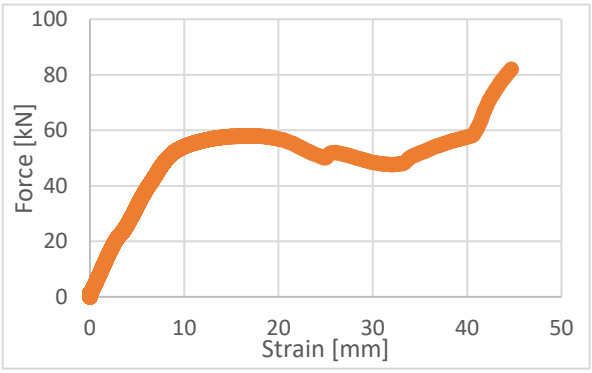

e)

Fig. 62. Test results after loading of specimen T12.

The sum of all the strains in Fig. 62 is 343.72 mm. The manually measured length of specimen T12 after crushing, as seen in the upper-left picture in Fig. 63, was 71.3 mm, which equals a strain of 328.7 mm. After the first test run, the specimen was measured and revealed a shortening of around 2 mm, and the deformation can be seen in the top-right picture in Fig. 63. This means that only the first two millimeters of the strain in Fig. 62a should be accounted for. The measured length after the second test run confirms this, as adding two millimeters to the total strain seen in Fig. 62b matches almost perfectly with the length of the specimen after the second test run, seen in the bottom in Fig. 63. This adjustment results in a total strain from Fig. 62 equal to 340.67 mm, which is close to the manually measured strain, and the strain from the test runs after the adjustment will therefore be assumed to correct and related to permanent deformation. With this assumption, the strain at 48 kN was equal to 11.04 mm.

After the second test run the specimen was examined, and an opening of the cut had started to form in the top section of the tube, which can be seen in the bottom picture in Fig. 63, marked with the number “1”. This area of the pipe seemed like an inflection point of the sinusoidal shape of the specimen, and on the upper side of the opening, the tube had a decreased radial curvature. This flattening would make this a weak point in the structure, acting like a hinge, which was confirmed both by the force required to initiate crushing in the third run, which was only 2 kN above the end-force in the previous test run, and by inspection inside the constraining tube after the third test run. This inspection revealed two hinges in the test specimen, one at the opening in the cut, marked with the number “1”, and the other at what seems to be a local minimum of the sinusoidal shape of the pipe, marked with the number “2” (this can be seen in Fig. 83).

Fig. 63. The top-left picture shows specimen T12 after loading and ejection from the constraining tube. The top-right picture shows the bent test specimen after the first test run, and the bottom picture shows the buckled specimen after the second test run.

The force required to push specimen T12 out of the constraining tube can be seen in Fig. 64. The strain at the very start of the curve is due to the piston not being in contact with the prism at the start of the test, and is therefore not related to movement of the crushed tube. At around 4.2 kN, the curve deviates from its linear characteristic, and the crushed tube was pushed out as force increased until a peak load of 5.92 kN was reached.

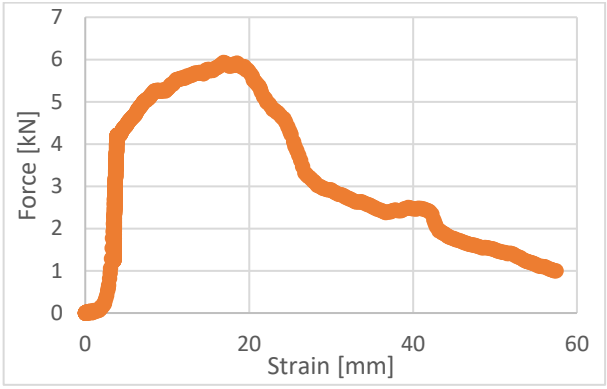

Fig. 64. Frictional force as specimen T12 was pushed out from the constraining tube.

7.3.9. Specimen T13, 4 and 3 cuts

Test specimen T13, seen in Fig. 65, was placed inside the 36.8 mm ID steel tube and loaded in 4 test runs to a maximum load of 42.02 kN. This was a different steel tube than the one that was deformed

during testing of T5, but was made from the same original pipe. Since the previous constraining steel tube of the same dimensions had only been deformed at the bottom where the crushed tube was, the deformation may have been due to the large forces during the last test runs. It was therefore decided to test this tubular size again to see if the inner tube could be loaded to 48 kN without the constraining tubular being plastically deformed. One of the test runs stopped due to an unknown error, and the specimen was ejected using the digital press.

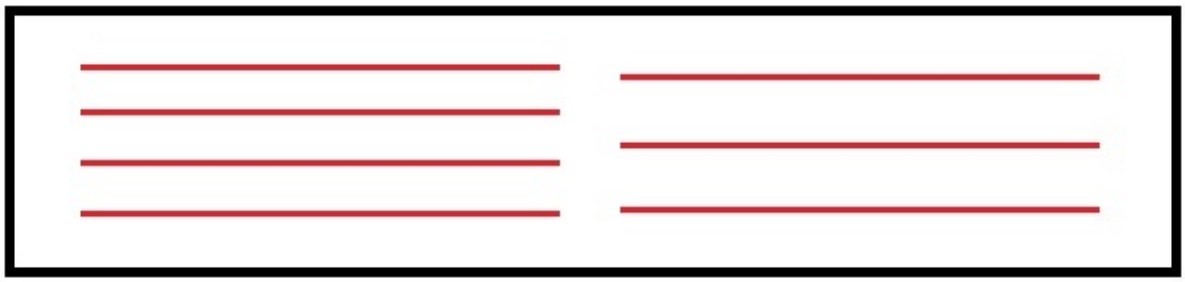

Fig. 65. Cutting pattern of specimen T13, which was similar to that of specimen T10, only this would be compacted within the small steel tube. The uncut ends were approximately 10 mm long, while the cuts were around 185 mm long. The longitudinal spacing between the cuts was roughly 10 mm.

The test results from specimen T13 can be seen in Fig. 66. The first test run, seen in Fig. 66a, had a steep increase in force until a peak load of 27.70 kN was reached, after which the force decreased as crushing progressed. The force built up to a new peak of 32.28 kN before dropping rapidly until the test commenced at 19.04 kN. The second test run, seen in Fig. 66b, started with a near-linear curve until reaching a peak load of 30.05 kN. Subsequently, three other peaks were reached, each higher than the previous, with semi-linear drops in force in between. The last peak of 38.48 kN was followed by a steadily decrease in force as the inner tube deformed and ended with a load of 21.93 kN. The third test run, seen in Fig. 66c, reached a maximum force of 9.74 kN before the test ended abruptly for no known reason. What seems to be plastic deformation in the beginning of Fig. 66d started almost immediately, which was expected after the end-force of 0.41 kN in the third test run. The last test run was supposed to reach a maximum force of 48 kN, and it is not known why it only reached 42.02 kN. It was not discovered until reviewing the results a couple of weeks after the experiment was finished, but the most logical reason is that 42 kN was set as the predetermined maximum load by mistake. The reason for this may be the likeliness between this number and the previous force limit of 82 kN.

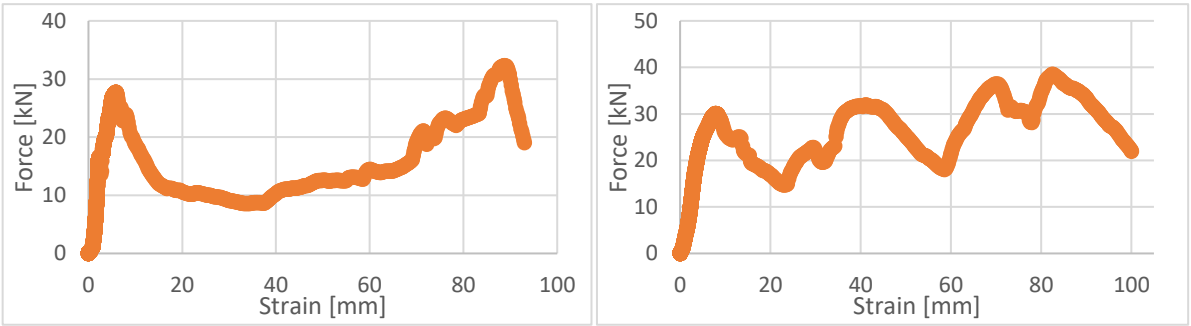

a) b)

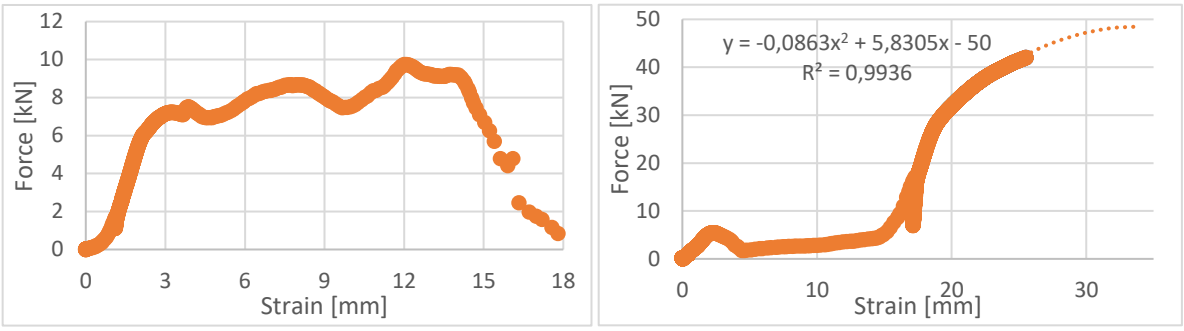

c) d)

Fig. 66. Test results from loading of specimen T13.

The total strain in Fig. 66 adds up to 236.67 mm. Manual measurement of specimen T13 after crushing, as seen in the top of Fig. 67, gave a length of 200.7 mm, which equals a strain of 199.3 mm. This is much lower than what was measured by the press, but this may be due to abnormally high elastic strain during this test. Between the 15 and 16 cm marks in the top picture in Fig. 67, the shape of the crushed test specimen looks like it could build up over a centimeter of elastic strain, and looks similar to the shape of some modern prosthetic legs. Elastic deformation may therefore be the reason for the big difference between the strain measured by the press and the manually measured strain. To estimate the strain at 48 kN, polynomial extrapolation was performed based on the values between 30 kN and the end data point. This gave an additional strain of 5.92 mm, but there is high uncertainty related to this value, as there is no way of knowing how the curve would look like beyond what was measured. Both the extrapolation equation and the R^2 value are presented in Fig. 66d. The results from the first test run will assumed to be correct for the discussion in Section 7.4.

After the first test run, the inside of the constraining tube was inspected, which revealed a much greater compaction of the lower section of the test tube compared to the upper section. However, from the upper picture in Fig. 67, it can be observed that the compaction of specimen T13 was much greater in the top than in the rest after ejection. It is believed that the lower part of the tube was not weakened enough, so deformation of the upper section started too early. After the second test run, some deformation of the constraining tube was observed, as seen in the bottom picture in Fig. 67. This deformed area was located approximately in the middle of the tube. By inspecting the inside of the constraining tube, it was clear that the inner tube has been crushed past this deformed point. Still, during the second test this deformation may have acted as an anchoring area for the inner tube, which could require increased force to move past. However, it will be assumed that this deformation had to effect on the results.

Fig. 67. The top picture shows specimen T13 after loading and ejection from the constraining tube. The bottom picture shows deformation of the constraining tube, as seen after the second test run.

The force-strain curve during the process of pushing out the crushed specimen, as seen in Fig. 68, started to flatten out at around 17.4 kN and reached a plateau with a maximum force of 23.24 kN. The ejection process was performed in two test runs, and forces above 20 kN was also seen in the last one. This suggests that most of the friction was related to the top of the crushed tube, which is where compaction was the greatest. The sudden spike at the end of Fig. 68 was caused by the prism touching the constraining tube.

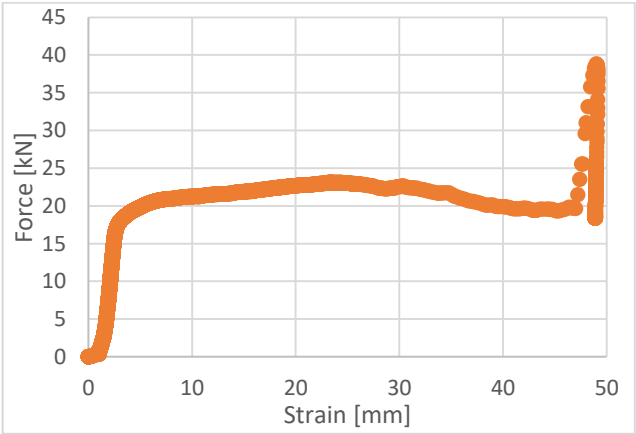

Fig. 68. Frictional force as specimen T13 was pushed out of the constraining tube.

7.3.10. Specimen T14, 2 cuts

Test specimen T14, seen in Fig. 69, was placed inside the 49.3 mm ID steel tube and loaded in 5 test runs to a maximum load of 42.31 kN. The maximum load was meant to reach 48 kN in this test as well, but the input from the previous specimen was still saved in the software. The first two test runs stopped abruptly for unknown reasons, and one test run terminated early because a maximum strain of 10 mm was fed into the software instead of 100 mm. The specimen was ejected using the digital press.

Fig. 69. Cutting pattern of specimen T14, where the uncut ends were around 10 mm long and the cuts were roughly 380 mm long.

The test results from specimen T14 can be seen in Fig. 70. An unknown error caused the first test run, seen in Fig. 70a, to stop abruptly. In the second test run, seen in Fig. 70b, the force increased near-linear until reaching an initial peak of 8.65 kN, before dropping rapidly. The force then continued to increase with increasing strain, until it reached a new peak of 16.63 kN, followed by a near-linear decrease in stress during what seemed to be crushing of the inner tube. The second test run ended due to an unknown error with a decreasing force-strain curve at a load of 0.86 kN, which is far below where the third test run, seen in Fig. 70c, starts to deviate from linear, which was around 2.9 kN. The peak force-value during the third test run was equal to 3.46 kN, and after passing this, the strain rate started to increase until the test stopped due to a wrong predetermined maximum strain limit of 10 mm. The graph in the fourth test run, seen in Fig. 70d, shows an almost continuously increasing force until reaching a maximum of 38.03 kN. In the fifth test run, seen in Fig. 70e, the curve starts to deviate from linear at around 9 kN less that the end-load of the fourth test run. The load then dropped, before increasing to a second peak of 41.74 kN, followed by a new drop and increase in force, after which the test was automatically stopped at 42.31 kN.

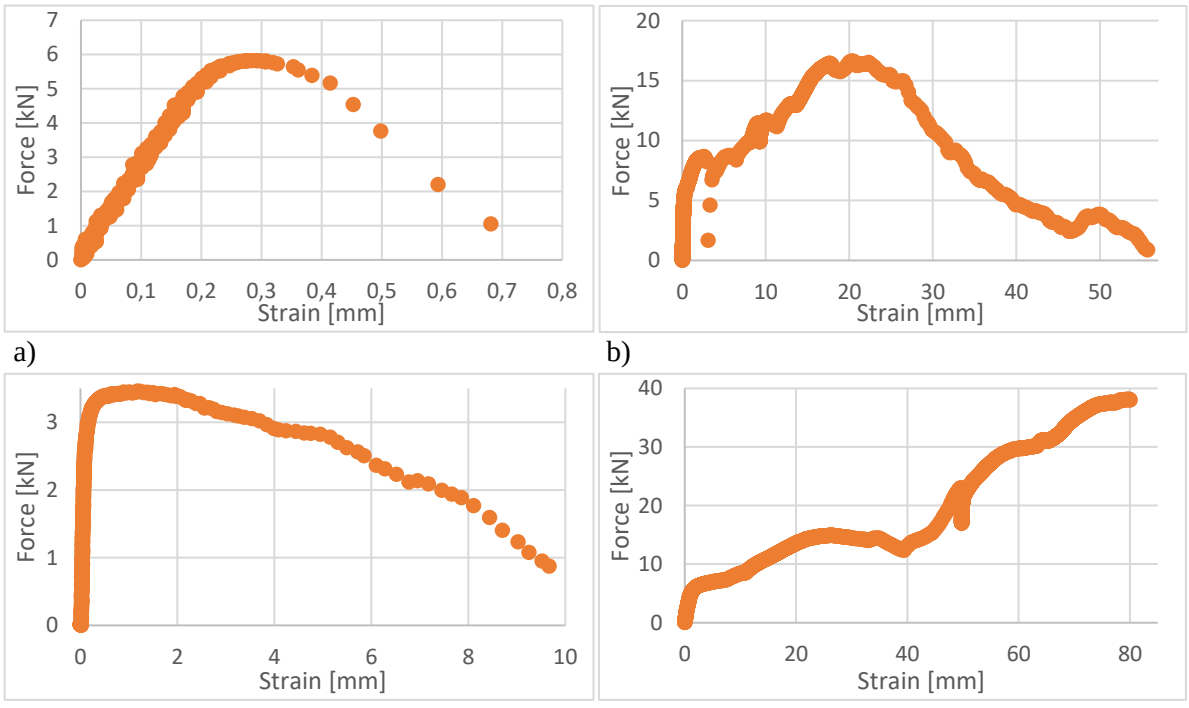

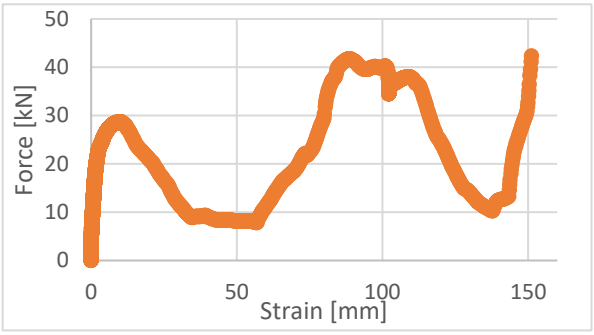

e)

Fig. 70. Test results from loading of specimen T14.

The cumulative strain in Fig. 70 is 297.28 mm. Using a fractional caliper, the length of specimen T14 after crushing, seen in the upper-left picture in Fig. 71, was measured to 95.9 mm, which equals a strain of 304.1 mm. The two measurements are very close to each other. Because of the steep force-strain curve at the end of the final test run, it may be assumed that no significant permanent deformation would take place if the specimen had been loaded to the intentional load of 48 kN. Compared to the test results from the other specimens at approximately the same total strain, this assumption seems valid. It will therefore be assumed that the measured length of the crushed specimen would be the same if it was loaded to 48 kN.

After the first test run, the specimen was examined and measured. The lower picture in Fig. 71 shows the sinusoidal buckling of the pipe. The shortening due to this plastic deformation was barely measurable, as seen in the top-right picture in Fig. 71, which was also confirmed by the results in Fig. 70a.

Fig. 71. The upper-left picture shows specimen T14 after loading and ejection from the constraining tube. The bottom picture shows the specimen after the first test run, while the upper-right picture shows the insignificant strain after this test run.

During ejection of the crushed tube, the force rose steeply until reaching an initial peak of 7.73 kN, as seen in Fig. 72. Continuing to increase, the force subsequently reached a maximum load of 9.17 kN, after which it decreased while the crushed pipe was pushed out from the constraining tube. At the end

of this test run, the hydraulic pump registered some negative force values, like it had in previous test, but this has no impact on the results from the ejection.

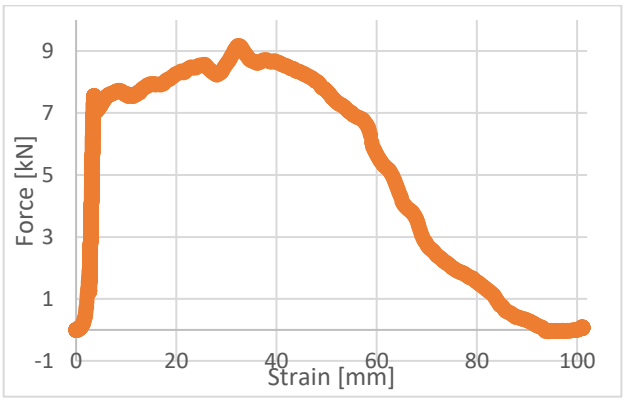

Fig. 72. Frictional force as specimen T14 was pushed out of the constraining tube.

7.3.11. Specimen T15, 2 cuts

Test specimen T15, seen in Fig. 73, was placed inside the 49.3 mm ID steel tube and loaded in 2 test runs to a maximum load of 42.08 kN. As with the two previous tests, the maximum load was intended to be 48 kN. In addition, this specimen was initially intended to be compacted within the small steel tube, but after the deformation of this constraining tube during crushing of T13 it was instead decided to use the large steel tube. The crushed pipe was ejected using the digital press.

Fig. 73. Cutting pattern of specimen T15, which was aimed to be identical to that of specimen T14. The uncut ends had a length of around 10 mm and the cuts were roughly 380 mm long.

The test results from specimen T15 can be seen in Fig. 74. In the first test run, seen in Fig. 74a, the force increased linearly until reaching a peak load of 28.06 kN. The force then dropped and increased two times before reaching a third peak load of 32.52 kN, after which crushing presumably occurred. Towards the end of the test run, the force increased to 42.03 kN before the test ended. The second test run, seen in Fig. 74b, reached a peak load of 39.51 kN before large strains took place while the force decreased. After a relatively large strain, the force started to increase again, reaching a maximum value of 42.08.

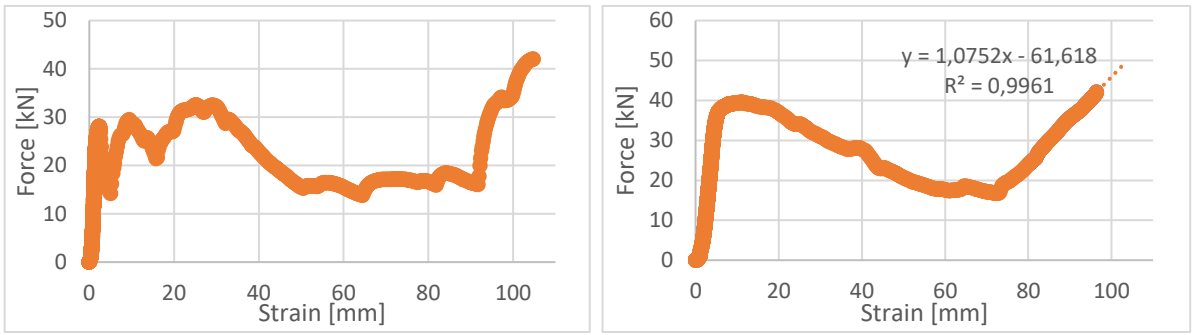

Fig. 74. Test results from loading of specimen T15.

The total strain from the two test runs seen in Fig. 74 is 201.13 mm. The manually measured length of the crushed tube, as seen in Fig. 75, was 201.3 mm, giving a strain of 198.7 mm. The two measurements are very similar. Linear extrapolation of the force-strain curve, using the values between 24.10 kN and the last data point as inputs, gives a strain of 101.95 mm at the intended force limit during the second test run. This results in an additional strain of 5.56 mm at 48 kN. Both the extrapolation equation and the R^2 value are presented in Fig. 74b. It will be assumed that the extrapolated value is correct when discussing the results, but there is a large uncertainty related to this assumption.

Only the top of specimen T15 was compacted during the test runs, as seen in Fig. 75. The crushing of the upper part of the tube most likely distributed some of the axial compressive force to the walls of the constraining tube, increasing friction and reducing the load on the lower part of the specimen.

Fig. 75. Specimen T15 after loading and ejection from the constraining tube.

The load during ejection of specimen T15 from the constraining tube is presented in Fig. 76. The crushed tube started to move at around 3 kN, which can be seen in Fig. 76 as where the curve deviates from its initial linear characteristic. The force continued to increase until reaching a maximum load of 7.26 kN.

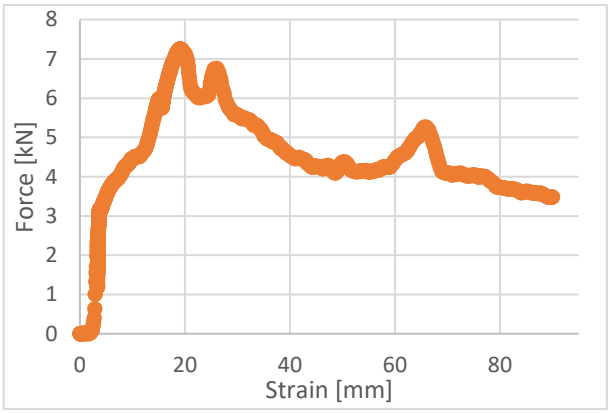

Fig. 76. Frictional force as specimen T15 was pushed out from the constraining tube.

7.4. Summary and Discussion

7.4.1. Summary of Results and Analysis

A summary of the results from the experiment is presented in Table 9. Here, several different foundations for comparison are presented, and the reason for these are given below:

- *Constraining tube:*
  The ID of the constraining tube should have a significant impact on the compaction process, as discussed in Section 6.6.2, and will be discussed further in Section 8.3.2.

- *Cutting pattern:*
  The different selections regarding the cutting pattern will affect the load capacity of the tube. The number of cuts in Table 9 represents the number of longitudinal cuts. Dashed means that the longitudinal cutting pattern is dashed instead of continuous.

- *Maximum force for 10% strain:*
  To compare the forces required to initiate crushing, 10% strain was used to ensure that buckling would not be considered as crushing.

- *Maximum force for 50% strain:*
  Based on the results from the first full-scale experiment in Chapter 5, the expected compaction ratio in the planned full-scale experiment in Chapter 6 is around 50%. Therefore, it might be interesting to compare the forces required to reach this strain value.

- *Strain at 48 kN and 82 kN:*
  It is important to compare the effects of different cutting patterns and radial clearances to the achieved compaction ratios at different applied loads. The selected loads are meant to represent scaled values of the forces planned for the full-scale experiment in Chapter 6, as discussed in Section 7.2. For the specimens that were not loaded to 48 kN, the extrapolated additional strains were added to the manually measured values.

- *Maximum force during ejection:*
  The maximum force during ejection of the crushed specimens from the constraining tubes should represent the friction between the specimen and the wall.

Table 9. Summary of the results from the experiment.

Specimen	Cons-training tube*	Cutting pattern	Max force for 10% strain [kN]	Max force for 50% strain [kN]	Max force during ejection [kN]	Strain at 48 kN [%]	Strain at 82 kN [%]
T3	BS	2 cuts	-	-	Low	-	-
T4	AL	3 cuts	-	-	Low	-	-
T5	SS	4 cuts	14.89	39.69	41.2	56.87	71.22
T6	BS	5 cuts	4.47	11.47	Low	76.88	81.15
T7	BS	3 cuts	21.22	22.37	15.54	74.61	81.15
T8	BS	No cuts	50.34	70.08	11.49	20.33	65.75
T9	BS	4 cuts	9.25	16.82	5.00	75.90	81.78
T10	BS	4 & 3 cuts	15.52	26.65	2.11	72.78	80.85
T11	BS	4 dashed	29.18	29.18	<2.11	74.88	75.50
T12	BS	1 cut	50.05	50.05	5.92	2.76	82.18
T13	SS	4 & 3 cuts	27.70	38.48	23.24	51.30	-
T14	BS	2 cuts	16.63	38.03	9.17	76.03	-
T15	BS	2 cuts	32.52	43.42	7.26	51.07	-

Note: *BS = Big Steel tube, SS = Small Steel tube, AL = Aluminum tube

The results in Table 9 are presented in Fig. 77 through Fig. 80. Fig. 77 shows that increasing the number of continuous longitudinal cuts reduces the required force to initiate compaction, and reduces the necessary force to continue compaction up to 50% strain. Using a mixture of different number of cuts gave results that lies in between the results from the respective number of cuts. The results from dashed cuts indicated far less reduction in strength compared to a continuously cut pipe with the same number of longitudinal cuts. When more than 3 longitudinal cuts are used, the friction seems to be reduced compared to a lower number of cuts. There is however no clear pattern, and large differences in total compaction ratio between specimens T8, T14, and T15 creates additional uncertainty when comparing their respective ejection results. The results from the ejection tests runs also indicate that using a mixture of different number of cuts can reduce the friction, and dashed cuts seems to give less friction than the same number of continuous cuts. The ejection results from specimen T14 and T15, both cut twice, showed that the ejection force was higher for T15. One of the major reasons behind this is likely that T15 was less crushed so that there was less contact area between the specimen and the constraining wall. Based on this, one can assume that the frictional force would increase with an increasing specimen length. It should be noted that the friction forces presented in Fig. 77 are neither adjusted for different maximum loads applied during the tests nor the different lengths of the crushed specimens. Adjusting for the lengths is not straightforward, since the whole length of the crushed tube is not contributing to friction. Multiplying the yield strength of the test specimen with its cross-sectional area gives a yield force of 33.96 kN. The compaction initiation forces for specimens with no cuts and 1 cut were higher than this yield force, while the specimens with 2 or more cuts were crushed at much lower forces.

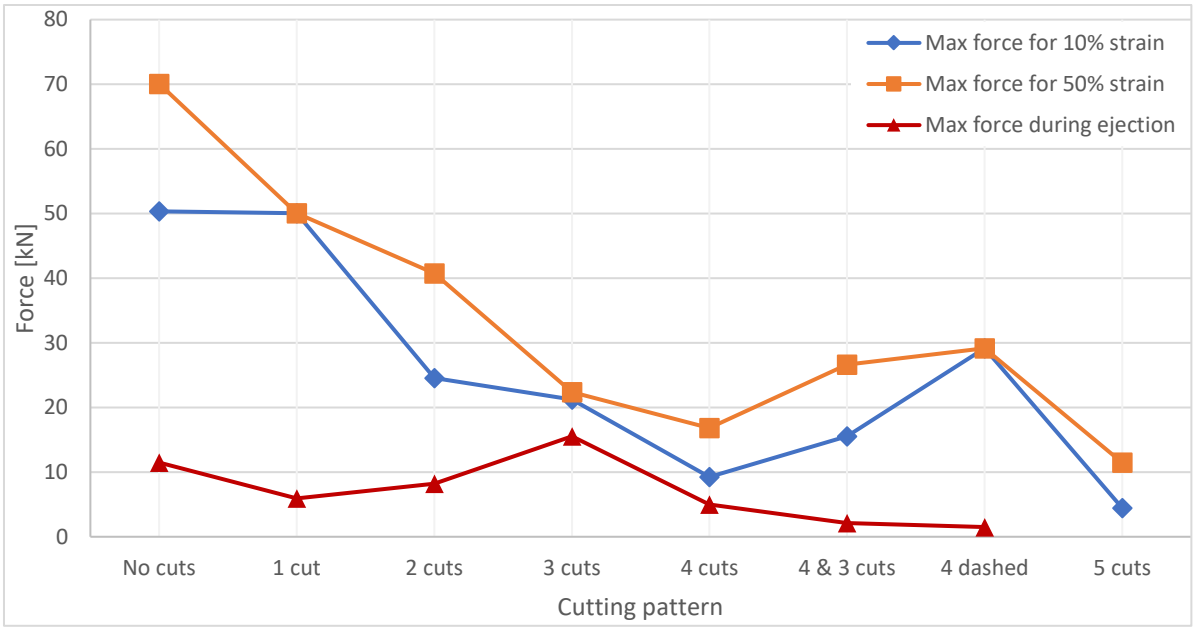

Fig. 77. Plot of different forces resulting in different strains, in addition to maximum forces during ejection of the specimens, using the largest constraining steel tube. For the 4 dashed cuts, the maximum ejection force was arbitrary selected to 1.5 kN, and the average values of T14 and T15 were used for "2 cuts".

Fig. 78 shows that increasing the number of cuts increases the resulting compaction ratio at a load of 48 kN, but the results from a single cut does not follow this trend. The compaction ratio increases insignificantly when more than 3 cuts are used. Dashed cuts and mixed number of cuts gave strains that were less than their continuous and single-pattern cut counterparts. For a load of 82 kN, a single cut gave the highest compaction ratio, but the results for all the cut specimens are very close to each other. Except from the uncut specimen, dashed cuts gave the lowest compaction ratio at 82 kN.

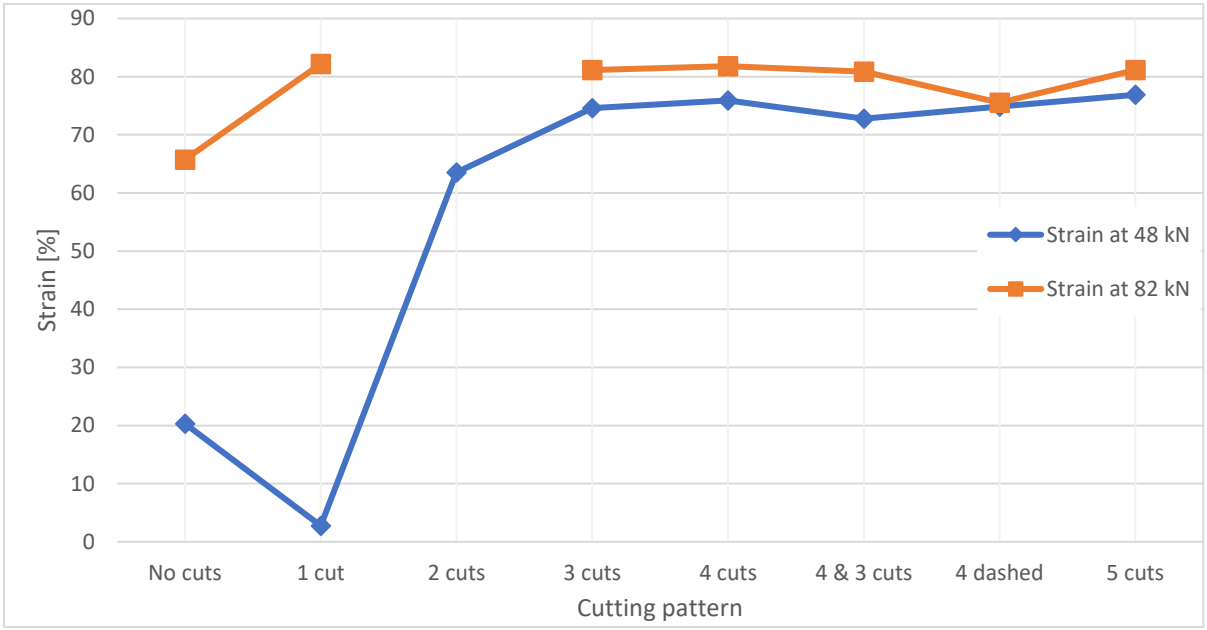

Fig. 78. Plot of strains at different loads for the different cutting patterns using the largest steel tube.

The results show that the specimen with a single cut was less compacted at 48 kN compared to the uncut specimen. This is illogical, and is most likely due to one or several of the sources of error discussed in Section 7.4.3. In Fig. 77 and Fig. 78, the average values of the results for the specimens with 2 cuts were used. However, the results from these specimens are significantly different. This is

most likely also linked to one or several of the sources of error discussed in Section 7.4.3, and will also be used as a foundation for the discussion of repeatability in Section 7.4.4. It should be noted that the large strain difference between specimen T14 and T15 at 48 kN could be a result of a small difference in axial strength. In the last test run during loading of specimen T14, the force reached a peak load of 41.74 kN, just after reaching a total strain of 210 mm, before the specimen was compacted the last 17%. At a cumulative strain of around 200 mm, specimen T15 had a similar load-strain curve as that of specimen T14, but the test was ended at a load of 42.08 kN. If the last test run on specimen T14 had been ended just before reaching 41.74 kN, the total strain for this test would have been 59%, which is much closer to the results of specimen T15.

Fig. 79 compares the measured forces when using the biggest and the smallest constraining steel tubes. The two tests with the smallest constraining tube both showed higher forces for initiating compaction and for reaching 50% strain compared to the same cutting patterns on specimens in a larger tube. The effect of the constraining tubes was most significant during ejection of the crushed specimens, where the measured friction was several times higher when using the smallest constraining tube. This might indicate much greater forces on the walls of a smaller constraining tube compared to a larger one, but might also be a result of deformation and non-flush ID of these tubes, which will be discussed in Section 7.4.3.

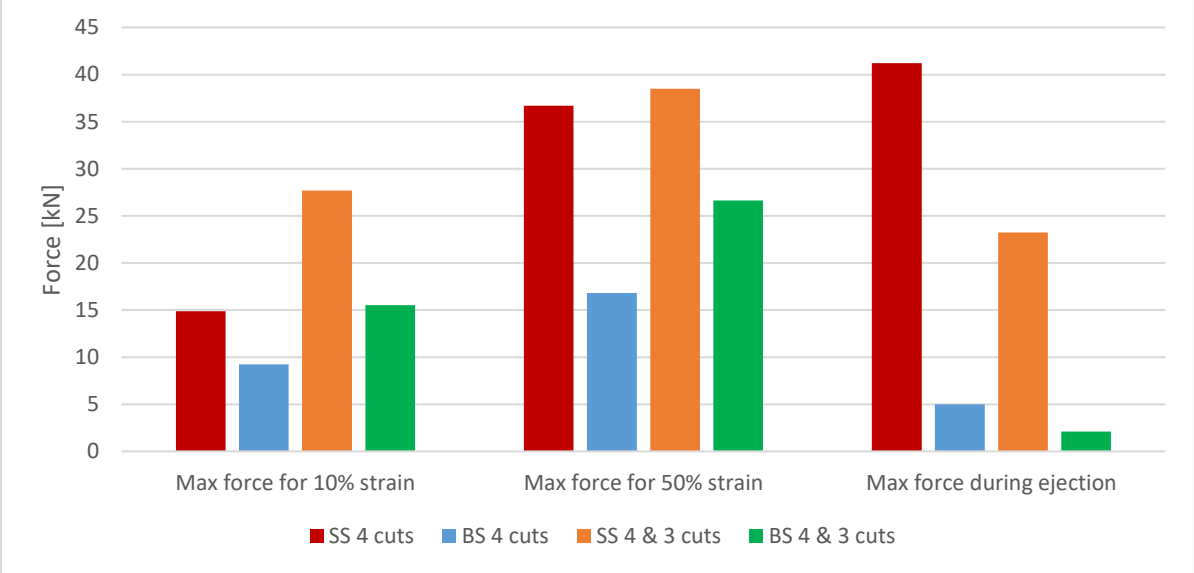

Fig. 79. Comparison of forces between the different constraining tubes and cutting patterns.

The resulting strain between the different constraining tubes are compared in Fig. 80. Both at 48 kN and 82 kN, using a bigger constraining tube gave higher compaction ratios. This was expected, as there was more space for the specimen to be compacted into. A better way of comparing the compaction results between the big and small constraining tube is to look at the occupied cross-sectional area inside the constraining tube, which can be seen in Fig. 81.

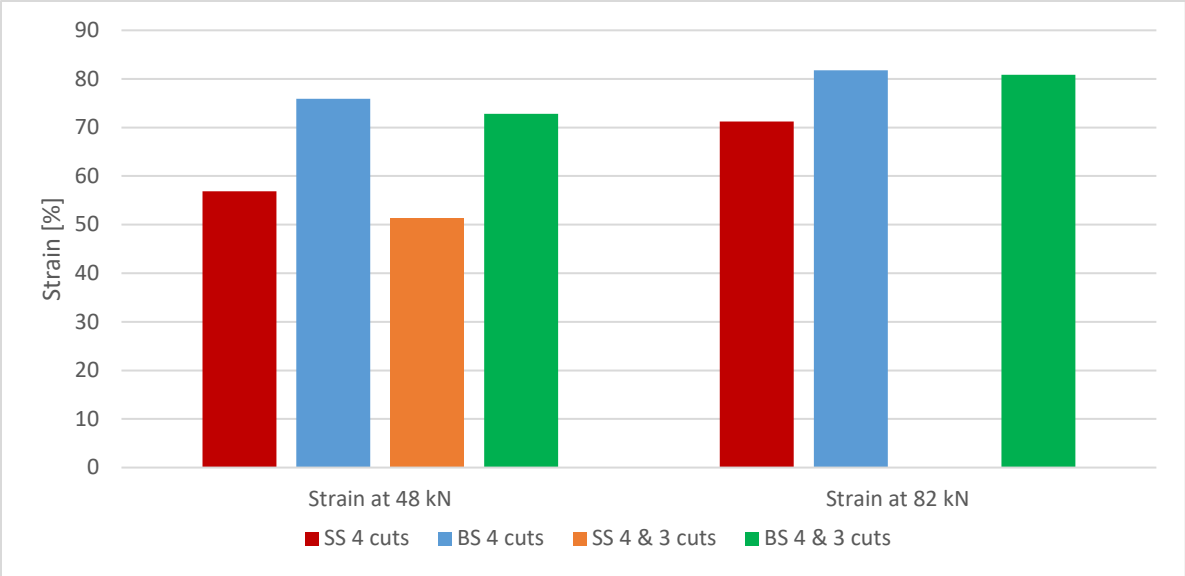

Fig. 80. Comparison of strains between different constraining tubes and cutting patterns.

Fig. 81 compares the occupied cross-sectional area inside the big and small constraining steel tube at different loads. Before any load was applied, the specimens naturally occupied a greater percentage of the area inside the smaller tubes. By calculating the steel volume of the specimen and dividing this by the volume inside the constraining tube with a height equal to the length of the crushed specimen, one obtains the percentage of the cross-sectional area which the specimen occupies. The results presented in Fig. 81 show that the occupied cross-sectional area is almost identical for the same cutting pattern at a load of 48 kN. At a load of 82 kN, the results show that the compaction, or degree of crushing, is greater inside the small tube, even though the compaction ratio is smaller.

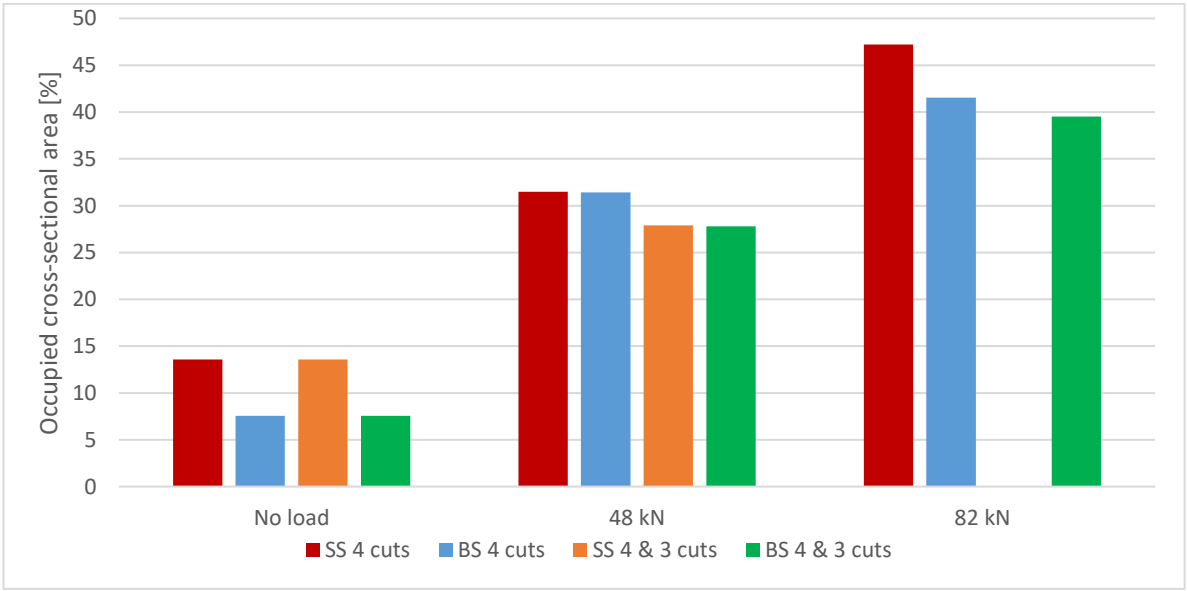

Fig. 81. Comparing occupied liquid space after compaction for different constraining tubes. The load represents the load at which the values where measured.

7.4.2. Compaction Process

The compaction results from specimen T8 in Section 7.3.4, which was uncut, showed evidence of helical buckling in the crushing pattern. The radial clearance between the inner and the outer tube made the moment arm long enough for the tube to be crushed downwards under the applied load. The

same process is evident from the tests on specimen T14, which was cut two times. After the second test run, the top of the specimen had been crushed while the lower section was helically buckled, as seen in Fig. 82.

Fig. 82. Picture taken after the second test run during loading of specimen T14. The specimen in seen from the bottom.

No evidence of helical buckling was seen during loading or after ejection of specimen T12, which was cut a single time. Fig. 83 shows that the specimen may have been sinusoidally buckled instead. The pipe could have been helically buckled in the elastic region before unloading, since it was extruding from the constraining tube after the test run, but not permanently as was the case for specimen T14.

Fig. 83. Picture taken after the third test run during loading of specimen T12. The specimen is seen from the bottom.

For specimen T4, which was cut three times, one of the strands was buckled while the other two were fairly straight, as seen in Fig. 84. This is contrary to specimens with fewer cuts, where the whole pipe buckled instead of individual strands. This compaction initiation is also evident in many of the other specimens in Section 7.3 which had more than two cuts.

Fig. 84. Picture taken after the first test run during loading of specimen T4. The specimen is seen from the bottom.

From what was observed during this experiment, there seems to be no link between the length of the test specimen and the compaction initiation. For all the tests, except the ones with a higher number of cuts in the bottom, the compaction started in the top of the specimen. Specimens T8 and T14 both show evidence of this after ejection, and it is clear that crushing the top section first reduces the transfer of axial force to the bottom of the specimen. Based on what was observed when looking through the constraining tubes after some of the test runs, it seemed like the radial clearance influenced the first bend, since this is directly linked to the moment arm that was created. This was also discussed in Section 6.6.2. Furthermore, increasing the number of cuts seems to enable the initiation crushing before reaching the HBL, and maybe also the LBL, during loading.

7.4.3. Sources of Error

The measured strain from the hydraulic press did not match the manually measured strain for many of the tests. There might be several reasons for this, some of them being:

- *Elastic deformation:*
  Some of the deformation in each test run should be elastic. Since the hydraulic press stopped recording force and strain after the test was stopped, it is not possible to know how large this elastic strain was. The shape of the specimen during loading may influence the amount of elastic strain, and the top picture in Fig. 67 shows a shape that can potentially store large amounts of elastic energy. The total strain related to elastic deformation should increase with the number of test runs and with the load during each test run. This is consistent with specimen T11 and T15, which had the least amount of test runs and the best match between digitally and manually measured strains.

- *Hammering the end of the constraining tube:*
  After most of the test runs, the elastic strain in the bottom of the crushed tube caused it to extrude from the constraining tube. The length of extrusion was barely visible in most cases, but was still enough to make the constraining tube unstable when placed upon a flat surface. To solve this, the bottom of the crushed tube was forced inside the constraining tube by using a hammer. The balance of the constraining tube was checked after each hit with the hammer to minimize the movement of the crushed specimen before the constraining tube was stable. This source of error is believed to be of little importance.

- *Prism not in full contact with extension rod:*
  Before starting each test run, the piston was lowered until touching the prism. A small load was applied on the prism, before some of this load was released. In some test runs, the release of this load caused the inner tube to move slightly, resulting in the extension rod not making full contact with the prism. When the test run started some of the measured deformation would then we related to the extension rod aligning with the prism. In some of the test runs, this source of error was visible enough to be removed before the strain was calculated, like for specimen T8.

- *Extension rod landing on extruding metal:*
  The extension rods did not fill the entire internal area of the constraining tubes. This created a flat area on the top of the crushed specimen where the extension rod made contact, and often some extruding metal adjacent to the extension rod, as seen in Fig. 85. If the extension rod was located on top of this extruding metal before the test was initiated and then proceeded to crush the extruding metal, the height of this extruding metal would then be included in the digital measured strain. This is an error, as this length would have already been accounted for. This is difficult to avoid unless a perfectly fitting extension rod is used. Another way to reduce this error would be to measure any extruding metal pieces after each test run, and then see if they were crushed in the following test run. This was not done in this experiment and would also be difficult to perform accurately, since the crushed specimen cannot be removed from the constraining tube until the test is finished. The extension rod could also land on the extruding metal and slide into the flat area during loading, which would not crush the extruding metal (as most likely happened with specimen T10).

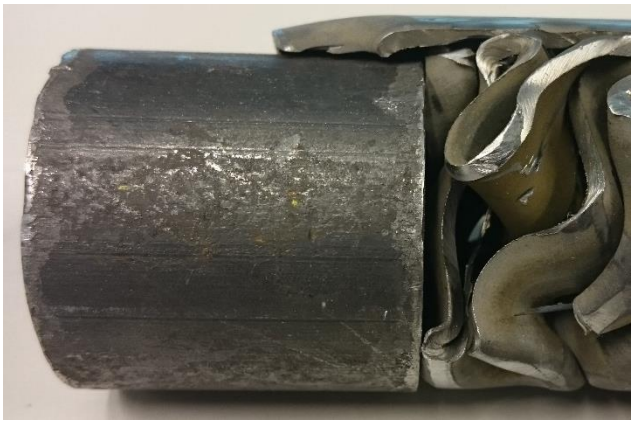

Fig. 85. The extension rods did not fill the entire internal area of the constraining tube. This caused metal pieces to extrude adjacent to the extension rod.

Other sources of error may affect the reliability of the measured forces during the experiment. Some of these are:

- *Hydraulic press calibration:*
  The negative values seen in some of the test runs may have been due to the hydraulic press not being calibrated correctly. In that case, all the results from the experiment should be higher, but the error should be the same for all of them. However, the press was calibrated in 2014, and a professor who frequently used the press had compared the measured forces of this press with another one several times during the last two years without getting any significant

variations. It is therefore assumed that the negative measured force values are related to very low loads.

- *Friction related to extruding metal pieces:*
  Only the friction between the crushed specimen and the constraining wall due to crushing should be present during the experiment. Additional friction caused by extruding metal pieces being lodged between the constraining wall and the extension rods will therefore be a source of error. It is difficult to measure how much friction is related to this and it is not known how much of an impact this may have caused on the results.

- *Not seamless small steel tube:*
  The smallest steel tubes had a welding seam on the inside, most likely resulting in additional friction. It is not known if this additional friction could cause a significant impact on the results.

- *Deformation of small steel tube:*
  The deformation of the smallest steel tubes could affect the compaction results. For the constraining tube used with specimen T5, this deformation did most likely increase the required ejection force. The deformation could also have affected the compaction results, both for T5 and for T13, but the severity of this is not known.

- *Weight of extension rods and prism:*
  The weight of the extension rods and the prism is insignificant compared to the forces used in the experiment. The combined mass of the longest extension rod and the prism equals around 3 kg, while a force of 1 kN equals a mass just below 102 kg. The mass of these objects is therefore not believed to have any significant impact on the results.

7.4.4. Repeatability

The sources of error discussed in Section 7.4.3 reduces the quality of the results. Poor repeatability can also reduce this quality. Because of manual preparation of the test specimens, the repeatability of the cutting patterns is to some extent poor. Not all cuts started and ended exactly 10 mm from the ends of the specimen, and as was seen in Fig. 34, many of the cuts were not straight. The latter resulted in different radial distances between the cuts on the same specimen. There was also some difference in the total length of the test specimens, but this is believed to be negligible.

The only setup that was performed multiple times was two cuts inside the large steel constraining tube. The results from T14 and T15 are significantly different, especially for the required force to reach 10% strain. This poor repeatability is most likely caused by several reasons, which would also be the case for all the other specimens if there had been performed more repeated tests. The main reason for the different results is believed to be the chaotic crushing process together with the inaccurate cuts. The point where the specimen first bends can be a product of the cuts, the eccentricity of the test specimen at test start, the contact area between the extension rod and the test specimen, and several other factors. The poor repeatability can be a result of all these factors varying between each test. However, the comparison of strain for different constraining tubes showed good repeatability when the results were calculated as a percentage of occupied cross-sectional area inside the constraining tubes.

7.5. Conclusions and Recommendations

With minimal repeated tests, it is hard to know the accuracy of the results. However, some conclusions can be made from the experiment:

- Increasing the number of cuts reduces the compaction initiation load and the required force to reach 50% strain.

- Using a smaller constraining tube resulted in higher compaction initiation forces and forces required to reach 50% strain.

- A mixed cutting pattern can be used for selective compaction initiation.

Other observations were also made, but these are not regarded as conclusions:

- Increasing the number of cuts increases the obtainable strain at a load of 48 kN, but the increase is insignificant above 2 cuts.

- Using dashed cuts resulted in a significantly higher compaction initiation force compared to the same number of continuous cuts, and required a higher force to reach 50% strain. The friction, however, was reduced. The strain at 48 kN was approximately the same as for the same number of continuous cuts, but the strain at 82 kN was lower. The results from the slotted specimen is believed to be highly dependent on the slot lengths and spacing.

- Using mixed cutting patterns gave an initial crushing force that was between the two mixed cutting patterns, while the required force to reach 50% strain was higher than both the respective cutting patterns. On the other hand, the friction was much lower. The strain at 48 kN was a little lower for the mixed cutting pattern compared to the individual patterns, but at 82 kN they were roughly the same.

- Using different constraining tubes resulted in the same occupied cross-sectional area at 48 kN, and it was significantly higher for the smaller tube at 82 kN.

- The crushing process seems to be independent on specimen length.

- Increasing the number of cuts seems to reduce the friction when more than 3 longitudinal cuts are used.

Further testing should try to minimize the errors discussed in Section 7.4.3 and aim to maximize the repeatability. Some recommendations for further work are:

- *Center the test specimens by using specially constructed extension rods:*
  By welding a short solid cylinder with an OD slightly less than the specimen ID to the center of an extension rod with an OD slightly less than the constraining tube ID, the tip of the extension rod can be seated inside the constraining tube. This will center the specimen inside the constraining tube during the loading, which will also be the case for a real case of DTD, as discussed in Section 4.2. The surface which the bottom of the specimen rests upon can also

be modified in a similar way. The specially constructed extension rod should be long enough so that the whole compaction sequence can be done in one test run, and stability is provided by the minimal radial clearance between the extension rod and the constraining tube.

- *Use a wider range of tubes:*
  Using different constraining tubes can give a better understanding of the effect of radial clearance. It is important to select tubes with flush IDs that are strong enough to handle the applied forces without deforming. Different lengths and dimensions of test specimens should also be used.

- *More repeated tests:*
  To reduce the uncertainty in the results, many tests should be performed with the same setup.

- *Increase repeatability of cutting pattern:*
  By using a machine or a tool that can make more accurate cuts, the repeatability would increase. It is important to make correct measurements of the radial distance between the cuts, and minimize the amount of removed steel during the cutting process. A small tube would be more weakened by a 2 mm thick cut than what a bigger tube would be with the same cut thickness.

- *Confirm load measurements of hydraulic press:*
  To be sure that the load readings from the press are correct, the press should be tested, and if necessary, calibrated. The software settings on the hydraulic press should be thoroughly reviewed to minimize errors during the experiment. If possible, the hydraulic press should measure strain while unloading the test specimen, so that elastic strain can be accounted for.

- *Adjust setup to represent a real case of DTD more accurately:*
  Some adjustments to the setup can be made to better represent a real case of DTD, such as filling the constraining tube with water and a friction-reducing additive during testing.

Chapter 8

Discussion

8.1. Introduction

This chapter will discuss the method of DTD with respect to compaction and economic viability, and will also point out some limitations of the method. Even though the planned full-scale compaction experiment was not completed, parts from the discussion of this experiment will be used, in addition to the experience from the first full-scale test and the small-scale test.

8.2. Differences Between the Planned Experiment and a Real Case

The main objective of the second full-scale compaction experiment is to check whether it is possible to compact a 4 ½" tubing within production casing sizes commonly found on the NCS. There will be several differences between the experiment and a real case of DTD, and some of these differences will be highlighted in this section.

8.2.1. Well Obstructions and Orientation

In the experiment, the tubing will be forced against a flat casing end cap, distributing the contact force over the cross-sectional area of the tubing. In a real case, the tubing will be connected to the casing through the production packer. Production packers are usually held in place by slips, which is a kind of cone with teeth that grip on the inside of the casing. Below the production packer follows the tail pipe, which ends in the polished bore receptacle (PBR). The clearance between the bottom of the PBR and the end of the tailpipe is usually not more than a meter, which means that if the production packer slips loses grip, the packer will still not be able to travel much more than a meter downwards. If the to-be-compacted tubing length is measured from the production packer, then the end conditions for a real case would be similar to that of the experiment. If one decides to cut longitudinally far above the production packer, the to-be-compacted tubing section can be crushed adjacent (side-by-side) to the rest of the tubing below the selected compaction interval, which means that the entire to-be-compacted tubing section could be removed. This case would be very different from what will be done in the full-scale experiment.

The orientation of the casing and tubing may also differ between the experiment and a real case of DTD. Accurate cement placement is notably more complicated in extended reach drilling (ERD) wells due to different factors, including high deviation angles (Farahani, Brandl and Durachman 2014). Therefore, operators often aim to place PP&A cement plugs in vertical or near-vertical sections. However, many ERD wells remain deviated after kick-off, featuring no near-vertical sections to place primary barriers. Using DTD in a horizontal or near-horizontal section may therefore be necessary, should the method be verified and adopted by the industry. The main issues regarding DTD in a horizontal wellbore have been discussed in Section 5.3. To investigate the benefits of crushing tubing within a vertical section, the gravitational assistance and friction reduction can be estimated. A 100 m long, 12.6 ppf tubing, as the one to be used in the experiment in Chapter 6, will have a total dry weight of 18,388 N. Using Eq. 1 with this weight and a friction factor of 0.24, which is used for CT when no lubricant is used (Livescu, Craig and Aitken 2016), results in a static frictional force of 4,413 N between a horizontal tubing and casing before buckling and crushing in a dry well. After vertical slicing of the tubing, the same fluid is assumed to be present inside and outside the tubing. Assuming a well fluid density of 1.03 sg, and using Eq. 3 to calculate the buoyancy factor, the effective weight of the tubing, equal to 15,960 N, would result in a frictional force of 3,830 N. In a horizontal scenario, the weight would not increase the axial loading on the tubing, and the effective frictional force would reduce the axial load on the tubing end furthest from the piston. The exact opposite would be the case for a vertical situation, where none of the frictional force would be present, and the full effective weight of the tubing would contribute to the axial load at the bottom of the tubing. Together, this would result in an increase in the axial compressive force at the bottom of the tubing equal to 19,790 N, compared to a horizontal case. As stated in Section 7.3, the internal minimum yield pressure for the 9 5/8” casing is 473.7 bar, and using this pressure will result in a piston force of 1,808,840 N. In this context, the effect of gravity and normal friction is minuscule, but much lower pressures may be more appropriate to use, which will be discussed in Section 8.5. The most important disadvantage of a horizontal situation is therefore believed to be the higher load near the piston. It should be noted that the calculations in this section did not include the force required to lift the tubing up from the constraining casing during the compaction process, and the assumptions regarding fluid density and the friction factor are pessimistic.

8.2.2. Formation Dependent Well Parameters

During compaction, the available fluid volume below the piston gets smaller. The fluid present will have to be displaced, either through a travelling valve arrangement in the piston or into the formation. In the latter case, perforations would have to be placed through the tubing and casing in order to provide a passage for the fluid. To force the fluid inside the well into the formation, the formation injection pressure would have to be overcome. This means that to move the piston, the differential pressure must exceed the compaction forces associated with crushing of tubing, the accompanying friction, and the formation injection pressure. There are limitations on the maximum piston pressure that can be used for DTD, which will be discussed in Section 8.5.

8.2.3. Tubing Related Parameters

Many wells today are termed “smart wells” by having hydraulic and/or electric cables attached on the outside of the tubing to control different devices downhole and send data to surface (Dekui, et al. 2012), as seen in Fig. 86. The second full-scale experiment will only use regular tubing joints with

nothing attached on the outside. A real case of DTD in a smart well may experience problems related to the control lines. If the cables are not cut when the tubing is severed they may be pushed against the casing by the inflated packer and act as a leak path. However, the leakage may be acceptable, and different viscous fluids may be used to reduce the leakage. When the piston is pushing the tubing downwards, any uncut cables that are pushed against the casing wall are believed to break and coil into the bottom of the well, as expressed by Oilfield Innovations in a confidential document. Some control lines have tensile strengths that can reach up to 56,275 N (Fine Tubes 2017), but it is not known how cables of this strength would influence the compaction process

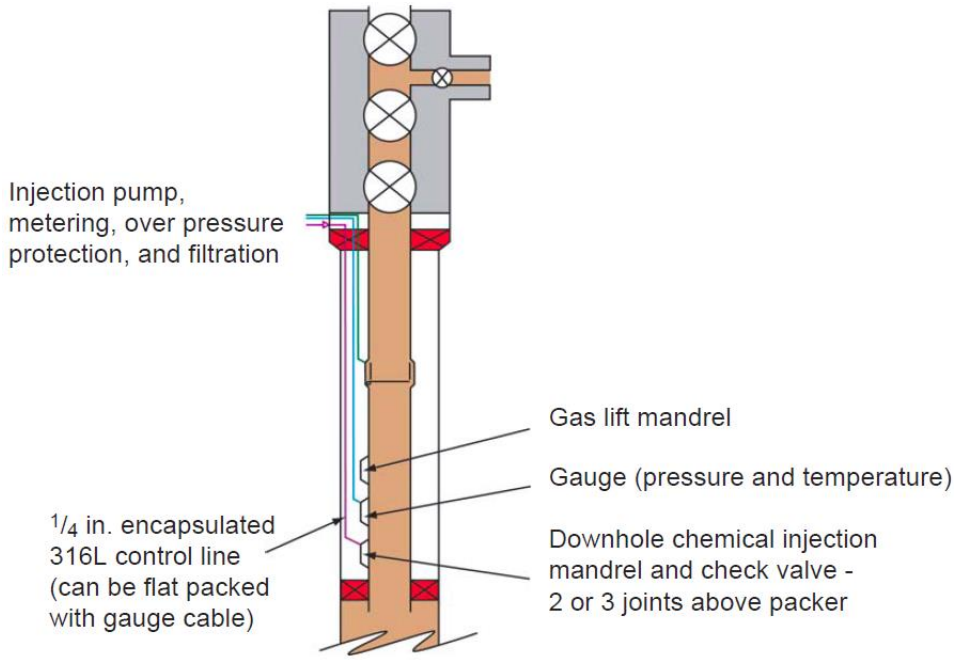

Fig. 86. Illustration showing control lines and downhole equipment attached to the tubing (Bellarby 2009).

The tubing that is planned to be compacted in the full-scale experiment in Norway is regular tubing with no equipment attached to it. During a real case of DTD, depending on the tubing interval that is planned to be compacted, downhole equipment may cause disadvantages. Control line clamps and protectors may not be cut during the weakening process, and can influence the compaction process. Other equipment can be pressure and temperature gauges, a chemical injection valve, and side pocket mandrels, as shown in Fig. 86. The influence of such equipment would need to be tested, but it may be used as a rule of thumb to not include the length of such equipment when determining the required tubing length to create a specific unobstructed casing space.

Another parameter related to the tubing is the cutting method. In the experiment, a plasma cutter is planned to be used, which creates the cuts by removing steel. A Gator Perforator (see Appendix C) or the vertical cutting tool introduced in Section 4.1 are believed to remove far less steel, if any at all. A reduction in the cross-sectional area will reduce the strength of the tubing, but making the cuts by forcing a tool against the tubing wall may cause convex surfaces which may also assist in lowering the required compaction force. Additionally, a plasma cutter will have no problem with cutting through connections in the tubing string. Depending on the cutting method used in a real case of DTD, this may not be as simple.

8.2.4. Compaction Fluid Parameters

The plan for the experiment is to only use water, possibly with friction reducing additives. For a real case, other fluids may be used instead, but no detailed plan on this have been proposed. However, the use of a viscous fluid to reduce leakage around the piston have been discussed (Oilfield Innovations 2016b). A thixotropic fluid has shear-thinning properties, and, while having a large viscosity when static, is able to flow when shaken or otherwise stressed (Oxford University Press n.d.). This enables the fluid to be pumped down the well in a real case of DTD. By placing this fluid above the piston, its gel-like state may reduce leakage around the piston during compaction.

8.3. Compaction Ratio and Friction

As discussed in Section 6.6.2, several parameters may influence the compaction of tubing within casing. It is important to determine which of them are manageable in a real case of DTD, and how we can use them to maximize the compaction ratio and/or the likelihood of success. Since we have a considerably long string of tubing available, maximizing the compaction ratio should not necessarily be the ultimate goal, and maybe the focus should be to minimize friction to avoid getting stuck with the crushed pipe. This section will look at the extension of influence from different compaction related parameters.

8.3.1. Fixed Parameters

Assuming DTD proves to be a viable method for PP&A, several considerations would need to be accounted for to determine if DTD should be used for a particular well. Fixed parameters cannot easily be changed, if possible at all, and serves as a foundation for potential models. Some of the fixed parameters associated with the tubing and constraining casing/liner at the planned depth of compaction are:

- Casing wall roughness
- Casing ID
- Casing inclination and dogleg severity
- Tubing condition
- Tubing grade, OD, and ID
- Mechanical failure of either casing or tubing
- Obstructions caused by downhole equipment

8.3.2. Manipulable Parameters

Manipulable parameters can be tuned to an operator's needs, and should also be used in potential models to determine if DTD is viable for the well. Some of these were discussed in Section 6.6.2. Out of these variables, the cutting pattern is arguably the most important one because of the large impact on the compaction forces, as seen in Section 7.4. By carefully selecting the cutting pattern, one can manipulate how the tubing will behave during the compaction process. The selection depends upon

the goal of the compaction, whether it is to maximize the compaction ratio, or to minimize the friction, where the former is to some extent dependent on the latter.

The compaction ratio is an important aspect when discussing DTD. By focusing on having a large compaction ratio, the length of the to-be-compacted tubing section can be as short as possible. To maximize the compaction, the tubing needs to fill as much of the liquid space inside the constraining casing as possible. Based on the results from the small-scale compaction experiment in Chapter 7, it may be possible achieve greater compaction inside smaller casing sizes at relatively high loads, but the resulting compaction ratio will be smaller compared to larger casing sizes. At moderate loads occupied liquid space seems to be roughly the same for different casings. By using the tubulars in the planned full-scale experiment, wherein a 4 ½" OD, 3.958" ID tubing, an 8.681" ID casing, and a 6.625" ID casing were to be used, the tubing makes up 6.1% and 10.4% of the internal areas of the casings, respectively. For comparison, the tubing used in *model run [4]* in the first full-scale experiment in Chapter 5 made up 7.3% of the internal casing area before compaction and 13.4% afterwards, where the compaction ratio was 45.9%. Using the tubular sizes from the planned full-scale experiment, the same occupied cross-sectional area as *model run [4]* would mean a compaction ratio of 54.7% and 22.3% for the 9 5/8" and 7 5/8" casing, respectively. It should be noted that these figures are based on the first full-scale experiment, which was run dry with a weak pump, but also using roughly a quarter of the length planned for the second full-scale experiment. These calculations do not take into consideration the force that would be required to reach these compaction ratios.

Based on the results from the small-scale experiment, a mixed cutting pattern can be used to influence which section of the tubing that will compact first. This is believed to be crucial when a considerable long tubing length is planned for compaction. When a uniform cutting pattern was used, the top of the tube was always crushed first. For a full-scale situation, this would mean that the top of the crushed tubing would have to be pushed through the casing while more friction is added as compaction progresses. By dividing the 100 m tubing into several sections, where the number of cuts increases towards the bottom, crushing could be initiated in the lower part first. The results from the small-scale experiment showed a small decrease in the compaction ratio when a mixed cutting pattern was used, but the benefits of selective compaction initiation are believed to surpass this potential disadvantage by far. In a horizontal case, the difference in number of cuts between two sections may be required to be greater compared to a vertical case, since the normal friction reduces the transfer of axial compressive force.

The longest tubing string that have been compacted had a length of 28.86 m (see Section 5.2). For a real case of DTD, almost four times this length is planned to be compacted. Without any results from a compaction length of this size, the extent to which friction will limit the crushing is not certain. The best way to reduce friction is to avoid contact between the crushed tubing and the casing wall. By using absorber deformation theory (see Section 2.5), it may be possible to induce axisymmetric sequential folding in the tubing. This process is believed to be much closer to the static tests than the dynamic tests, and the theory will be used accordingly. A 4 ½" OD, 3.958" ID tubing has a D/t ratio of 16.6, which classifies it as thick-walled. As stated in Section 2.5.1, an L/D ratio above 6 gave Euler collapse for all tubes of this D/t ratio and lower, but these results were based on aluminum tubes. However, tests have also been performed on mild steel tubes with a D/t ratio of 15. By cutting wide external grooves in these tubes, the sequential crushing was stabilized, which could mean that a much longer tube length can be used without initiating Euler buckling. Instead of grooves, the tubing could be slotted which may induce the same sequential folding pattern. Only a single concertina fold was developed in each groove, and this fold moved outwards during the compaction, as seen in the model

in Fig. 8. By assuming the same hinge-formation, the slot length can be selected so that the folds do not touch the constraining casing wall after compaction, and friction may be minimized. After a fold have been formed, it may also serve as to center the tubing within the casing, which may further stabilize compaction. During the small-scale experiment, sequential folding was not observed. This may be due to several factors, such as a D/t ratio of 12.5, eccentricity inside the constraining tube, too few or short slots, too long tube, or that it is not possible to induce sequential folding by using slots instead of grooves. If a Gator Perforator was used to create the slots, each slot would be pushed outwards, which should increase the likelihood of creating a fold compared to slots created by a plasma cutter. This method may work best in a vertical well where the radial clearance is small, and by creating support between the casing and the tubing at different depth intervals.

If this method was proven to work, the compaction ratio would be much lower compared to crushing of the tubing, since only a small part of the cross-sectional area of the casing is occupied after compaction. Because of the lower compaction ratio, a much longer tubing string would need to be used, which could result in a significant increase in cutting time. This method is therefore not believed to be advantageous over crushing of tubing, but if the friction during crushing becomes an issue, the sequential folding method may be an alternative.

8.4. Economic Viability

The motivation behind the development of DTD was mainly the high cost of PP&A. Oilfield Innovations have proposed a fully rigless procedure for field abandonment phase 1 and 2, which can be categorized as either complexity type 1 or 2. Rigless completion of phase 3 have already been proven to be safe and reliable (Saasen, et al. 2013).

By using wireline and coiled tubing there is no need for mobile drilling rigs, and for platform wells the derrick can be used for drilling operations, and thus sustaining or increasing hydrocarbon production which is the core function of a drilling rig. This can result in significant cost reductions. Aarbakke Innovation (2015) have estimated that by performing PP&A using WL and CT instead of mobilizing a jack-up rig, total cost savings for a PP&A batch operation on 10 wells can reach up to $183,490,000. It should be noted that these estimates assume the same number of days for performing abandonment with both jack-up utilization and rigless, which might be unrealistic. According to the same estimates, the main cost contributor in using a rig is not the rig rate, but rather the overhead costs, where the difference between a jack-up rig and a RLWI vessel can reach up to $422,500 per day (Aarbakke Innovation 2015). This results in a jack-up rig being roughly twice as costly to hire each day, while the modification and demobilization costs can be over 7 times as expensive for a jack-up rig (Aarbakke Innovation 2015). Cost savings related to transferring some P&A operations from rigs to RLWI vessels have already been proven by a risk based probabilistic approach (Moeinikia, et al. 2014), and safe and reliable methods for rigless execution of phase 1 and 2 abandonment could increase the cost savings.

Oilfield Innovations have provided a comparative cost estimate to an operator between using a drilling rig for conventional PP&A and performing DTD through wireline and coiled tubing on a platform well[8]. This estimate served only as a basis for further discussion between the two parties, and is

[8] Confidential document provided to ConocoPhillips regarding abandonment of a specific well.

presented in this thesis to give a rough estimate of cost savings related to a rigless abandonment using DTD. The two alternatives presented in the document were to either hire a jack-up rig or to use wireline, coiled tubing, and a jacking unit, all deployed from the platform, where the platform would be used for living quarters and other facilities. It should be noted that the operational sequence presented is different from that in Chapter 4, which was only a general proposal. For the comparison, the following cost estimates was proposed:

- Wireline rig-up: $60,000/day including spread rate (boats, helicopters, and other associated costs)
- Coiled tubing rig-up: $100,000/day including spread rate
- Jacking unit with abrasive jet cutting tools: $75,000/day[9]
- Jack-up drilling rig: $600,000/day including spread rate

Based on above costs, a drilling rig abandonment program is presented. The total duration of the operation is estimated to 17 days and includes:

- *Slickline rig-up (3 days)*:

Operation	**Days**
Rig-up and rig-down	2
Set temporary plugs to prepare well for drilling rig	1

Total cost: 3 × $60,000 = $180,000

- *Drilling rig (15 days):*

Operation	**Days**
Kill the well	1
Remove XMT and install BOPs	1
Remove tubing above annular safety valve (ASV)	1
Remove FLX tubing hanger packer	1
Remove tubing above production packer	1
Mill casing for the first plug	2
Set first cement plug, wait on cement, and tag	1
Mill casing for the second plug	2
Set second cement plug, wait on cement, and tag	1
Set bridge plug and cut and pull the 13 3/8” casing	1
Set cement plug in the 20” casing	1
Rig down BOPs	1
Cut and pull conductor	1

Total cost: 15 × $600,000 = $9,000,000

[9] In the document, this jacking unit would be hired for a batch operation after all the planned abandonments had been performed.

An additional $420,000 was added to account for tangible costs such as cement plugs, packers, and cutters. This adds up to a total of $9,600,000 for the drilling rig abandonment program.

Based on the costs for wireline and coiled tubing rig-up, an abandonment program using DTD and a method proposed by Oilfield Innovations to avoid milling and pulling casing is presented. The total duration of the operation is estimated to 26 days and includes:

- *Slickline rig-up (4 days):*

Operation	**Days**
Rig-up and rig-down	2
Vertically cut 152 m of tubing (for primary plug)	1
Sever tubing and compact it with an inflatable packer	1

Total cost: 4 × $60,000 = $240,000

- *Coiled tubing rig-up (17 days):*

Operation	**Days**
Rig up	1
Perforate and clean casing and wellbore for cementing	1
Vertically slice 9 5/8” casing	1
Set first cement plug, wait on cement, and tag	1
Split the tubing (for secondary plug)	1
Compact the tubing	1
Perforate and clean the casing and wellbore for cementing	1
Vertically slice the 9 5/8” casing	1
Set second cement plug, wait on cement, and tag	1
Split the tubing (for surface plug)	1
Compact the tubing	1
Perforate and clean the 9 5/8” and 13 3/8” casing	1
Vertically slice the 9 5/8” casing	1
Set surface plug, wait on cement, and tag	1
Split the tubing (to compact upper part of tubing below mudline)	1
Compact the tubing	1
Rig down	1

Total cost: 17 × $100,000 = $1,700,000

- *Jacking unit (5 days):*

Operation	**Days**
Rig-up with abrasive cutter	1
Cut conductor through 9 5/8” casing	1
Jacking conductor and 9 5/8” casing, and cutting them into pieces for backload	2

Rig-down	1

Total cost: 5 × $75,000 = $375,000

Tangible costs are estimated to $710,000, making the total cost of the rigless abandonment equal to $3,000,000.

The total cost savings from using a rigless approach instead of a drilling rig based on these estimates are $6,600,000 per well. Neither the drilling rig total cost nor the rigless total cost include non-productive time or other potential issues, but these are usually roughly the same[10]. The time estimations for rigging up and down coiled tubing and wireline are based on the average of a batch operation, but does not include moving the equipment for each new well. This is also the case for the jack-up program, where the required time for getting equipment and the derrick in place for a new well is not included. Additional expenses not included in the tangible cost estimates, such as handling and disposal of scale for a drilling rig abandonment, are not accounted for in the comparative cost estimate.

The largest uncertainties with the rigless abandonment program are related to cutting of tubing and casing. Cutting the casing as to provide access to annuli is an alternative method to the established "Perf & Wash" technology, and will not be discussed in this thesis. The accuracy of the time estimates related to cutting will depend on the technology that will be used for this process. Apart from the estimates around these operations, ConocoPhillips have expressed that the proposed abandonment programs are reasonable, assuming that the wells are able to be abandoned through DTD[10].

8.5. Limitations

Assuming that DTD of 4 ½" tubing is possible, and that it will also work for larger tubing sizes common on the NCS, there are still limitations for the use of the method. Some of these will be discussed below:

- *Restricted access:*
  Mechanical failure of tubing that reduces the effective ID may block the passage for the inflatable packer. This can usually be solved by running a swaging tool on slickline to force open the tubing. Collapse of casing, however, can in many cases not be solved with wireline or coiled tubing deployed tools, and is often solved by milling away the collapsed area and replacing it with a casing patch or expandable liner. Should a collapsed casing result in a drift diameter smaller than the minimum required casing ID for the piston packer, a drilling rig may be required to solve this issue before optionally performing DTD.

- *Maximum allowable piston pressure:*
  It is mainly the casing that determines the maximum allowable piston pressure. As mentioned in Section 8.2.2, the formation injection pressure would have to be overcome in addition to the friction and deformation forces associated with tubing compaction. Minimum internal

[10] From oral correspondence with ConocoPhillips.

yield pressure data for the specific casing along with degradation factors should be the upper limit for what pressures that are allowed downhole.

- *Open hole:*
  Even though a packer can seal in an open hole section (TAM International 2012), moving it in an open hole may cause excessive wear compared to a cased hole application.

- *Annular safety valve (ASV):*
  If a gas-lift completion is utilized on a well, there will be a problem circulating fluids on the outside of the tubing during operations with wireline. As proposed by Oilfield Innovations in a confidential document, the tubing can be punched above and below the ASV, and a straddle can be installed over the punches to allow fluids past the ASV. Using coiled tubing instead of wireline during circulation operations is another solution proposed by Oilfield Innovations.

Chapter 9

Conclusions and Recommendations

9.1. Overview

This thesis has presented a new method for rigless PP&A called Downhole Tubing Disposal (DTD). The method has been tested in a full-scale experiment that have been presented and discussed. A second full-scale experiment was planned to be conducted during the writing of this thesis, and this experiment have also been presented and discussed. When it became clear that the experiment would be postponed, a small-scale experiment was planned and executed, and the results were discussed. The discussions from all three experiments were combined and used as a foundation for a discussion of DTD in a real case.

From the work of this thesis, shortcomings of the full-scale compaction experiments have been highlighted and important factors during the crushing of tubing have been identified. A short economic analysis was also performed to investigate cost savings related to the use of DTD. A summary of the work and conclusions will be presented in this chapter.

9.2. Summary

- A full-scale experiment has been performed to verify if compaction of a small tubing was possible, and what compaction ratios that could be obtained. The results were believed to be pessimistic, and the data from the experiment was limited.

- A second full-scale experiment has been planned. A bigger tubing of significantly increased length would be loaded to see if compaction and DTD is possible with tubular sizes found on the NCS. The setup of this experiment was reviewed, recommendations were given, and important compaction variables were discussed.

- A small-scale experiment was conducted to look at the effect of different cutting patterns, and to evaluate the influence of different constraining tubes. Based on this experiment, several conclusions were made:

  - Increasing the number of longitudinal cuts in a tube reduces the axial strength of the tube.

  - Smaller constraining tubes reduce the compaction ratio.

  - Mixed cuttings patterns can be used for selective compaction initiation. A section with a higher number of cuts is more weakened than a section with a lower number of cuts, and by making the lower part of the tube compact first, friction can be reduced.

- Several important differences between a real case of DTD and the planned experiment was highlighted. The effects of gravity assistance and normal friction were discussed, and the influence of tubing, formation, and well related parameters were highlighted.

- An alternative method to tubing crushing was presented, based on absorber theory used in the car industry. This method would give a lower compaction ratio, but could also significantly reduce friction.

- A short economic analysis was performed based on a comparative cost estimate presented by Oilfield Innovations, which presented significant cost reductions by using DTD with rigless abandonment.

9.3. Recommendations for Further Work

- Conduct the planned full-scale experiment, preferably by including additional larger tubing sizes, since the 4 ½" is not the most common tubing on the NCS. Use mixed cutting patterns with a higher number of cuts at the bottom at least once. Create models based on the results if the data is sufficient.

- Perform a vertical compaction experiment with slotted tube, preferably weakened by a tool similar to the Gator Perforator that pushes against the inside of the tubing wall. See if sequential folding of thick-walled tubes is possible by using a high number of radially placed slots.

- Perform small-scale experiments based on the recommendations in Chapter 7 to build empirical models for the effect of cutting patterns and constraining tubes, and preferably also length of compaction tubes.

- Conduct a detailed economic analysis of cost savings related to DTD, which can be used as a foundation to provide further funding for development of the method.

- Verify if the cutting tool proposed by Oilfield Innovations can be used to efficiently cut tubing downhole. The use of other cutting/weakening tools should also be investigated.

References

Aarbakke Innovation. "Norsk Olje & Gass P&A Seminar." October 29, 2015. https://www.norskoljeoggass.no/Global/PAF%20seminar%202015/08%20-%20New%20PA%20Tool%20Concepts%20for%20Rigless%20PA,%20AArbakke.pdf?epslanguage=no (accessed March 30, 2017).

Aasen, Jan Aage. *Buckling in Oil And Gas Wells.* Stavanger, Norway: University of Stavanger, 2007.

American Petroleum Institute. *API Spec 5CT.* American Petroleum Institute, 2005.

Andrews, K. R. F., G. L. England, and E. Ghani. "Classification of the axial collapse of cylindrical tubes under quasi-static loading." *International Journal of Mechanical Sciences, Vol. 25, Issue 9,* 1983: 687-696.

Belayneh, Mesfin Agonafir. "Materials and Material selection, lecture notes." University of Stavanger, 2016.

Bellarby, Jonathan. *Well Completion Design.* Amsterdam, The Netherlands: Elsevier, 2009.

Birkeland, Fredrik. *Final Field Permanent Plug and Abandonment – Methodology Development, Time and Cost Estimation, Risk Evaluation.* University of Stavanger, 2011.

Callister, W.D., and D.G. Rethwisch. *Materials Science and Engineering, Eight Ediдtion, SI Version.* John Wiley & Sons, 2011.

Chen, Y.C., Y.H. Lin, and J.B. Cheatham. *An Analysis of Tubing and Casing Buckling in Horizontal Wells.* Houston, Texas: Offshore Technology Conference, 6037, 1989.

Dawson, Rapier, and P. R. Paslay. *Drillpipe Buckling in Inclined Holes.* Journal of Petroleum Technology, October, 1734-1738, 1984.

Dekui, Xu, et al. *Smart Well Technology in Daqing Oil Field.* Abu Dhabi, UAE: Society of Petroleum Engineers, 161891, 2012.

Farahani, Hamidreza S., Andreas Brandl, and Ridwan Durachman. *Unique Cement and Spacer Design for Setting Horizontal Cement Plugs in SBM Environment: Deepwater Indonesia Case History.* Offshore Technology Conference, 24768-MS, 2014.

Fine Tubes. April 21, 2017. http://www.finetubes.co.uk/uploads/images/Control%20Lines.pdf.

Ghani, Eskandar. *Static and dynamic collapse behaviour of cylindrical tubes and tube assemblies.* Faculty of Engineering of the University of London, Department of Civil Engineering, King's College, 1982.

Halliburton. "Cementing Wiper Plugs." 2009. http://www.halliburton.com/public/cem/contents/Books_and_Catalogs/TECH/Sect07_ce.pdf (accessed April 18, 2017).

He, X., G.W. Halsey, and Å. Kyllingstad. *Interactions between Torque and Helical Buckling in Drilling.* Society of Petroleum Engineers, 30521, 1995.

Hsu, S. S, and N Jones. *Quasi-static and dynamic axial crushing of circular and square stainless steel tubes.* Boston, MA: Proceedings of the 7th International Conference on Structures Under Shock and Impact, Structures Under Shock and Impact VII, 2002.

Interwell. November 15, 2016. http://www.interwell.com/newsroom/oil-gas-uk-award-to-centrica-based-on-the-trials-of-interwell-p-a-solution-article1347-521.html (accessed March 30, 2017).

Khalifeh, Mahmoud. *Plug & Abandonment Lecture Notes.* 2016.

Kyllingstad, Å. *Buckling of tubular strings in curved wells.* Journal of Petroleum Science and Engineering, 1995.

Livescu, Silviu, Steven Craig, and Bill Aitken. *Coiled Tubing Friction in Extended-Reach Wells.* Society of Petroleum Engineers, 179100-MS, 2016.

Lubinksi, Arthur, W. S. Althouse, and J. L. Logan. *Helical Buckling of Tubing Sealed in Packers.* Journal of Petroleum Technology, 655-670, 1962.

Lubinski, A. *A Study of the Buckling of Rotary Drilling Strings.* Dallas, Texas, 178-214: American Petroleum Institute Drilling Production Practice, 1950.

Maurer Engineering Inc. "Bureau of Safety and Environmental Enforcement." August 1993. https://www.bsee.gov/sites/bsee.gov/files/tap-technical-assessment-program//300an.pdf (accessed 03 30, 2017).

Mehari, Elsa Taeme. *P&A In Artic Conditions.* University of Stavanger, 2014.

Miska, S., W. Qiu, L. Volk, and J.C. Cunha. *An Improved Analysis of Axial Force Along Coiled Tubing in Inclined/Horizontal Wellbores.* Society of Petroleum Engineers, 37056-MS, 1996.

Miska, Stefan, and J.C. Cunha. *An Analysis of Helical Buckling of Tubulars Subjected to Axial and Torsional Loading in Inclined Wellbores.* Society of Petroleum Engineers, 29460, 1995.

Mitchell, R.F. *Effects of Well Deviation on Helical Buckling.* Society of Petroleum Engineers Drilling & Completion, 29462-PA, 1997.

Mitchell, Robert F. *Simple Frictional Analysis of Helical Buckling of Tubing.* Society of Petroleum Engineers Drilling Engineering, 13064-PA, 1986.

Mitchell, Robert F. *Tubing Buckling - The State of the Art.* San Antonio, Texas: Society of Petroleum Engineers Drillling & Completion, 104267, 2006.

Moeinikia, Fatemeh, Kjell Kåre Fjelde, Arild Saasen, Torbjørn Vrålstad, and Øystein Arild. *Evaluating Cost Efficiency of Rigless P&A for Subsea Multiwell Campaign.* Society of Petroleum Engineers, 167923-MS, 2014.

NORSOK D-010. *Well integrity in drilling and well operations, Rev. 4.* Standards Norway, 2013.

NPD. n.d. http://factpages.npd.no/factpages/Default.aspx?culture=nb-no&nav1=wellbore&nav2=TableView|Development (accessed May 17, 2017).

Oil & Gas UK. "Guidelines for the suspension and abandonment of wells, Issue 4." 2012.

Oil & Gas UK. "Guidelines on Well Abandonment Cost Estimation, Issue 1." 2011.

Oilfield Innovations. August 19, 2013. http://www.oilfieldinnovations.com/assets/oilfield-innovations-tubing-crushing-modelling-19-aug-2013-rev.pdf (accessed March 30, 2017).

Oilfield Innovations. "Crushing of Tubing within Horizontal Casing." 2013.

Oilfield Innovations. "Downhole tubing disposal general procedure." 2016a.

Oilfield Innovations. "Large Real Scale Tubing Compaction Simulations." 2017.

Oilfield Innovations. "Mitigating the high cost of offshore well P&A." 2016b.

Oxford University Press. *Oxford Dictionary.* n.d. https://en.oxforddictionaries.com (accessed March 30, 2017).

Persson, B. N. J. *Sliding Friction - Physical Principles and Applications, Second Edition.* Berlin: Springer Verlag, 2000.

Ramex. *RX-72TL Friction Reducer.* n.d. http://www.ramex.no/RX-72TL.pdf (accessed April 20, 2017).

Saasen, Arild, Kjell Kåre Fjelde, Torbjørn Vrålstad, Sanggi Raksagati, and Moeinikia Fatemeh. *Plug and Abandonment of Offshore Exploration Wells.* Offshore Technology Conference 23909, 2013.

Salehghaffari, S, M Tajdari, and F Mokhtarnezhad. *Collapse of thick-walled metal tubes with wide external grooves as controllable energy-dissipating devices.* Institution of Mechanical Engineers, Part C: Journal of Mechanical Engineering Science, Vol 223, Issue 11, 2009.

Subsea world news. September 14, 2016. http://subseaworldnews.com/2016/09/14/island-offshore-aims-for-riserless-heavy-well-intervention/ (accessed March 03, 2017).

TAM International . September 2015. https://www.tamintl.com/images/pdfs/gps/WP/SLIKPAK_02182014.pdf (accessed May 17, 2017).

TAM International. September 2012. https://www.tamintl.com/images/pdfs/brochures/SlikPakPlus_Brochure.pdf (accessed May 5, 2017).

Tarpon Pipe and Supply. n.d. http://www.tarponpipe.com/perch/resources/casing-table.pdf (accessed April 25, 2017).

ThyssenKrupp. March 2012. http://www.s-k-h.com/media/de/Service/Werkstoffblaetter_englisch/Praezrohre/Precision_acc._10305-4.pdf (accessed May 09, 2017).

Wicks, Nathan, Brian L. Wardle, and Demos Pafitis. *Horizontal cylinder-in-cylinder buckling under compression and torsion: Review and application to composite drill pipe.* International Journal of Mechanical Sciences, 538-549, 2007.

Wu, J., and H.C. Juvkam-Wold. *Study of Helical Buckling of Pipes in Horizontal Wells.* Society of Petroleum Engineers, 25503-MS, 1993.

Appendix A

TAM INTERNATIONAL

GENERAL PRODUCT SHEET

SlikPak™ Plus – *Slickline/E-line Conveyed Retrievable Inflatable Packer System*

PRODUCT DESCRIPTION:

The SlikPak™ Plus is a battery-powered assembly that can be used to run 2.13 in. to 14.5 in. (54 mm to 368 mm) inflatable bridge plugs or packers on slickline or electric line. The necessary inflation fluid can be obtained from the wellbore or carried on adaptable fluid chambers. Its electronic cartridge is preprogrammed at the surface in order to ensure the inflation process starts once the packer reaches setting depth. The SlikPak Plus system also contains a mechanically activated intensifier, which can be utilized for the inflation process as a backup to the electric/hydraulic components.

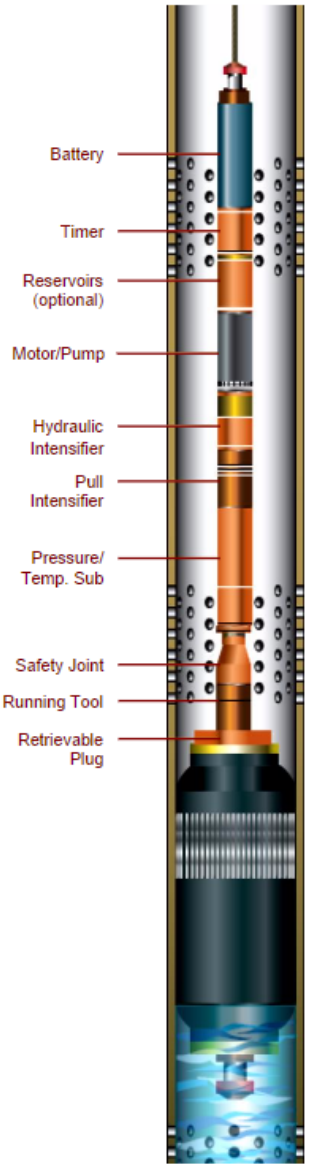

PROVIDE SOLUTIONS FOR:

- Water shut off
- Wellhead repair/change out
- Mechanical integrity testing
- Retrievable bridge plug for workover and recompletion
- Packer to hang off screens for thru-tubing sand control
- Modular scab liner for isolating mid-perf water leaks in screens or tubing
- Simultaneous Operations (SimOps)

FEATURES:

- Ideal for remote locations and small, unmanned platforms with restricted deck space
- Field-proven wellbore fluid inflation system reduces bottom hole assembly (BHA) length for platforms and rigs with restricted lubricator height
- Backup mechanical setting system if electric/hydraulic components fail to function properly as well as a secondary safety release mechanism
- Inflation fluid reservoirs for dry gas wells and heavy mud applications
- Capable of operation in up to 300°F (150°C)
- Optional cold weather package allows operation down to -40°F (-40°C)

BENEFITS:

- Reduced cost when run on slickline or electric line vs. coiled tubing
- Ability to run through tubing and set in large ID casing utilizing patented structure technology
- Pressure/temperature sensors monitor the inflation and setting processes and downhole well conditions at setting depth, and can also be used to measure the pressure gradient to determine the fluid type in the well

Fig. 87. General product sheet for SlikPak™ Plus (TAM International 2015).

Appendix B

A joint of casing will be severed and a thick plate will be welded on to the opposite site of the box or pin ends, as seen in Fig. 88. Several holes will be drilled through the thick plate to serve as bleed ports, and a pipe connection will be made in the center of the thick plate. The bleed ports will be made possible to close. The pad eyes seen in Fig. 88 is intended for use during a vertical experiment to serve as a lifting point, but this may not be included in the final design, since a vertical experiment is currently not planned.

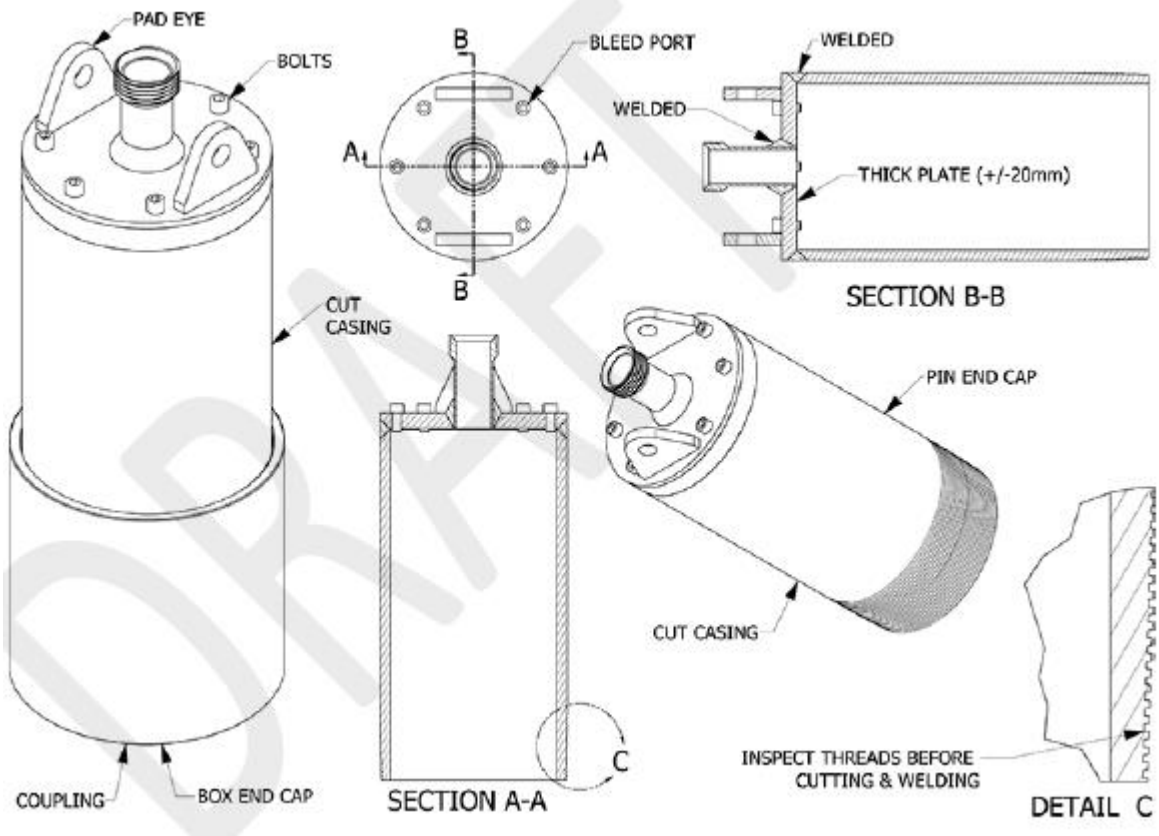

Fig. 88. Casing end cap design.

Appendix C

The blades on the Gator perforator, seen to the right in Fig. 89, are extended from the tool and pushed against the inside of the casing wall. This creates openings that are around 11.5 cm long, depending on the blades, which can be seen to the right in Fig. 89. This tool is used for cementing behind casing, but may weaken a tubing enough for compaction, especially if the tool is rotated 45° after the first perforations are made so that 8 longitudinal cuts are made along the tubing.

Fig. 89. To the left, a Gator Perforator tool designed by Lee Energy Systems Inc. To The right, a casting of a casing after being subjected to the Gator Perforator.

Appendix D

The first two tests were conducted with a hydraulic press operated manually with a pumping lever. There were no digital data readings, and since the manometer was insensitive to small loads, force recording was not available for these tests. The test specimen in the first two tests was a copper pipe with an OD of 12.00 mm and a wall thickness of 0.95 mm, which equals a D/t ratio of 12.63.

The cutting patterns and cut lengths of T1 and T2 are given in Fig. 90 and Fig. 92. All cuts in the copper tube were made with a Dremel-tool and were not very precise, and the cut lengths given in Fig. 90 and Fig. 92 are therefore averages.

The procedure for the first to tests was to place the test specimen within the constraining tubular and then place an extension rod on top that would transfer the force from the hydraulic piston to the test specimen. The rod was used because the piston was too wide to fit inside the constraining tubular, and the downward movement of the piston was limited to around 20 cm. The constraining tubular was not fixed in any locations. The piston was lowered slowly until it touched the extension rod, and then the test was started. Each time the piston reached the constraining tubular, the pressure was released so that the piston returned to its initial position. The rod was then changed with a longer one, so that force could again be transferred to the copper pipe. Both tests ended when the force required to pull the pumping lever markedly increased.

Specimen T1 was divided into three sections with one uncut part, one part that were cut 3 times, and the last part which were cut two times. The cuting pattern is seen in Fig. 90 and was selected to act as a foundation for further testing.

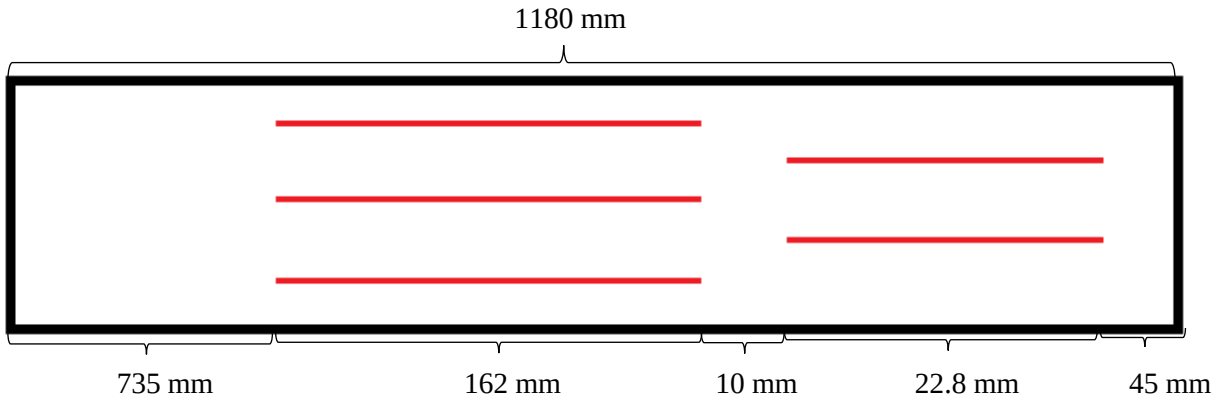

Fig. 90. Cutting pattern and cut lengths of specimen T1.

The specimen is depicted before and after crushing in Fig. 91. From this test, it was clear that a higher number of cuts resulted in less axial strength for the tube. It also seemed that using two cuts lowered the buckling load of the tube, since the upper section was permanently buckled while the lower section was straight. Another possibility is that both the upper section and lower section was buckled, but only the upper section was within the plastic range. A third possibility is that the crushed section with 3 cuts reduced the transfer of axial load to the lower section, but the effect of this is believed to be little since the compaction was relatively low and the ejection force seemed to be small.

Fig. 91. Top left picture shows specimen T1 after cutting and before compaction. Top right picture shows the 3-cut section after crushing, the second picture from the bottom shows the lower end of the specimen, and the bottom picture shows the upper section of the specimen.

Based on the results from specimen T1, a new test was conducted which only used 3 longitudinal cuts. Two different cutting patterns were used, as seen in Fig. 92.

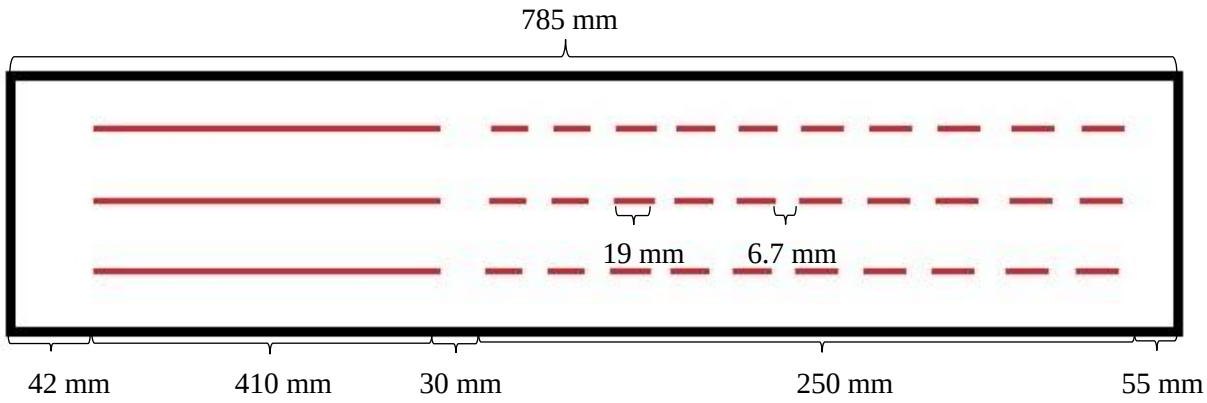

Fig. 92. Cutting pattern and cut lengths of specimen T2.

Specimen T2 is shown both before and after compaction in **Fig. 93**. It was clear that the part that were cut 3 times were much more crushed compared to the dashed cut part, where the latter was mostly compacted side-by-side.

Fig. 93. The upper picture shows specimen T2 after cutting and before compaction. The lower picture shows the tube after crushing, and in this picture, the left side of the specimen was at the top, unlike all the other figures.

No calculations were performed for the copper specimens since no force recordings or strength data were available.

Appendix E

Specimen T3, 2 cuts

Test specimen T3, seen in Fig. 94, was placed inside the 49.3 mm ID steel tube and loaded in 9 test runs to a maximum load of 100.00 kN. Since this was the first test with this hydraulic press, short extension rods were used to ensure stability, which is the main reason for the high number of test runs. A break criterion was also activated, which is commonly used during concrete testing, which was not detected and deactivated until later. This break criterion stopped the test if a certain strain criterion was reached. After the test, the crushed tube was ejected using the manual pumping press used during testing of T1 and T2, and because of the low required force, no readings were available.

Fig. 94. Cutting pattern and cut lengths of specimen T3.

The test results from specimen T3 can be seen in Fig. 95. The graphs from each test specimen in this experiment will be presented in the chronological order in which they were conducted, which means that Fig. 95a) belongs to the first test run, b) belongs to the second test run and so forth. The first and second test run both showed a smooth increase in force during small deformations, where they ended with a load of 31.01 kN and 38.40 kN, respectively. The pattern seen in Fig. 95c) after reaching the maximum load of 31.66 kN corresponds to crushing of the tube, based on the experience from this experiment. The two previous graphs in the same figure may correspond to buckling and elastic deformation, as later experience from two cuts suggests buckling before crushing. Fig. 95b) ends at 27.73 kN while the force decreases, which may be the beginning of the crushing process, since the first sharp fall in Fig. 95c) starts at 24.71 kN. Once crushing has initiated, large deformations take place below 25 kN, as can be seen in Fig. 95c), d), and f). Fig. 95g) and h) show approximately the same load-strain pattern, while Fig. 95g) shows a continuously increasing load while the tube is compacted.

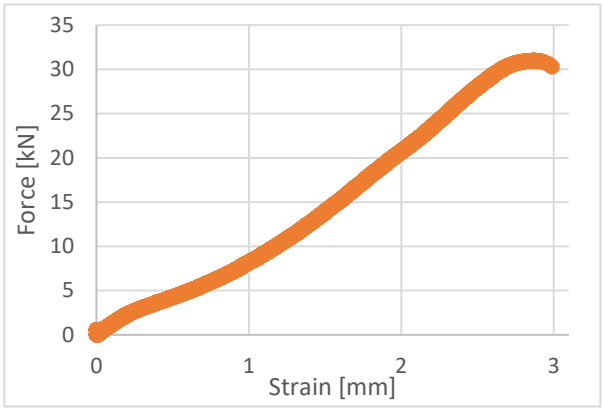
Force [kN]
Strain [mm]
0
5
10
15
20
25
30
35
0
1
2
3

a)

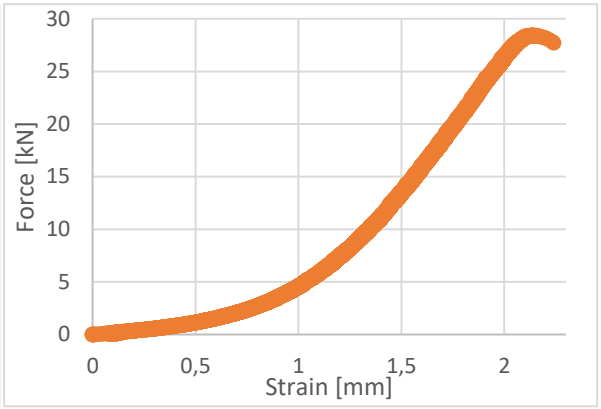
Force [kN]
Strain [mm]
0
5
10
15
20
25
30
0
0,5
1
1,5
2

b)

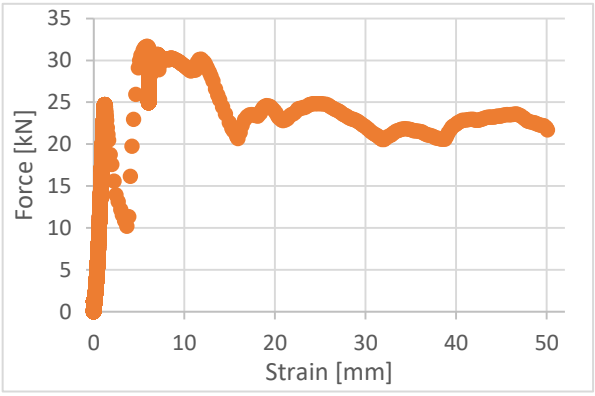
Force [kN]
Strain [mm]
0
5
10
15
20
25
30
35
0
10
20
30
40
50

c)

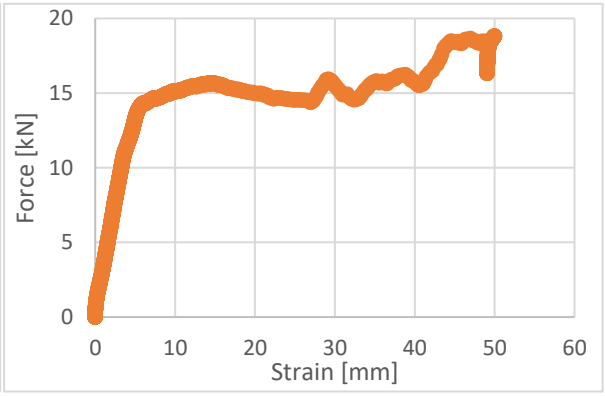
Force [kN]
Strain [mm]
0
5
10
15
20
0
10
20
30
40
50
60

d)

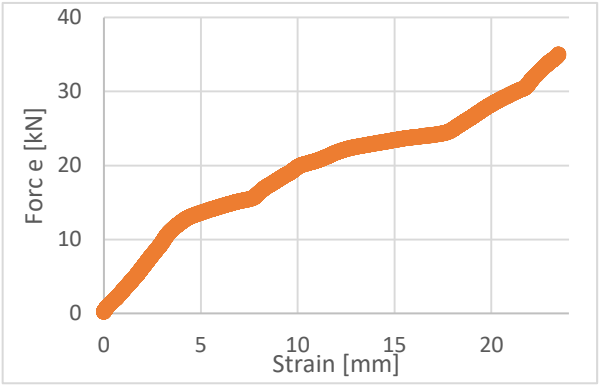
Force e [kN]
Strain [mm]
0
10
20
30
40
0
5
10
15
20

e)

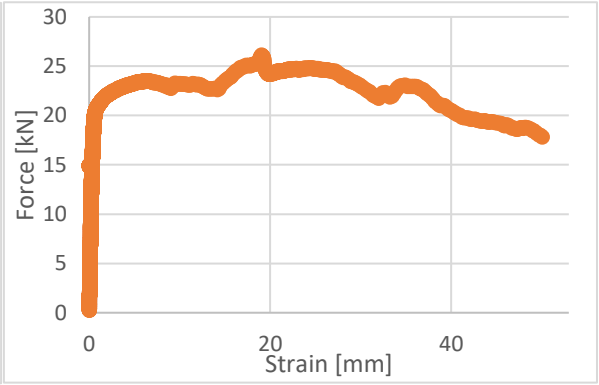
Force [kN]
Strain [mm]
0
5
10
15
20
25
30
0
20
40

f)

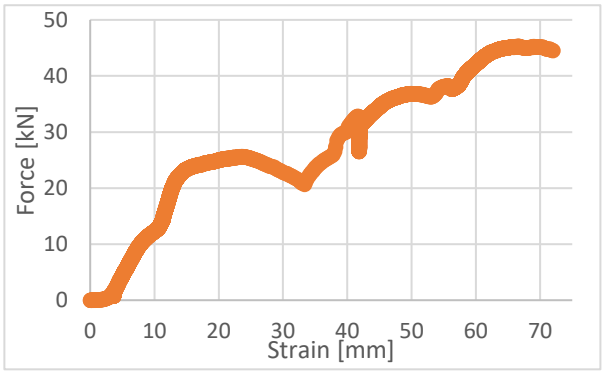
Force [kN]
Strain [mm]
0
10
20
30
40
50
0
10
20
30
40
50
60
70

g)

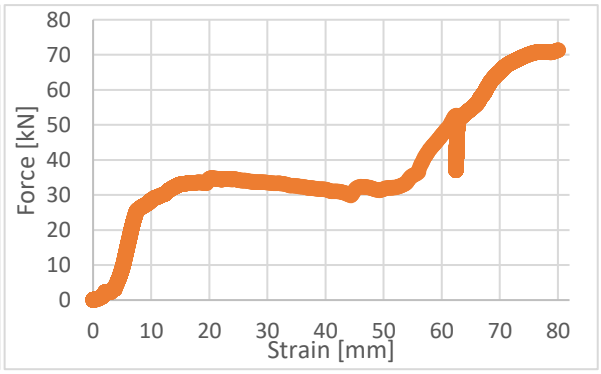
Force [kN]
Strain [mm]
0
10
20
30
40
50
60
70
80
0
10
20
30
40
50
60
70
80

h)

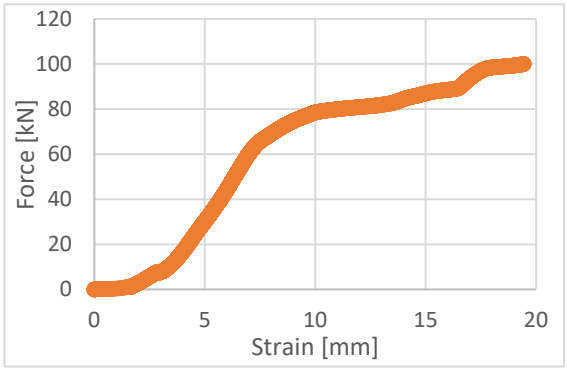

i)

Fig. 95. Test results from loading of specimen T3.

The total strain of all graphs in Fig. 95 adds up to 348.98 mm. The manually measured strain of the crushed specimen after ejection from the constraining tube, as seen to the left in Fig. 96, was 312.6 mm, giving a crushed length of 87.4 mm. Because of the big difference between the measured strain values, the results from this test will not be included in the discussion. The sources of error during the experiment will be discussed in Section 7.4.3.

The crushing pattern of specimen T3 can be seen to the left in Fig. 96. As seen in the middle and right picture in Fig. 96, crushing of the inner tube started at the top, where the lower part was buckled or slightly deformed. Further loading pushed down the crushed part of the tube, which started compaction of the lower part

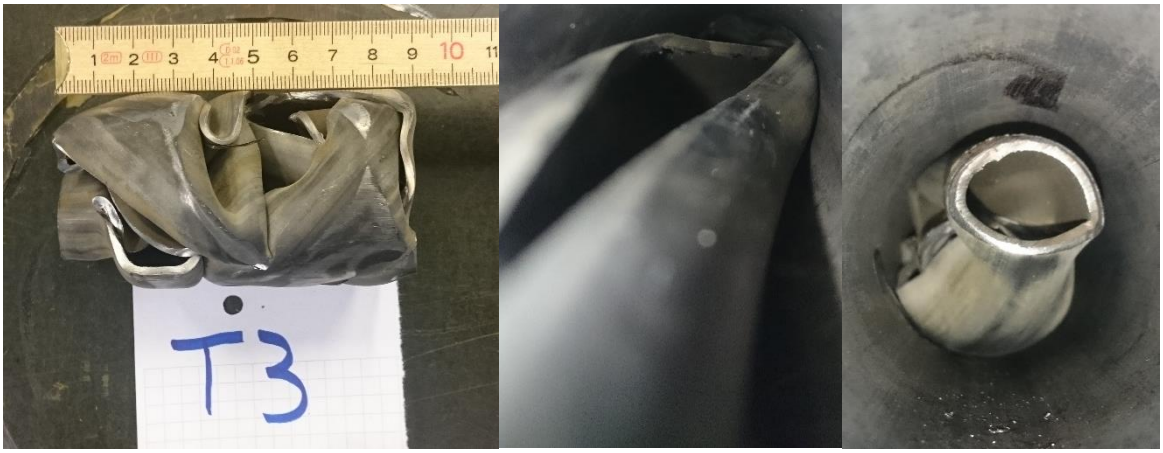

Fig. 96. To the left, specimen T3 is shown after crushing and ejection from the constraining tube. The middle picture shows the inner tube seen from below, and the right picture shows the inner tube from above, both after the second test run.

Specimen T4, 3 cuts

Test specimen T4, seen in Fig. 97, was placed inside the 39 mm ID aluminum tube and loaded in 2 test runs to a maximum load of 55.25 kN. The test was stopped when the constraining tube buckled in Euler mode and burst. This led to the decision that the 32 mm ID aluminum tube would not be used during this experiment, as it would be too weak. To release the crushed tube from the buckled constraining tube, the constraining tube was cut open using an angle grinder.

Fig. 97. Cutting pattern and cut lengths of specimen T4.

The test results from specimen T4 can be seen in Fig. 98. During the first test run, the force increased steadily until it reached 20.40 kN, where a short drop occurred, followed by small strains with increasing force, as seen in the beginning of Fig. 98. The force increased until it reached 32.22 kN, where it then dropped as large deformations took place, most likely bending and folding of the inner tube. The end of the graph in Fig. 98a) shows a force of 47.30 kN, and this is close to the first plateau in Fig. 98b) which had a maximum force of 45.13 kN. This shows that the crushing process at the end of the first test run most likely continued when the first plateau in the second test run was reached. The sharp drop in the end of Fig. 98b) is due to the Euler buckling of the constraining tube. One can see that this drop happened over a short time period since the density of the data points are much lower. This is also confirmed by the time measurements, which is not presented in the thesis.

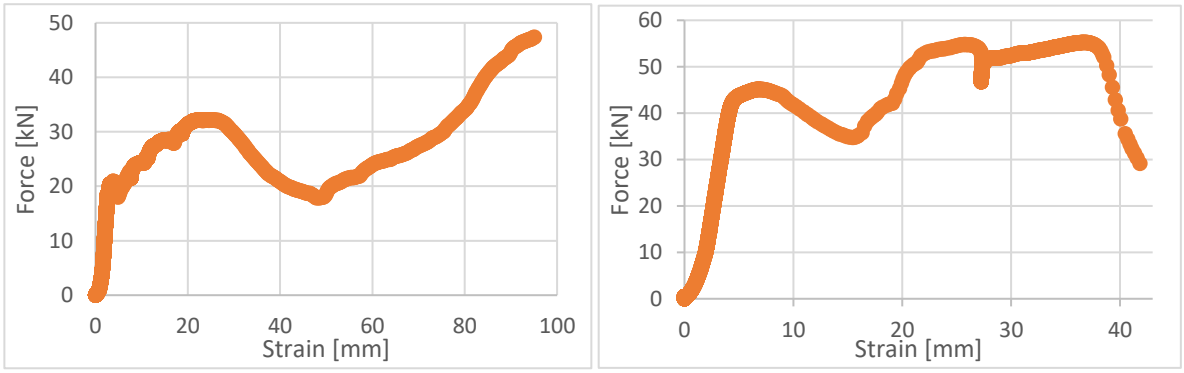

a) b)

Fig. 98. Test results from loading of specimen T4.

The total strain of the two test runs seen in Fig. 98 adds up to 133.13 mm, if the last part of Fig. 98b) is removed. This number may be a couple of millimeters bigger or smaller, depending on where the buckling process is assumed to start. The manually measured length of the specimen seen in the bottom right corner of Fig. 99 was 269.3 mm, which gives a strain of 130.7 mm.

From the bottom-right picture in Fig. 99 it can be seen that most of the deformation of specimen T4 took place at the top of the inner tube. During crushing of the inner tube, the constraining tube was deformed, which most likely created an anchoring point for the inner tube. This reduced the transfer of axial force to the lower part of the inner tube, which resulted in a focused load on the inner wall of the constraining tube and in the end, burst and buckling. Because of the possibly significant influence of the deformation of the constraining tube on the compaction process, none of the test results from this specimen will be used in the discussion.

Fig. 99. The left picture shows point where the constraining tube burst during loading of specimen T4 in the second test run. The upper-right picture shows the Euler failure mode of the constraining tube, and the bottom-right picture shows the test specimen after it had been removed from the constraining tube.